CHAPTER IV

RESULTS AND DISCUSSION

4.1 Infrared Analyses

We prepared starch-*g*-polystyrene copolymer by a simultaneous irradiation technique from a ^{60}Co source because the graft copolymers so obtained are clean, free from chemical initiator of the conventional free radical polymerization. It is necessary to avoid as much as possible the residue initiator because it may cause further polymerization upon irradiation. Although we added the dispersing agent in the composite, we do believe that starch-*g*-polystyrene might assist in better compatibility of starch and polystyrene. Starch-*g*-polystyrene copolymers were characterized in terms of the homopolymer content, grafting efficiency, grafting ratio, conversion, and percent add-on. FT-IR technique was used to follow up changes in graft copolymerization. The FT-IR spectra of cassava starch, polystyrene, the cassava starch-*g*-polystyrene graft copolymer before extraction, after extraction with toluene, and after hydrolysis of starch are given in Figures 4.1 through 4.5, respectively.

The infrared absorptions of cassava starch in Figure 4.1 give the O-H stretching peak at 3300-3500 cm^{-1}, the C-H stretching of CH_2 peak at 2850-2920 cm^{-1} and the C-O stretching at 960-1190 cm^{-1}. After γ-irradiation of styrene onto starch, one can observe the C-H stretching of aromatic ring at 3024 cm^{-1}, the aromatic C=C stretching peak at 1601 cm^{-1} and the absorption peak of starch at 3378.2 cm^{-1}, 2923.7 cm^{-1} and 960-1190 cm^{-1} still exist. It indicates that styrene was grafted on the starch backbone. The appearance of the absorption peak of starch at 3300-3500, 2850-2920 and 960-1190 cm^{-1} shows that starch was the framework of the graft copolymer. Polystyrene homopolymer that occurs during the graft copolymerization can be removed by toluene extraction and starch-*g*-polystyrene was hydrolyzed by hydrochloric acid (1.5 *N*, 2 hours) to determine percentage grafting efficiency. One can observe the decrease in the peak area of the stretching absorption peak of the O-H group at 3300-3500 cm^{-1} and the C-O stretching peak at 960-1190 cm^{-1}.

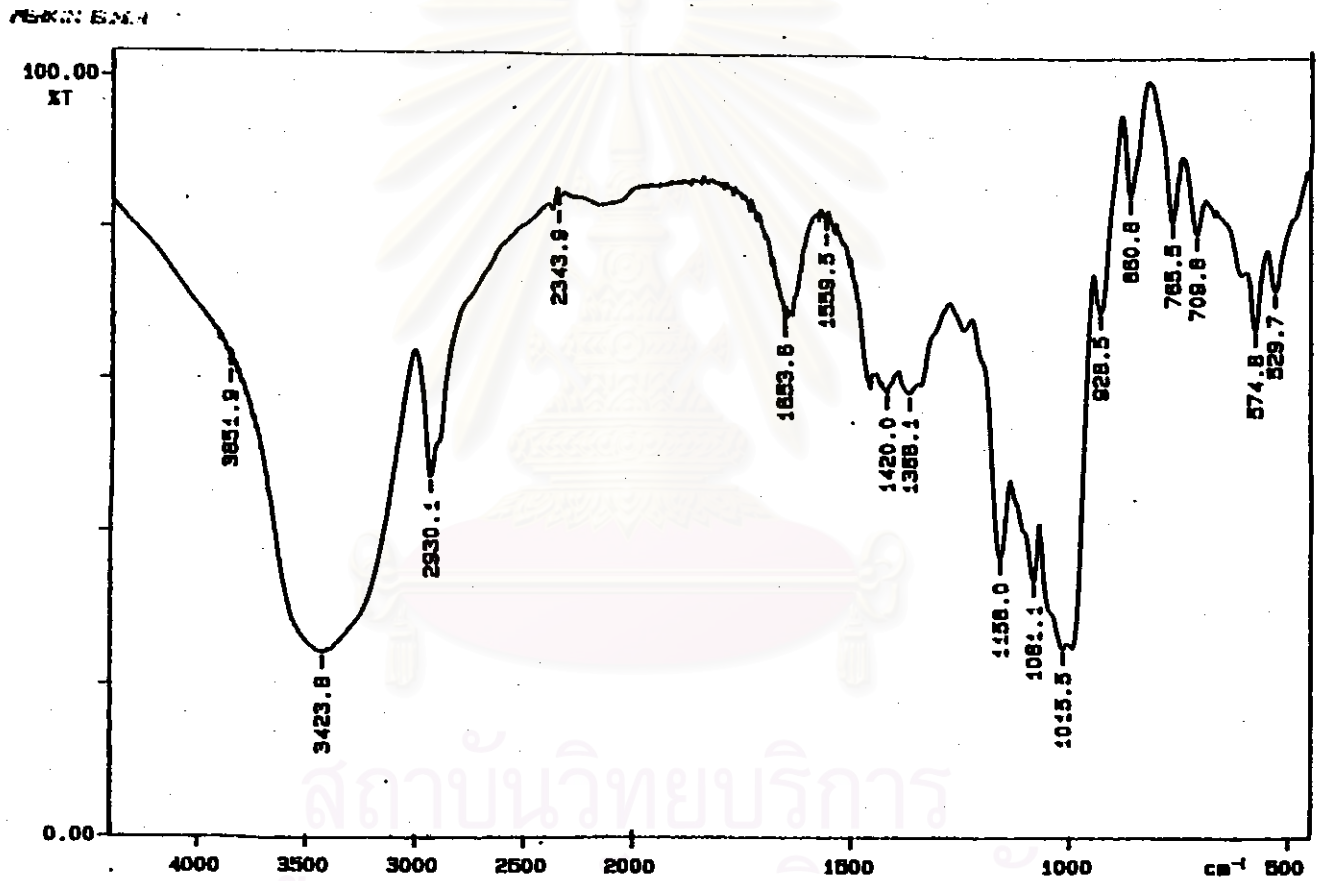

Figure 4.1 Infrared spectrum of cassava starch

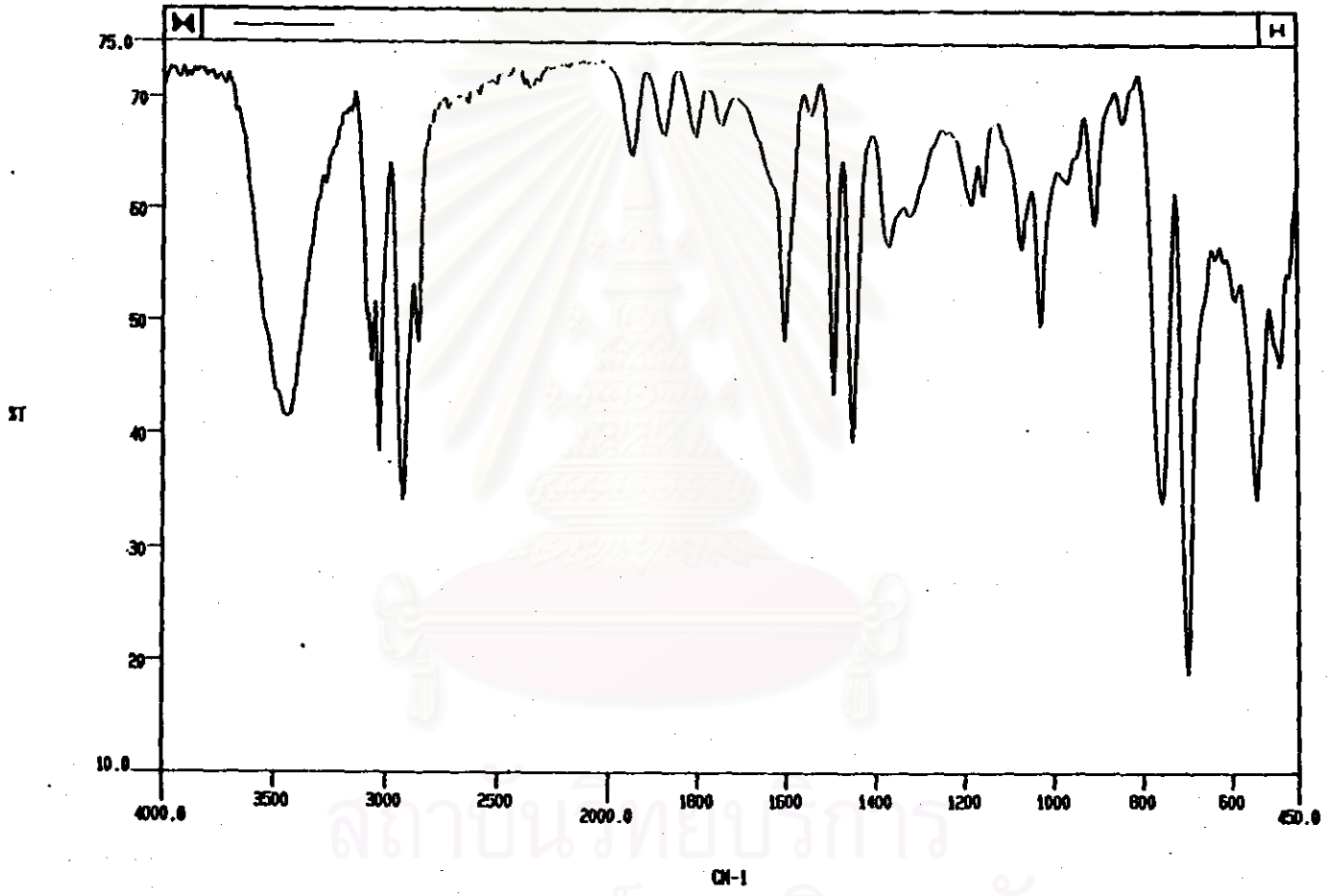

Figure 4.2 Infrared spectrum of polystyrene

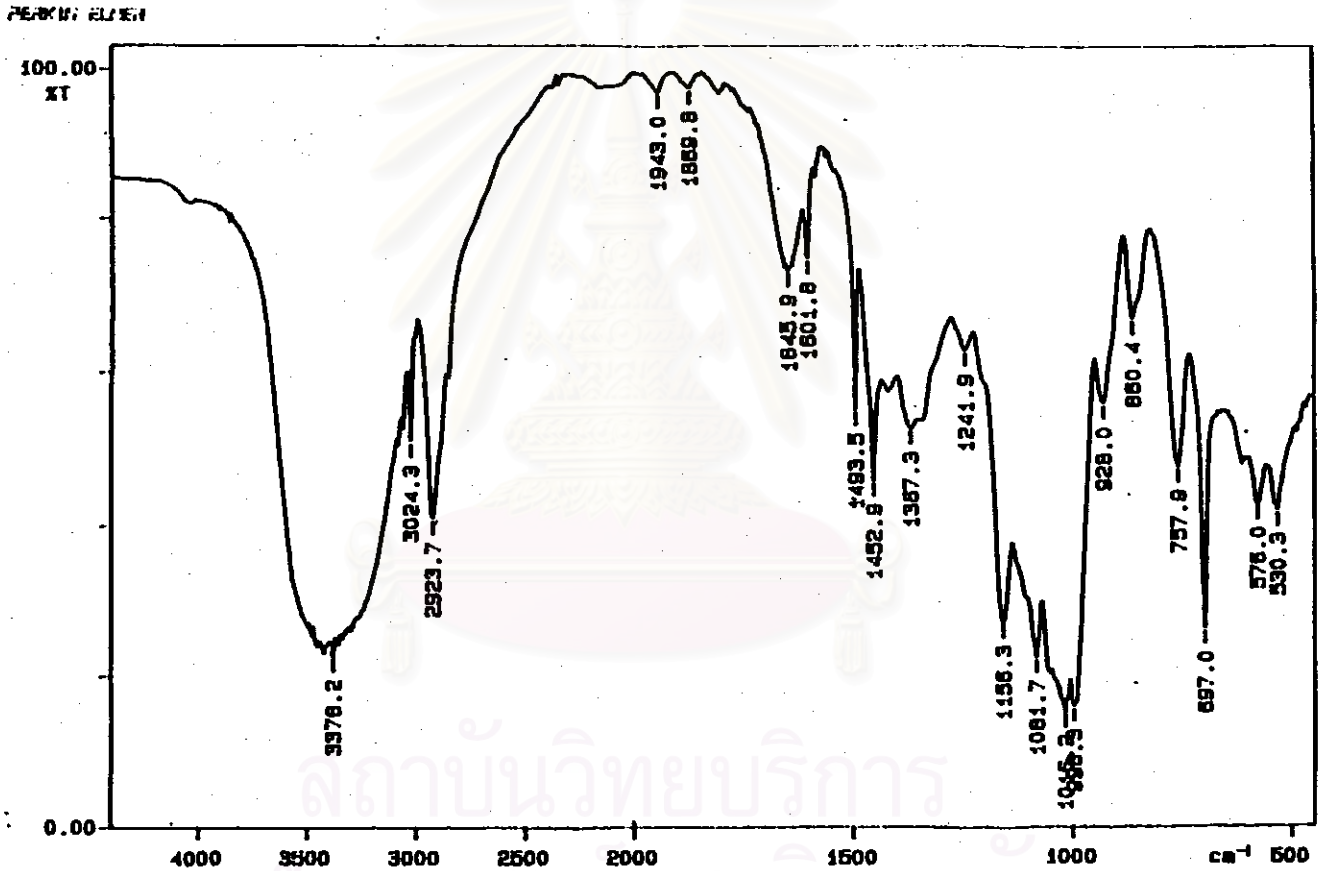

Figure 4.3 Infrared spectrum of the graft copolymer of cassava starch-*g*-polystyrene before extraction

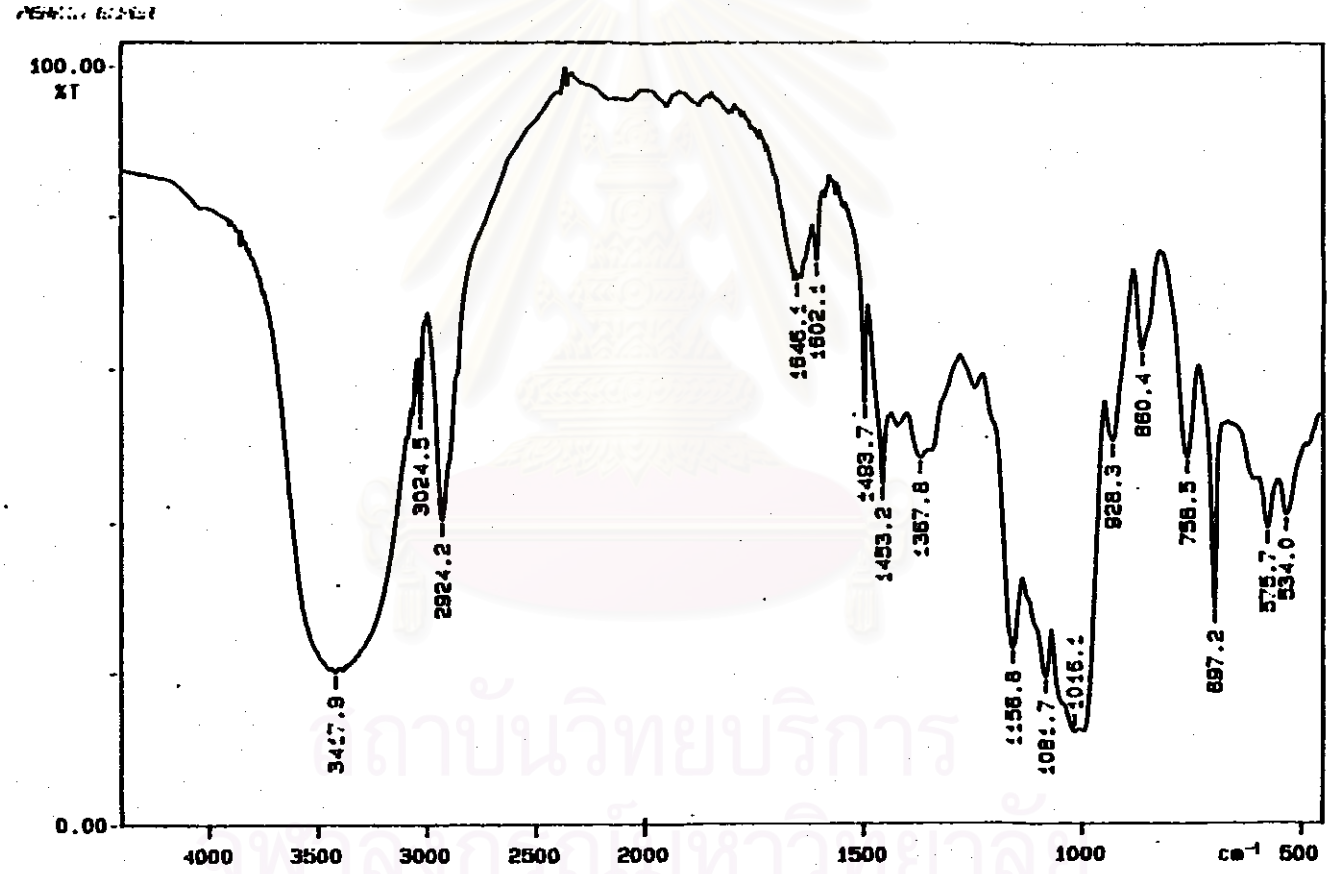

Figure 4.4 Infrared spectrum of the graft copolymer of cassava starch-*g*-polystyrene after extraction with toluene

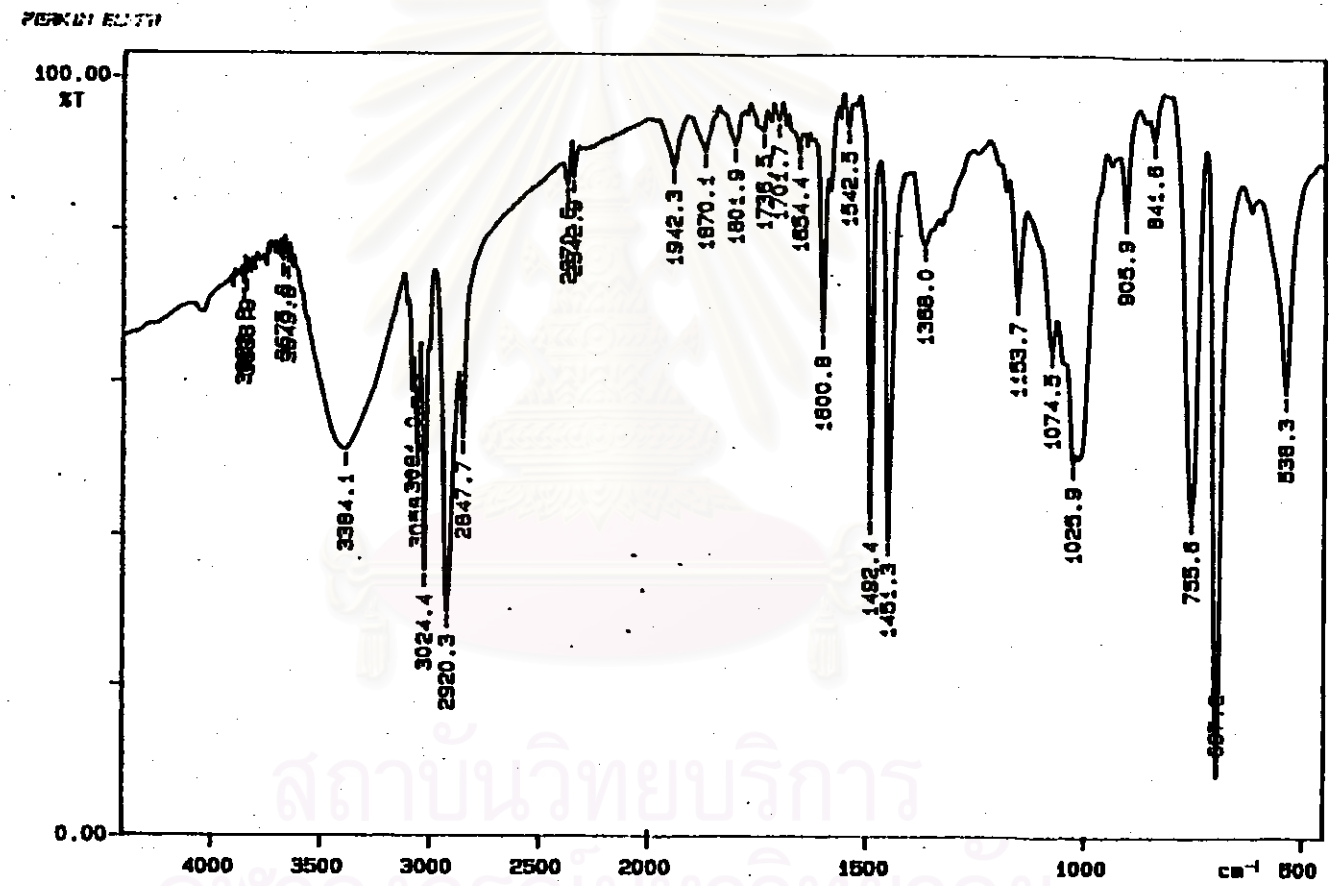

Figure 4.5 Infrared spectrum of the graft polystyrene after acid hydrolysis

4.2 Grafting of Styrene onto Cassava Starch by Simultaneous Irradiation Method

4.2.1 Effect of Total Dose on Graft Copolymerization

In this experiment, we studied the grafting of styrene with granular and gelatinized starch. When the gelatinized starch was used, the mixture of gelatinized starch and styrene tended to separate unless we stirred the mixture continuously because water, in gelatinized starch, is hydrophilic and cannot be miscible with styrene, a hydrophobic monomer. It was found that the grafting efficiency was higher with granular starch (62.6%, at total dose of 10 kGy) rather than with gelatinized starch (31.8%, at total dose of 10 kGy). Table 4.1 shows the effect of total dose on the grafting of styrene onto granular cassava starch.

Table 4.1 Effect of Total Dose (kGy) on the Grafting of Styrene onto Granular Cassava Starch

Total Dose* (kGy)	Homopolymer Formed (%)	Grafting Efficiency (%)	Grafting Ratio (%)	Conversion (%)	Percent Add-on (%)
2	13.4	16.2	8.7	2.3	8.0
4	12.6	26.2	14.8	14.1	12.9
6	11.1	41.5	23.7	17.7	19.2
8	8.1	57.5	27.6	24.2	21.7
10	7.8	62.6	35.6	38.3	25.2
12	13.8	60.2	38.4	40.7	27.3
14	18.1	57.9	39.2	42.3	28.2
16	22.1	56.3	41.8	66.0	30.1

*Starch (4 g), styrene (4 g) were blended with methanol (1.5 cm^3) and water (1 cm^3) at a fixed dose rate of 2.5 x 10^{-3} kGy/sec.

4.2.1.1 Relationship between Total Dose and Percent Homopolymer

Table 4.1 and Figure 4.6 show the correlation between the total dose and the homopolymer formed. The amount of homopolymer formed varied from

7.8 to 22.1% depending on the dose. The lowest homopolymer formed occurred at the total dose of 10 kGy and the homopolymer content increased when the total dose was higher than 10 kGy. To optimize the formation of graft copolymer with the minimum amount of the contaminating homopolymer, the yield of radicals from radiolysis of polymer (G value, starch = 10) are much greater than for the monomer (styrene = 0.69). This suggests that the higher irradiation dose gave a large amount of radiolysis product (in the absence of oxygen): $OH^{\cdot}$ and e^{-}_{aq} as $G(OH^{\cdot})$ and $G(e^{-}_{aq})$ are 2.8 and 2.7, respectively, which initiated homopolymerization rather than grafting reaction. The total irradiation dose at 10 kGy is thus just an optimum dose to generate the least amount of $OH^{\cdot}$ and e^{-}_{aq} for the chain transfer of homopolymer growing chains.

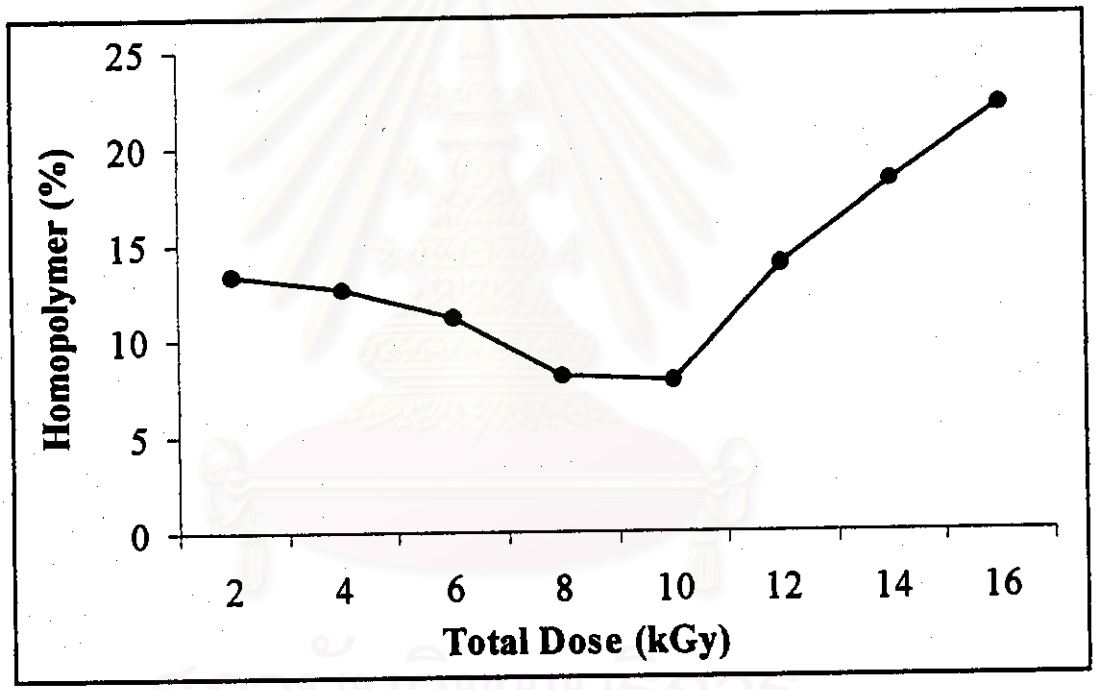

Figure 4.6 Effect of Total Dose on Percent Homopolymer

4.2.1.2 Relationship between Total Dose and Grafting Efficiency

Table 4.1 and Figure 4.7 show that the grafting efficiency is the highest at the total dose of 10 kGy. The grafting efficiency decreased with increasing the total dose of those higher than 10 kGy, and it decreased with decreasing the total dose of those lower than 10 kGy. This suggests that the decreasing grafting efficiency is due to the formation of small fragments of $OH^{\cdot}$ and e^{-}_{aq} to form homopolymer at the expense of grafting.

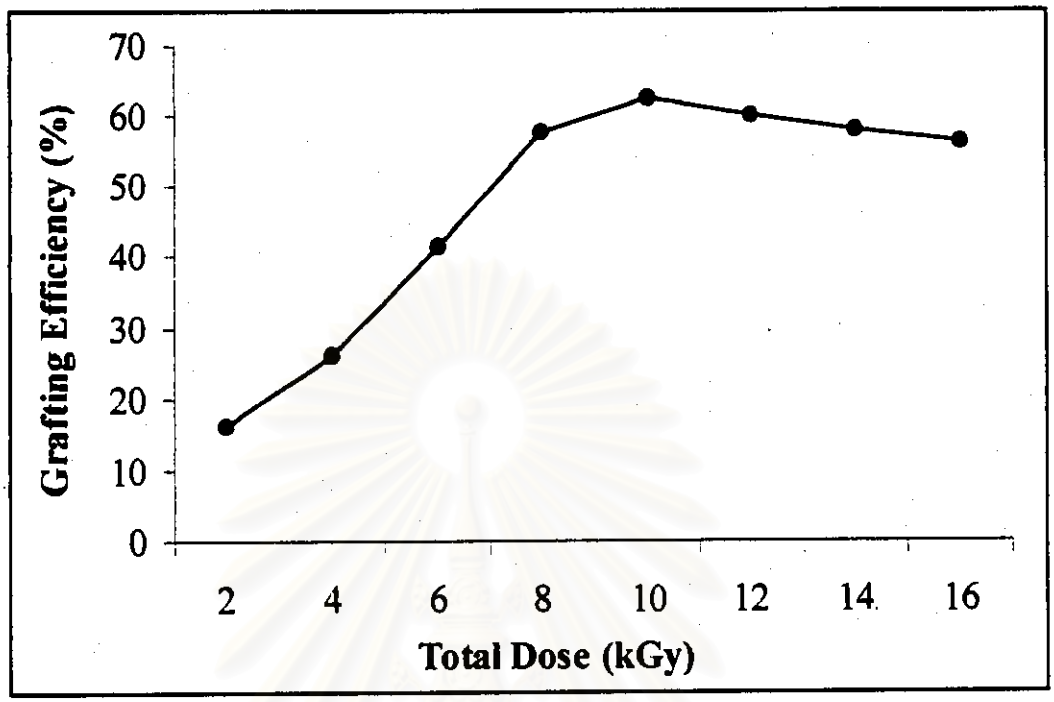

Figure 4.7 Effect of Total Dose on Grafting Efficiency

4.2.1.3 Relationship between Total Dose and Percent Conversion

Table 4.1 and Figure 4.8 show a continuous increase in percent conversion as the amount of total dose increases. An increase in the total dose enhances the formation of radicals in the reaction mixture: monomer, starch, water and methanol. All molecules are activated to induce a higher conversion for both homopolymer formation and the grafting reaction.

4.2.1.4 Relationship between Total Dose and Percent Add-on

The experimental data of the effect of the total dose on percent add-on are given in Table 4.1 and Figure 4.9. The curve indicates that after reaching a total dose at 10 kGy, the percent add-on changes slightly because of the amount of styrene added to the starch backbone decreases and a greater amount of polystyrene is formed as homopolymer at the expense of the grafting reaction.

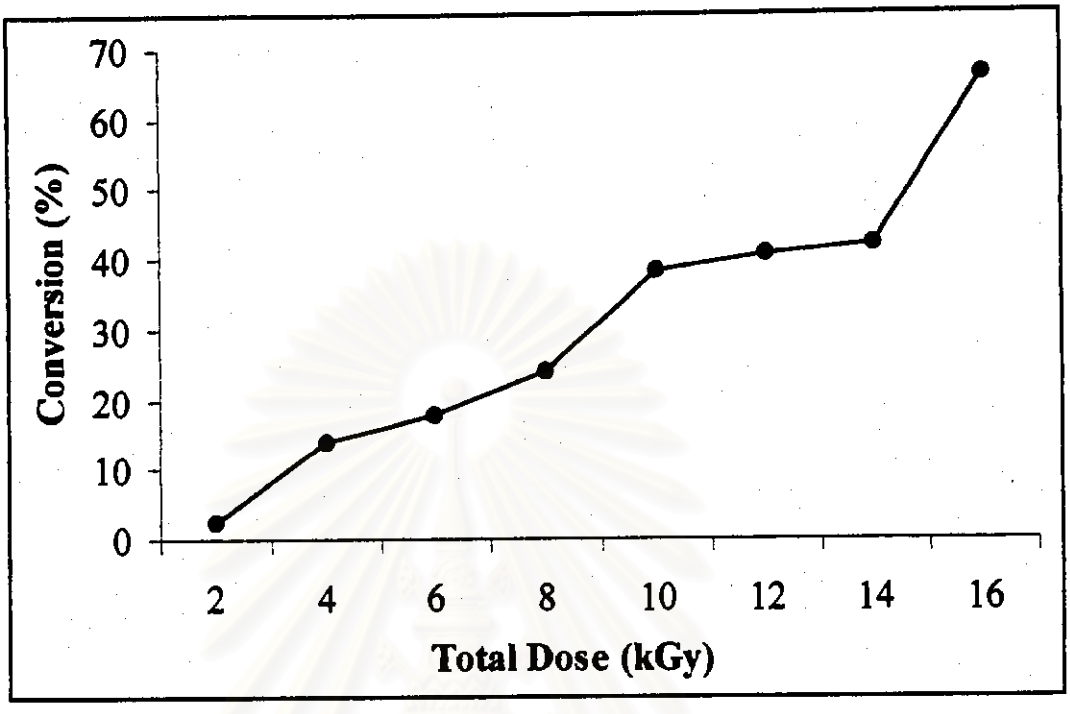

Figure 4.8 Effect of Total Dose on Percent Conversion

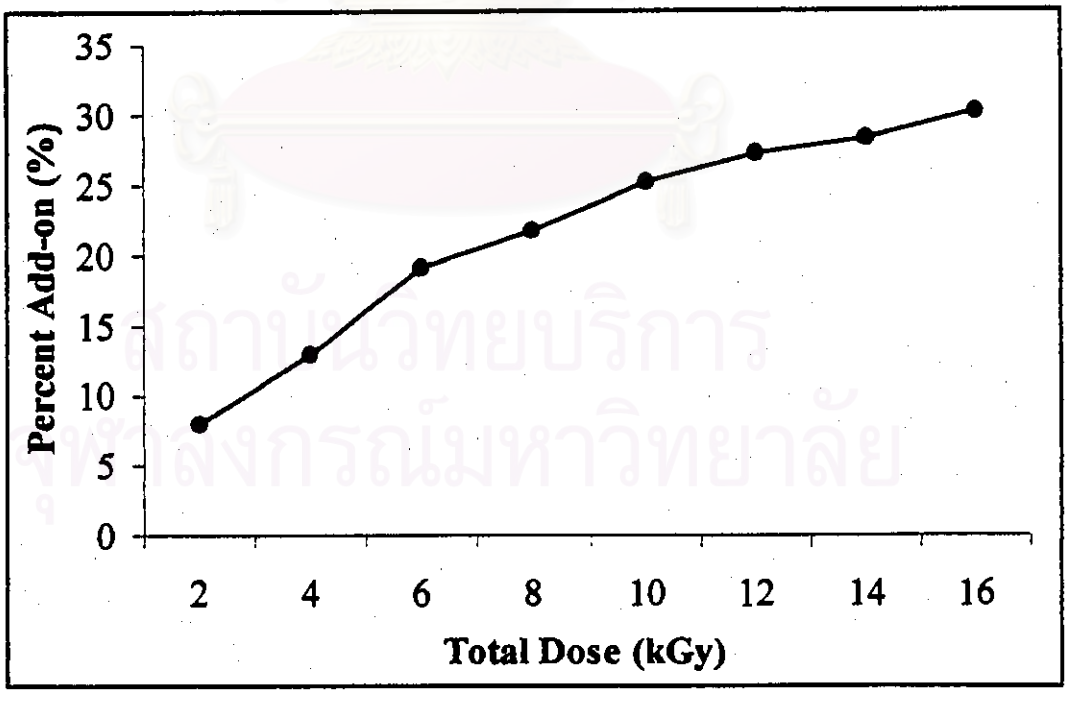

Figure 4.9 Effect of Total Dose on Percent Add-on

4.2.1.5 Relationship between Total Dose and Grafting Ratio

Table 4.1 and Figure 4.10 show the effect of total dose on grafting ratio. The results show that the ratio of the number of polystyrene in grafts to the weight of starch increased with increasing total irradiation dose. At the total dose higher than 10 kGy, radiolysis product ($G(OH^{\cdot}) = 2.8$, $G(e^{-}_{aq}) = 2.7$) induced homopolymerization rather than grafting reaction.

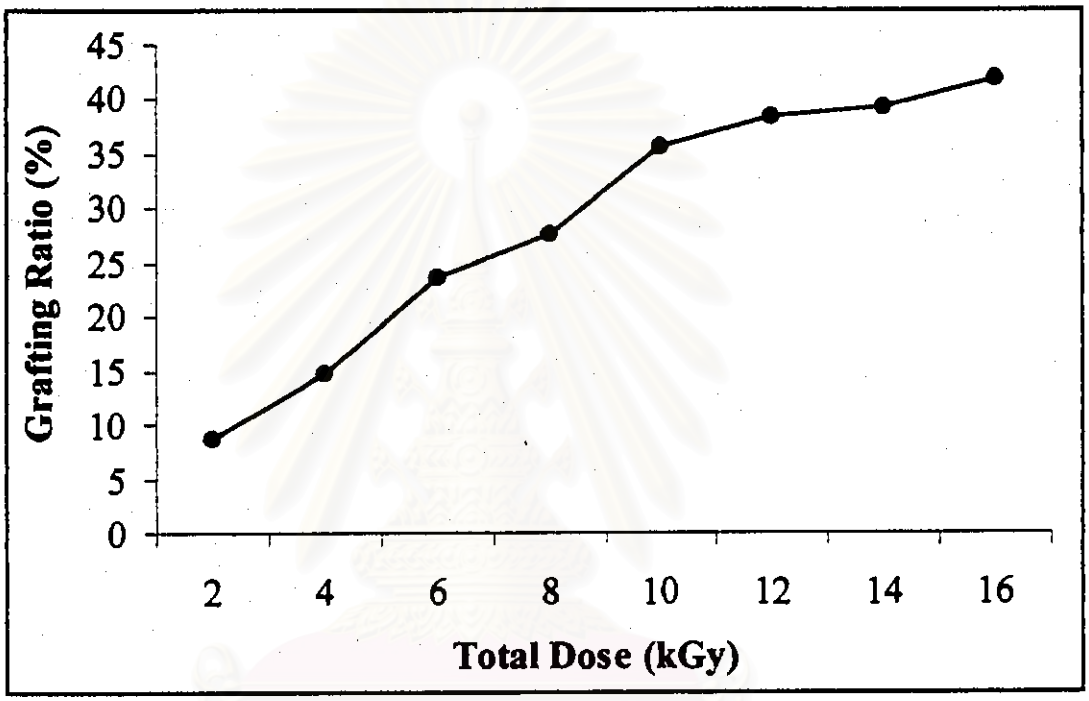

Figure 4.10 Effect of Total dose on Grafting Ratio

4.2.2 Effect of Nitric Acid on Graft Copolymerization

Table 4.2 Effect of Acid on Grafting of Styrene onto Cassava Starch

Sample	Homopolymer (%)	Grafting Efficiency (%)	Grafting Ratio (%)	Conversion (%)	Percent Add-on (%)
Without acid[a]	7.8	62.6	33.7	38.3	25.2
With Acid[b]	2.6	68.0	11.8	12.7	10.5

[a]Total dose = 10 kGy, [b]0.1 *N* HNO_3 (1 cm^3)

Table 4.2 shows the effect of nitric acid (0.1 *N*) for enhancing the grafting of styrene onto cassava starch. In acid media, the presence of H^+ ion can increase G(H·) value and increase the possibility of hydrogen radical (H·) produced by the following equations:

$$CH_3OH + H^+ \longrightarrow CH_3OH_2^+ \quad (4.1)$$

$$CH_3OH_2^+ + e^-_{aq} \longrightarrow CH_3OH + H\cdot \quad (4.2)$$

The hydrogen radical (H·) in the grafting systems, can lead to increased number of grafting sites by hydrogen abstraction reaction with starch backbone followed by increasing grafting probability [27].

$$CelloH + H\cdot \longrightarrow Cello\cdot + H_2 \quad (4.3)$$

Thus the grafting efficiency is increased and the homopolymer decreases accordingly. The conversion of monomer is decreased when an acid was used, because of the amount of acid might be too concentrate and the starch might be hydrolyzed before it can be reacted with styrene. Moisture and water exert a protective effect on starch, making it more resistant to irradiation. It is therefore suggested that more diluted nitric acid should be carried out.

4.3 The Plastic Compounding and Their Degradations

For a polymer to be degradable, the main chain with hydrolyzable groups must be present and accessible. Materials that contain an amide, urea, or ketone functional groups are susceptible to degradation such as poly(vinyl methyl ketone) can easily be degraded in sunlight. Because of the photosentivity of the carbonyl groups in the polymer chain, which will absorb photo-energy and convert this into chemical energy, thus producing free radicals which will accelerate the oxidation and chain scission. Polystyrene plastic does not contain any of the above-mentioned functional groups, it is therefore inherently non-degradable. In this research, we prepared starch-*g*-polystyrene graft copolymer, which was used with the polystyrene plastic for increasing the degradation of polystyrene plastic.

4.3.1 Effect of Starch and Graft Copolymer Content on Mechanical Properties of Polystyrene Plastics

The tensile strength and elongation at break of PS, PS-starch-graft copolymer (PS-S5-G5/1-9 and PS-S5-G10/10-18), PS-starch (PS-S15/19-27) and PS-graft copolymer (PS-G15/28-36) are shown in Table 4.3.

Table 4.3 Tensile properties of PS and composite PS sheets at various contents of soya oil and zinc stearate

Samples	Tensile Strength (MPa)	Elongation at Break (%)
PS	43.0	5
PS-S5-G5/1	31.2	4
PS-S5-G5/2	30.0	4
PS-S5-G5/3	27.6	4
PS-S5-G5/4	30.2	4
PS-S5-G5/5	28.4	4
PS-S5-G5/6	26.0	4
PS-S5-G5/7	29.7	4
PS-S5-G5/8	27.9	4
PS-S5-G5/9	24.6	4
PS-S5-G10/10	23.7	4
PS-S5-G10/11	22.1	3
PS-S5-G10/12	20.1	3
PS-S5-G10/13	22.0	3
PS-S5-G10/14	21.7	3
PS-S5-G10/15	20.0	3
PS-S5-G10/16	20.2	3
PS-S5-G10/17	19.2	3
PS-S5-G10/18	18.2	3

Table 4.3 (continued)

Samples	Tensile Strength (MPa)	Elongation at Break (%)
PS-S15/19	26.4	4
PS-S15/20	25.4	4
PS-S15/21	23.2	4
PS-S15/22	25.8	4
PS-S15/23	24.7	4
PS-S15/24	22.4	3
PS-S15/25	24.9	4
PS-S15/26	23.7	4
PS-S15/27	21.0	3
PS-G15/28	20.2	3
PS-G15/29	20.1	3
PS-G15/30	20.0	3
PS-G15/31	20.0	3
PS-G15/32	20.1	3
PS-G15/33	20.2	2
PS-G15/34	20.0	3
PS-G15/35	20.1	2
PS-G15/36	20.0	2

From Table 4.3, for PS sheet without cassava starch and graft copolymer, the tensile strength was 43.0 MPa and elongation at break was 5%. At the same starch content, it is found that tensile strength and elongation at break decrease with increasing graft copolymer content (PS-S5-G10 < PS-S5-G5). For PS-G15 sheets, the tensile strength and elongation at break are always lower than PS-S15 sheets (PS-G15 < PS-S15). The decrease in tensile strength of starch and grafted starch filled polystyrene could be cause by the presence of moisture (water) in the composites. The composites containing the graft copolymers (starch grafted polystyrenes) always have the lower tensile strengths. Water in the polymer matrix behaves as an external plasticizer to reduce tensile strength. The results may indicate that incorporation of

starch and starch-*g*-polystyrene in the presence of Epolene wax, a dispersing agent, cannot be well misible (wetting) with polystyrene. As known to the starch researchers, the mechanical degradation of dispersed starch was due to severance of the secondary bonds in the crystalline regions, and prolonged milling also causes some thinning presumably by cleavage of the glucosidic bonds. This explanation might possibly be the attribute to the decrease in tensile strength besides the suspected filler-polymer miscibility. From Figures 4.11 through 4.12, it is found that the amounts of zinc stearate and soya oil do not impose the significant effect on mechanical properties of the plastic sheets.

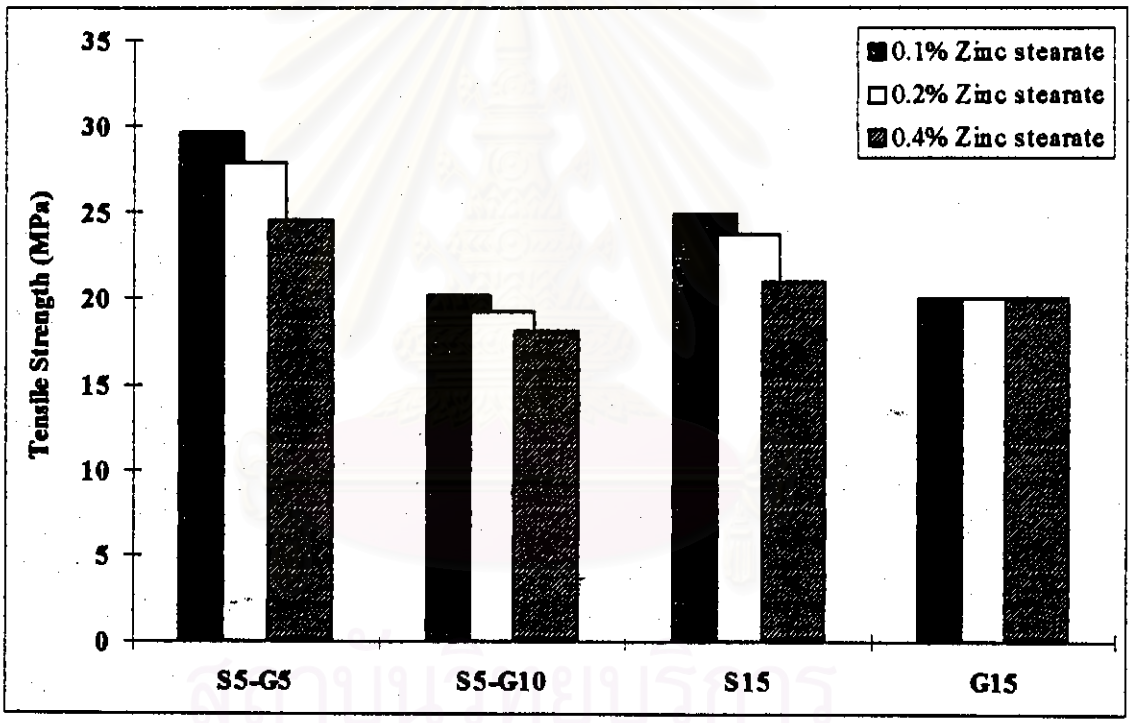

Figure 4.11 Effect of zinc stearate content on tensile strength of control composite PS sheets at 8% soya oil.

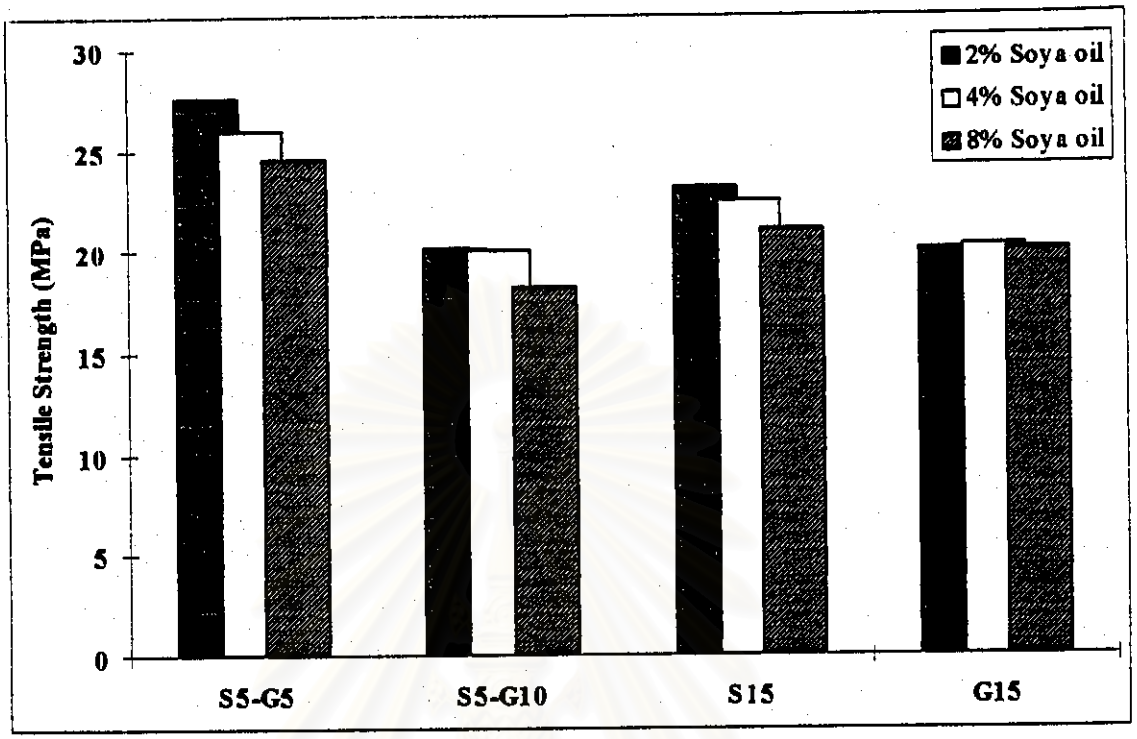

Figure 4.12 Effect of soya oil content on tensile strength of control composite PS sheets at 0.4% zinc stearate.

4.3.2 Sample Natural Exposure Test

The activities of cassava starch, graft copolymer and zinc stearate in PS degradation were studied by outdoor exposure. The environmental degradation of composite PS sheets were studied up to 6 months of outdoor exposure. The average temperature, humidity, rainfall and solar radiation are shown in Figures 3.2 and 3.3. For the effect of sunlight on mechanical properties of PS and composite PS sheets, the plastic samples were mounted on racks and tested for 6 months. The plastic samples were removed every month, after removal, it was found that the color of plastic samples becomes yellow, indicating the formation of conjugated double bonds in the polymer chain. The degradation of PS and composite PS sheets were measured by tensile property, molecular weight, infrared spectra and thermal stability.

4.3.2.1 Tensile Property Measurements

The samples were collected, at an interval of 2 weeks for the first two months and of 4 weeks afterwards, for the mechanical testing. According to the ASTM D638, tensile strength was measured by LLOYD tensile tester model LR 100K with a cross head speed of 100 mm/min. The thickness of test specimens was 1.0 mm with a gauge length of 50 mm. An average of five specimens was reported as a representative value. A typical study of the effect of UV exposure on the tensile strength of both unexposed and exposed PS and composite PS sheets is shown in Table 4.4 and Figures 4.13 through 4.16.

From Table 4.4, tensile strength of the PS sheet shows a gradual decrease after outdoor exposure. An initial tensile strength of PS sheet was 43.0 MPa and elongation at break was 5%; after 6-month exposure, tensile strength of PS sheet was 30.8 MPa and elongation at break was 3%. From Figure 4.17, it was found that the behavior of composite PS sheets (PS-S5-G5, PS-S5-G10, PS-S15, PS-G15) differs from PS sheet. Tensile strength and elongation at break decrease rapidly after 6-month exposure. Particularly, the tensile strength and elongation at break of PS-G15 sheet decrease sharply and then approach a zero value after 6-month outdoor exposure. The decrease in mechanical strength of PS-G15 sheet after 6-month exposure can be caused by the starch-*g*-polystyrene embedded in the PS matrix, which can easily absorb moisture in atmosphere and decreased the tensile strength of the PS-G15 sheet as described.

Table 4.4 Tensile properties of PS and composite PS sheets during outdoor exposure

a) Tensile strength (MPa)

Sample	Tensile Strength of Sample Exposure Time								
	Control	2 weeks	1 month	6 weeks	2 months	3 months	4 months	5 months	6 months
PS	43.0	41.1	40.8	39.3	38.3	36.2	35.0	32.7	30.8
PS-S5-G5/1	31.2	29.8	22.9	20.4	19.7	18.0	17.6	17.0	16.2
PS-S5-G5/2	30.0	28.2	25.9	23.7	20.1	18.8	16.9	15.2	15.0
PS-S5-G5/3	27.6	25.9	22.1	20.4	19.0	18.2	17.0	16.9	14.8
PS-S5-G5/4	30.2	29.0	25.1	23.0	22.3	20.0	16.9	15.2	14.6
PS-S5-G5/5	28.4	26.9	24.6	22.6	20.6	18.6	16.7	15.5	13.8
PS-S5-G5/6	26.0	24.9	22.2	20.6	18.4	16.2	15.9	14.8	13.6
PS-S5-G5/7	29.7	27.6	25.1	23.2	20.2	18.6	16.8	15.0	13.5
PS-S5-G5/8	27.9	26.0	24.5	20.3	18.4	17.0	16.6	14.3	13.3
PS-S5-G5/9	24.6	22.8	20.1	19.1	17.3	15.6	14.0	13.0	12.0
PS-S5-G10/10	23.7	22.2	17.3	12.6	11.0	10.5	8.3	7.9	6.6
PS-S5-G10/11	22.1	21.0	14.4	11.3	9.7	9.3	7.8	6.4	5.5
PS-S5-G10/12	20.1	19.8	13.3	10.6	8.6	8.5	6.5	5.8	4.0
PS-S5-G10/13	22.0	20.3	16.5	11.1	9.0	9.0	7.8	6.5	5.2
PS-S5-G10/14	21.7	19.7	13.4	10.2	7.4	7.2	6.2	5.8	4.4
PS-S5-G10/15	20.0	18.5	10.2	9.0	6.8	6.5	6.0	4.0	3.7
PS-S5-G10/16	20.2	19.8	14.8	10.1	8.7	8.3	6.1	5.6	4.1
PS-S5-G10/17	19.2	18.8	11.1	9.9	6.3	6.0	5.4	4.4	3.2
PS-S5-G10/18	18.2	17.8	7.7	6.5	5.4	5.1	4.0	3.2	2.2
PS-S15/19	26.4	24.6	22.3	17.1	13.5	11.9	11.4	10.6	9.4
PS-S15/20	25.4	23.7	17.9	15.2	11.8	10.2	9.9	8.6	7.5
PS-S15/21	23.2	20.4	15.9	13.1	11.5	10.2	9.9	8.0	7.0
PS-S15/22	25.8	24.3	20.6	15.6	11.7	9.7	8.8	8.0	7.2
PS-S15/23	24.7	22.5	15.5	13.2	11.1	8.6	7.6	6.8	6.2
PS-S15/24	22.4	20.1	14.1	12.9	11.0	8.2	7.1	6.2	5.9
PS-S15/25	24.9	22.2	17.4	15.3	11.7	9.6	7.6	6.6	6.3
PS-S15/26	23.7	21.6	14.9	13.3	10.8	8.2	6.7	5.9	5.0
PS-S15/27	21.0	18.9	12.1	10.9	9.1	6.6	5.7	4.3	3.7
PS-G15/28	20.2	15.5	13.0	11.2	10.1	9.5	7.6	6.4	3.2
PS-G15/29	20.1	12.3	11.2	8.8	7.4	6.6	5.4	4.3	2.8
PS-G15/30	20.0	9.8	6.4	5.6	5.4	5.0	4.5	3.4	2.6
PS-G15/31	20.0	14.1	12.3	11.1	9.2	7.1	5.3	4.2	2.4
PS-G15/32	20.1	10.8	8.6	7.2	6.8	6.0	5.5	4.1	2.2
PS-G15/33	20.2	8.6	5.8	5.4	5.3	4.5	4.2	3.3	2.6
PS-G15/34	20.0	13.8	10.9	9.0	6.3	5.6	3.6	2.7	2.4
PS-G15/35	20.1	8.9	7.1	4.2	4.1	3.1	2.4	2.2	2.0
PS-G15/36	20.0	15.8	5.0	3.6	3.1	2.1	2.0	1.1	0.0

Table 4.4 (continued)

b) Elongation at break (%)

Sample	Tensile Strength of Sample Exposure Time								
	Control	2 weeks	1 month	6 weeks	2 months	3 months	4 months	5 months	6 months
PS	5	5	5	4	4	4	3	3	3
PS-S5-G5/1	4	4	4	3	3	3	3	2	2
PS-S5-G5/2	4	4	3	3	3	3	2	2	2
PS-S5-G5/3	4	4	3	3	3	2	2	2	2
PS-S5-G5/4	4	4	3	3	3	3	3	2	2
PS-S5-G5/5	4	4	3	3	2	2	2	2	2
PS-S5-G5/6	4	4	3	2	2	2	2	2	2
PS-S5-G5/7	4	4	3	3	3	3	2	2	2
PS-S5-G5/8	4	4	3	3	2	2	2	2	2
PS-S5-G5/9	4	4	3	2	2	2	2	2	2
PS-S5-G10/10	4	4	3	3	3	3	2	2	2
PS-S5-G10/11	3	3	3	3	3	2	2	2	2
PS-S5-G10/12	3	3	3	3	3	2	2	2	2
PS-S5-G10/13	3	3	3	3	3	3	2	2	2
PS-S5-G10/14	3	3	3	3	2	2	2	2	2
PS-S5-G10/15	3	3	3	2	2	2	2	2	2
PS-S5-G10/16	3	3	3	2	2	2	2	2	2
PS-S5-G10/17	3	3	3	2	2	2	2	2	2
PS-S5-G10/18	3	3	3	2	2	2	2	2	1
PS-S15/19	4	4	4	3	3	3	3	2	2
PS-S15/20	4	4	3	3	3	3	3	2	2
PS-S15/21	4	3	3	3	2	2	2	2	2
PS-S15/22	4	4	3	3	2	3	2	2	2
PS-S15/23	4	4	3	3	2	2	2	2	2
PS-S15/24	3	3	3	2	2	2	2	2	2
PS-S15/25	4	4	3	3	3	2	2	2	2
PS-S15/26	4	3	3	2	2	2	2	2	2
PS-S15/27	3	3	3	2	2	2	2	2	2
PS-G15/28	3	3	3	3	3	2	2	2	2
PS-G15/29	3	3	3	3	3	2	2	2	2
PS-G15/30	3	2	2	2	2	2	2	2	2
PS-G15/31	3	3	3	2	2	2	2	2	2
PS-G15/32	3	3	3	2	2	2	2	2	2
PS-G15/33	2	2	2	2	2	2	2	2	1
PS-G15/34	3	2	2	2	2	2	2	2	1
PS-G15/35	2	2	2	2	2	2	1	1	1
PS-G15/36	2	2	2	2	2	2	1	1	0

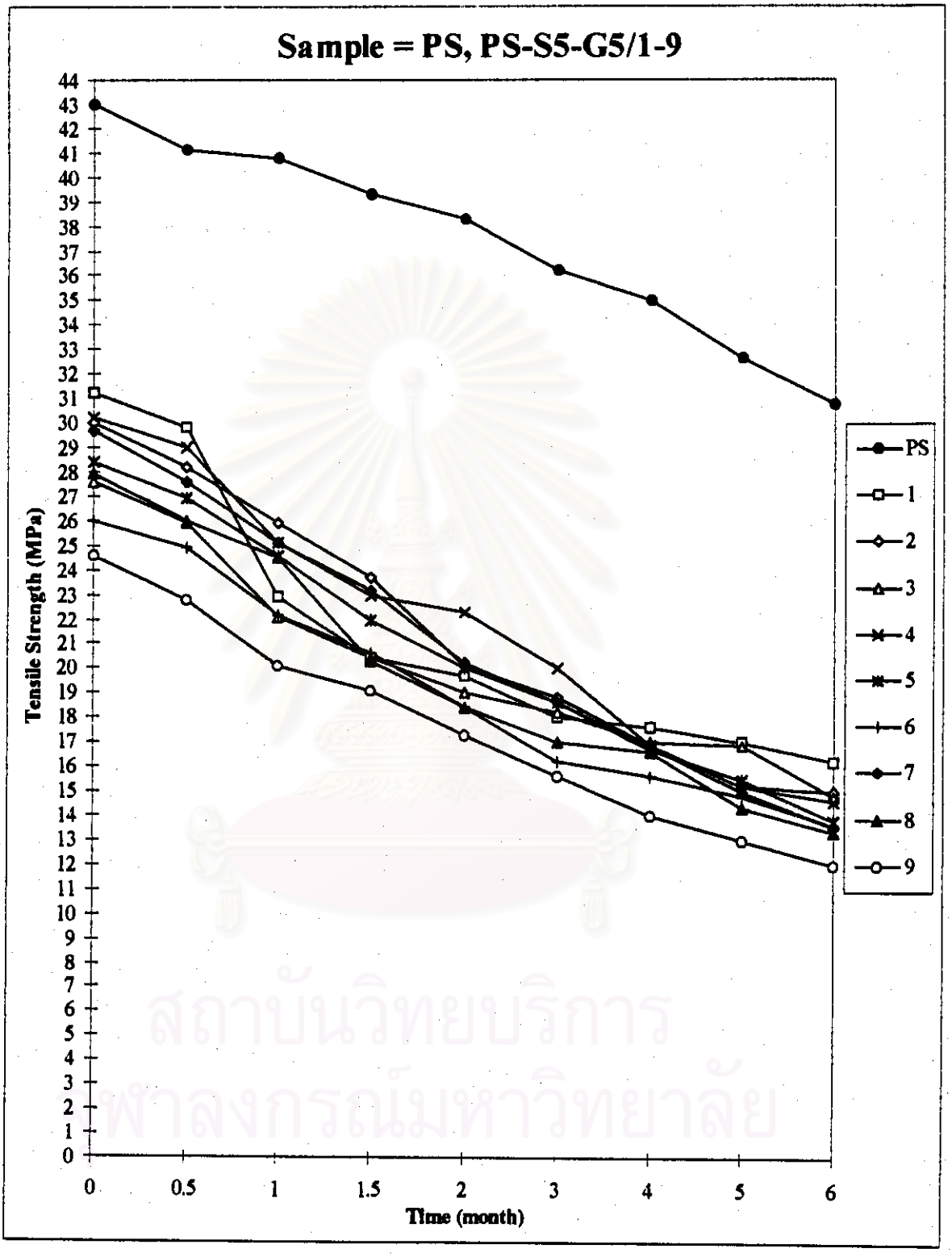

Figure 4.13 Tensile strength of PS and PS-S5-G5/1-9 sheets during outdoor exposure

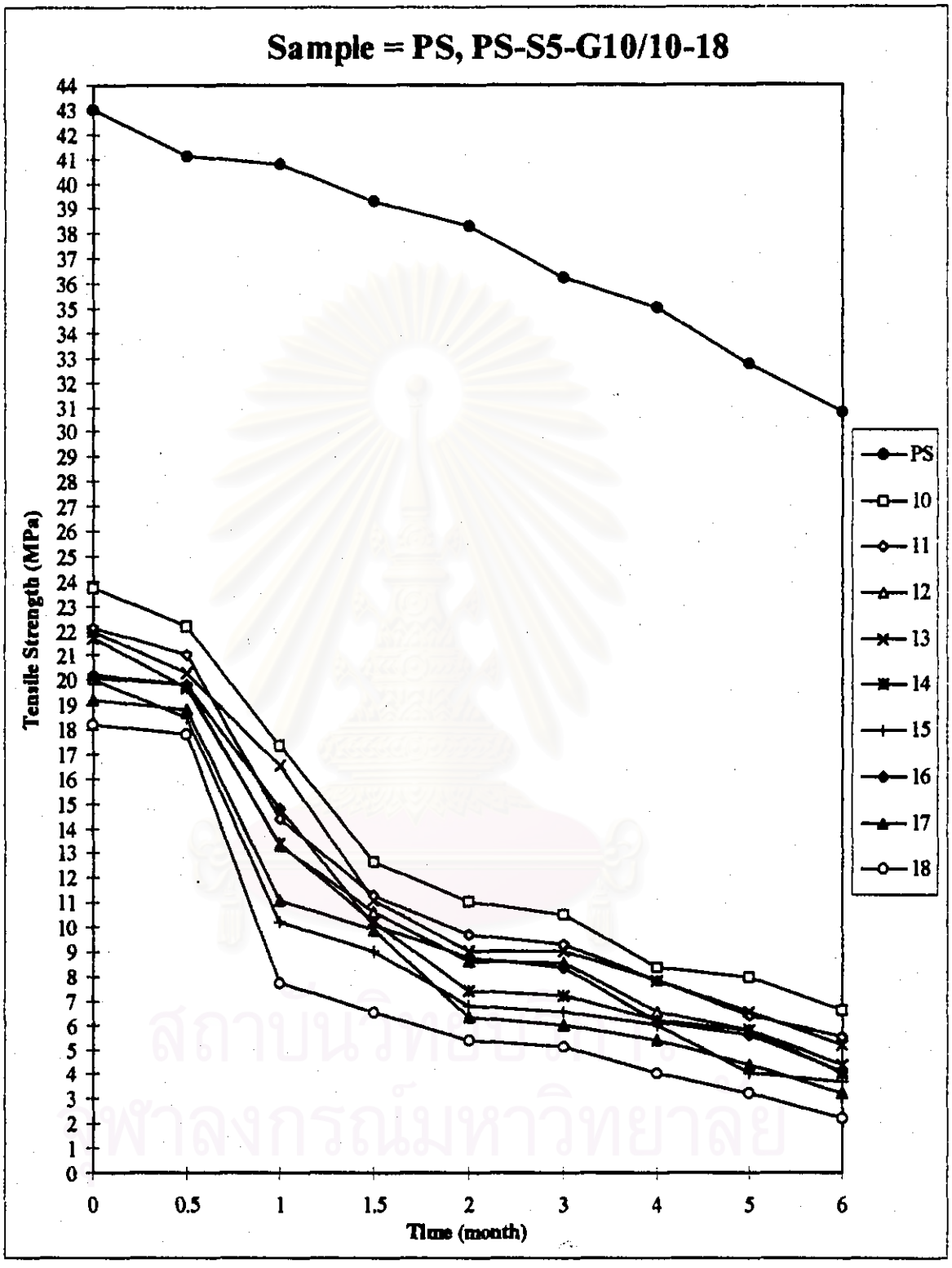

Figure 4.14 Tensile strength of PS and PS-S5-G10/10-18 sheets during outdoor exposure

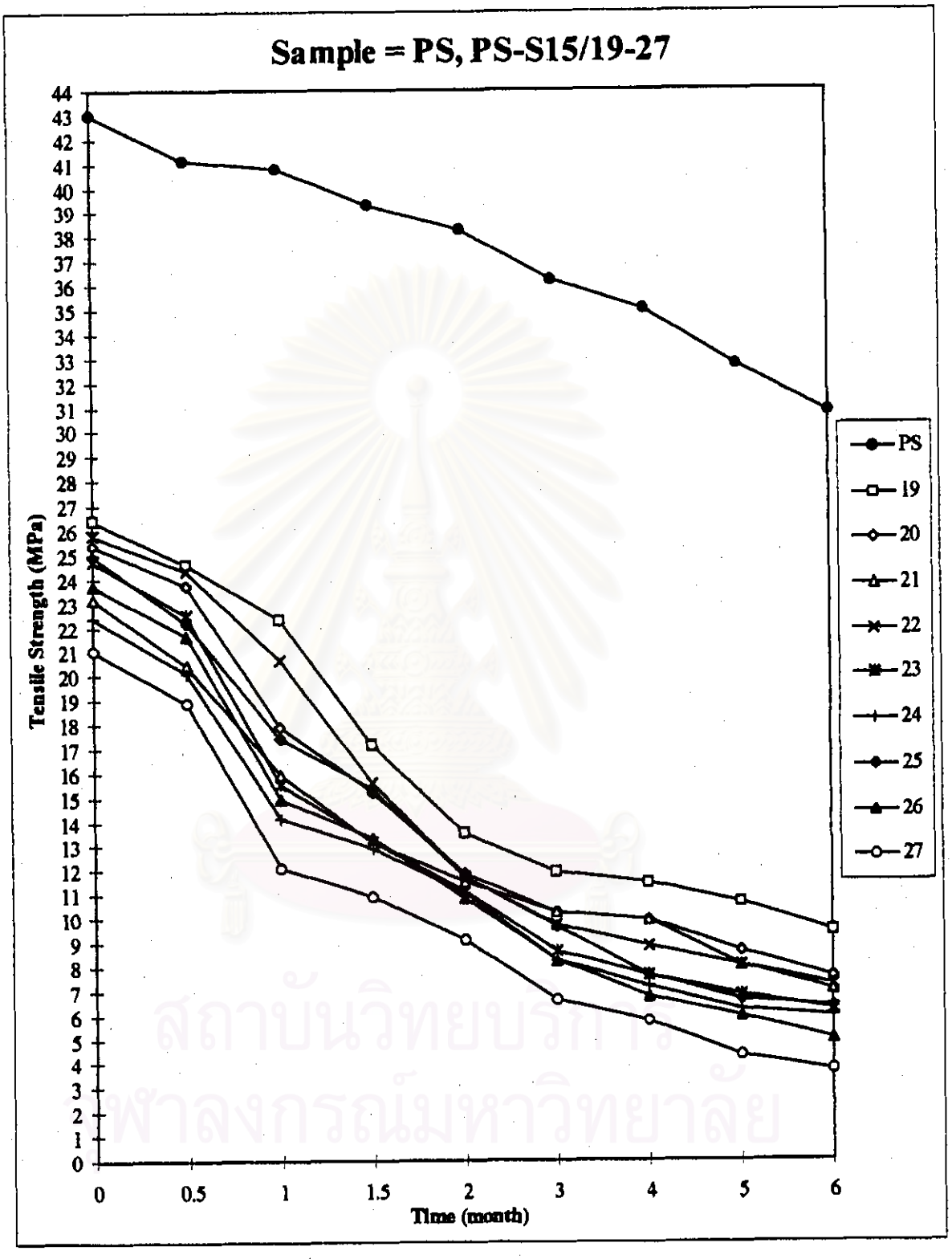

Figure 4.15 Tensile strength of PS and PS-S15/19-27 sheets during outdoor exposure

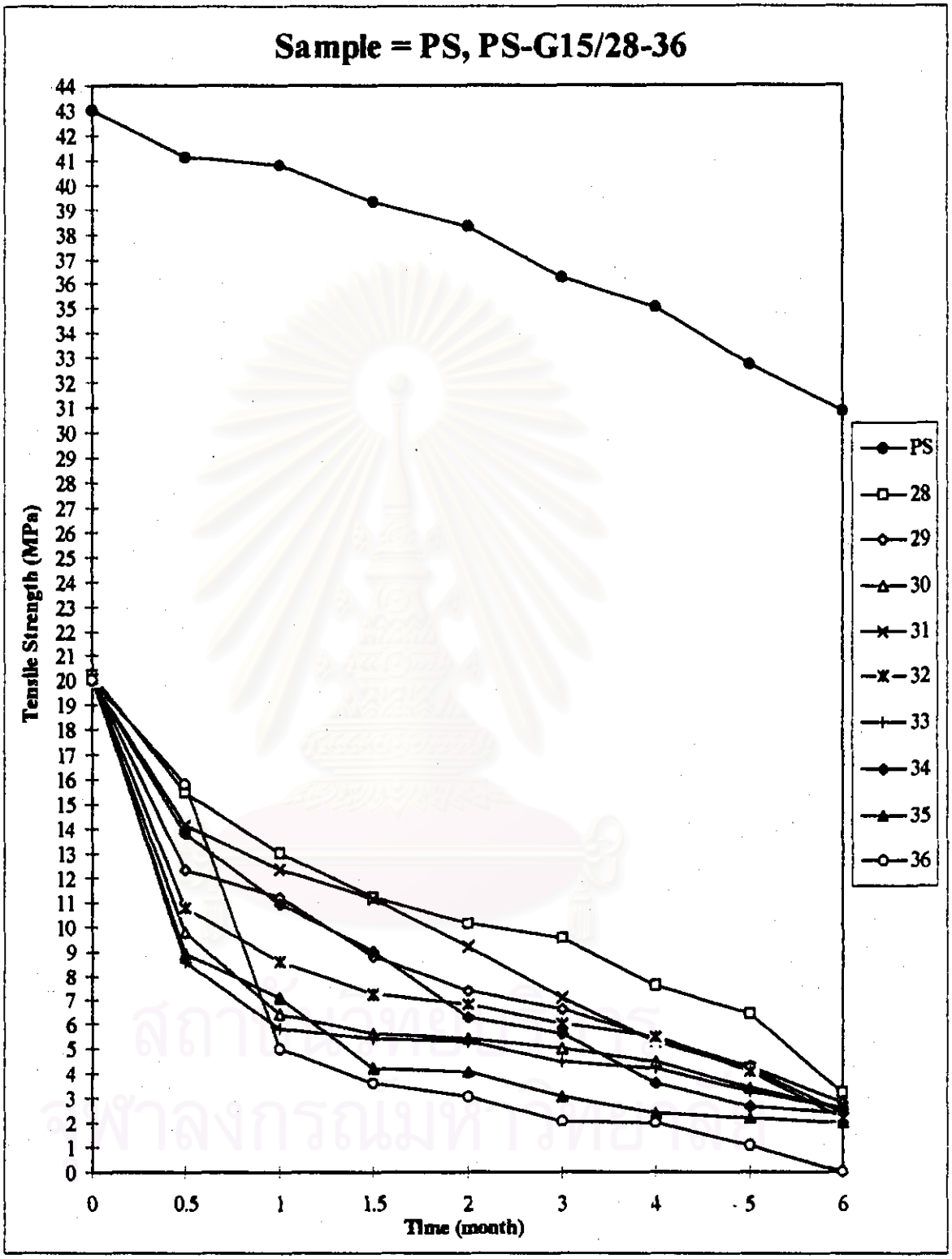

Figure 4.16 Tensile strength of PS and PS-G15/28-36 sheets during outdoor exposure

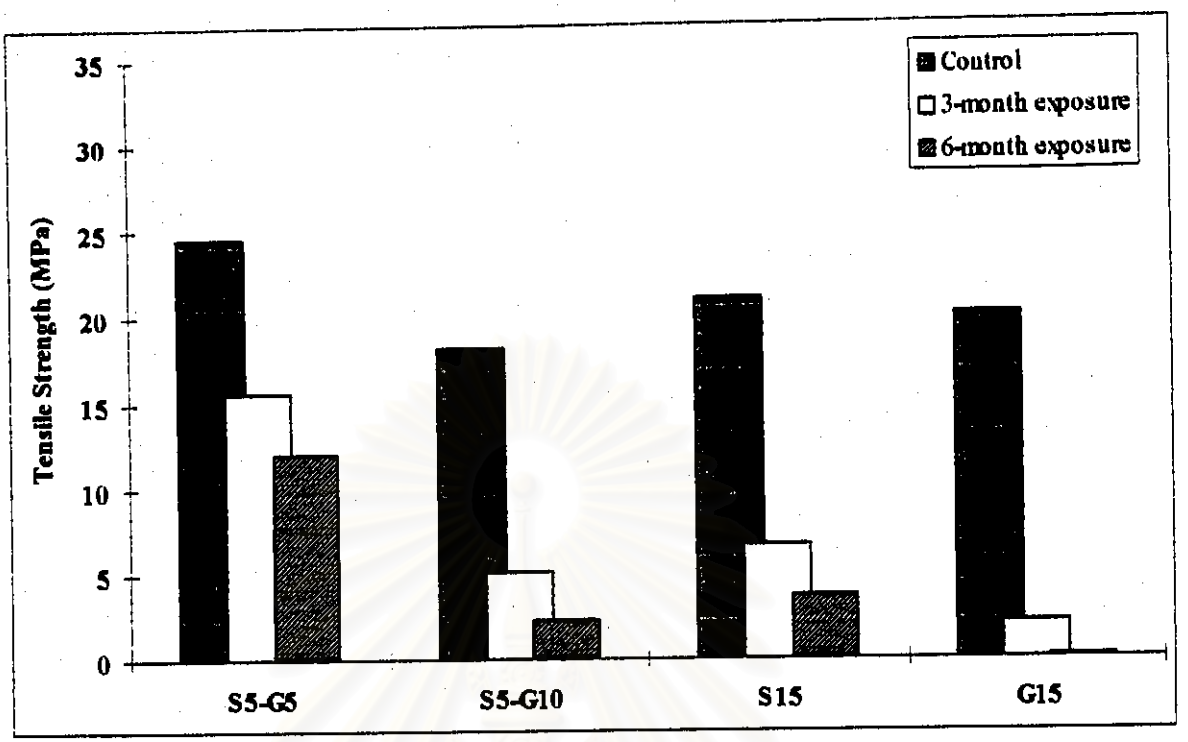

Figure 4.17 Effect of starch and graft copolymer content on tensile strength of composite PS sheets at 8% of soya oil and 0.4% of zinc stearate

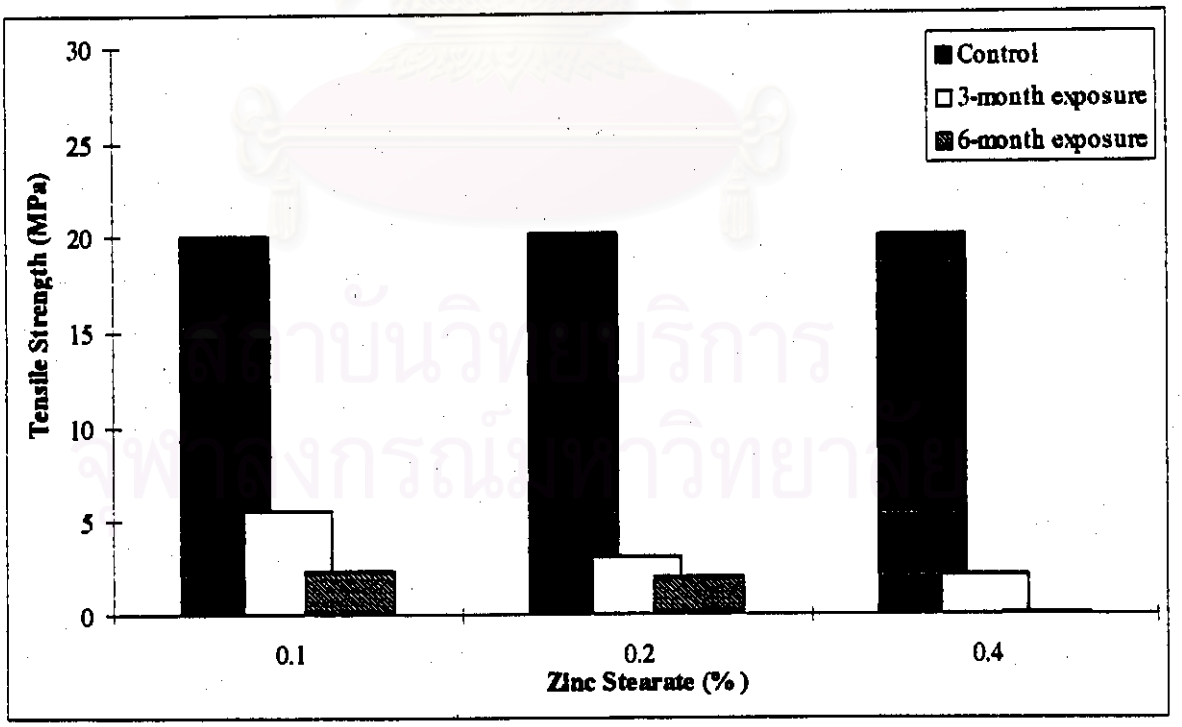

Figure 4.18 Effect of zinc stearate content on tensile strength of PS-G15 sheets at 8% of soya oil

From Figure 4.18, it was found that the content of zinc stearate has significant effect on tensile strength of PS-G15 sheets at outdoor exposure. The tensile strength of PS-G15 sheets shows a gradual decrease with exposure time, particularly, the tensile strength of PS-G15 sheet containing 0.4% of zinc stearate decreases sharply and then approach a zero after 6-month outdoor exposure. These can be explained that the zinc stearate acts as a prooxidant to catalyze the oxidation degradation.

The indoor exposure of PS and composite PS sheets are also conducted as blank samples for a comparison with the outdoor exposure. The tensile properties of the PS and composite PS sheets during indoor exposure are shown in Table 4.5 and Figure 4.19.

Table 4.5 Tensile properties of PS and composite PS sheets during indoor exposure

a) Tensile strength (MPa)

Sample	Control	2 months	4 months	6 months
PS	43.0	43.0	43.0	43.0
PS-S5-G5/9*	24.6	24.5	24.5	24.5
PS-S5-G10/18*	18.2	18.2	18.2	18.1
PS-S15/27*	21.0	21.0	21.0	21.0
PS-G15/36*	20.0	20.0	19.8	19.8

* all composite contain 0.4% w/w of zinc stearate

b) Elongation at break (%)

Sample	Control	2 months	4 months	6 months
PS	5	5	5	5
PS-S5-G5/9	4	4	4	4
PS-S5-G10/18	3	3	3	3
PS-S15/27	3	3	3	3
PS-G15/36	2	2	2	2

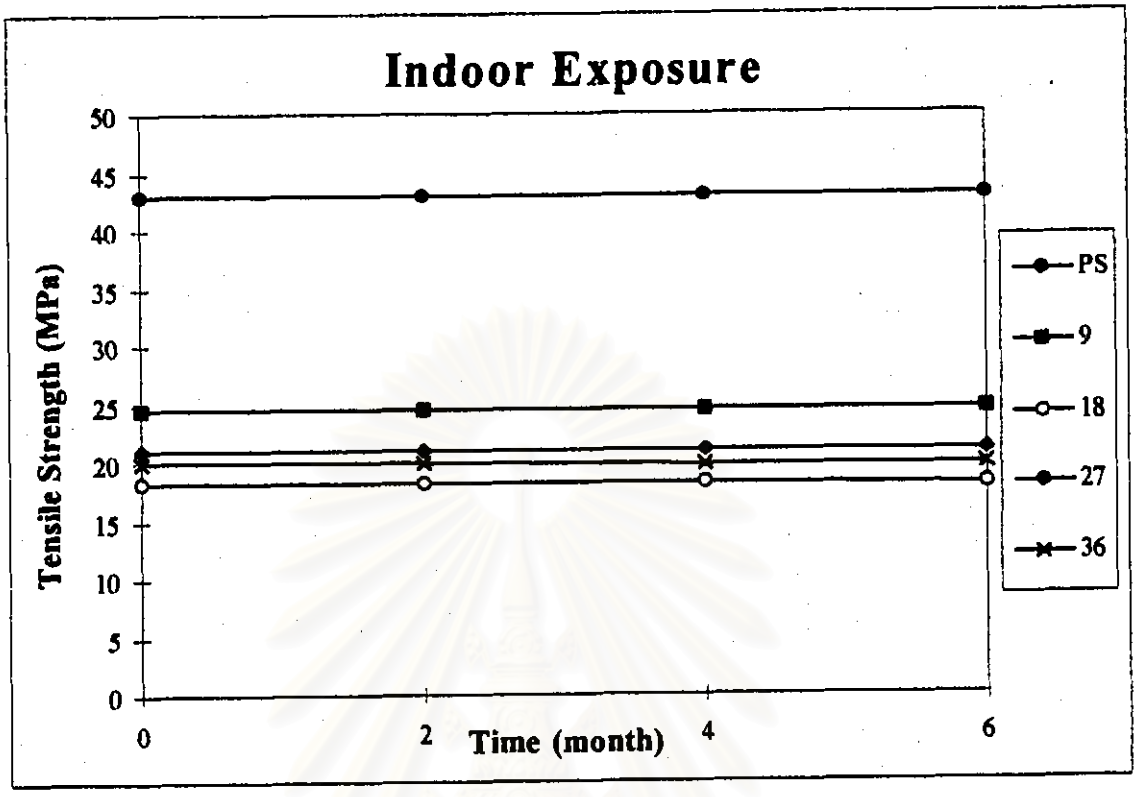

Figure 4.19 Tensile strength of PS and composite PS sheets during indoor exposure

It can be seen that the tensile properties of all samples change slightly or even do not change at all for indoor exposure. Therefore, it will take a long time for the degradation of composite PS sheets to take place when they are kept indoor. The indoor exposure is similar to a shelf life evaluation of the PS sheets. Therefore, we can state that all the PS sheets no matter they are incorporated by starch or starch grafted-derivatives, they functions well indoor. Studies on the photodegradation of polystyrene are important to develop methods to prevent photodegradation indoor and simultaneously to enhance photodegradation outdoor when they become waste or as litter.

4.3.2.2 Fourier Transform Infrared Absorption Measurements

The FTIR absorption spectra of the PS sheets were recorded on an FTIR spectrophotometer (Perkin-Elmer model 1760) that are used as a tool for estimating the changes in the carbonyl group C=O, in the chain at 1743 cm^{-1}. The polystyrene band at 1451 cm^{-1} served as an interval standard to which the absorbances of the other bands were related. The results were expressed by the carbonyl index defined as follows:

$$I_{co} = A_{1743} / A_{1451} \quad (4.4)$$

Where

I_{co} = Carbonyl index

A_{1743} = Absorbance of the carbonyl group at 1743 cm^{-1}

A_{1451} = Internal standard band in the PS backbone chain at 1451 cm^{-1}

The FTIR spectra of the PS and PS-G15/36 sheets reveal the formation of carbonyl group, which is identified as the ketone functionality (1742-1745 cm^{-1}), are given in Figures 4.20 through 4.25. The carbonyl indexes of the samples are shown in Table 4.6 and Figure 4.26.

Table 4.6 Changes in the carbonyl indexes of PS and PS-G15/36 sheets during control, 3 and 6-month outdoor exposure

Samples Exposure Time	Carbonyl Index (I_{co})	
	PS	PS-G15/36
Control	0.41	0.27
3 months	0.51	0.78
6 months	0.63	0.98

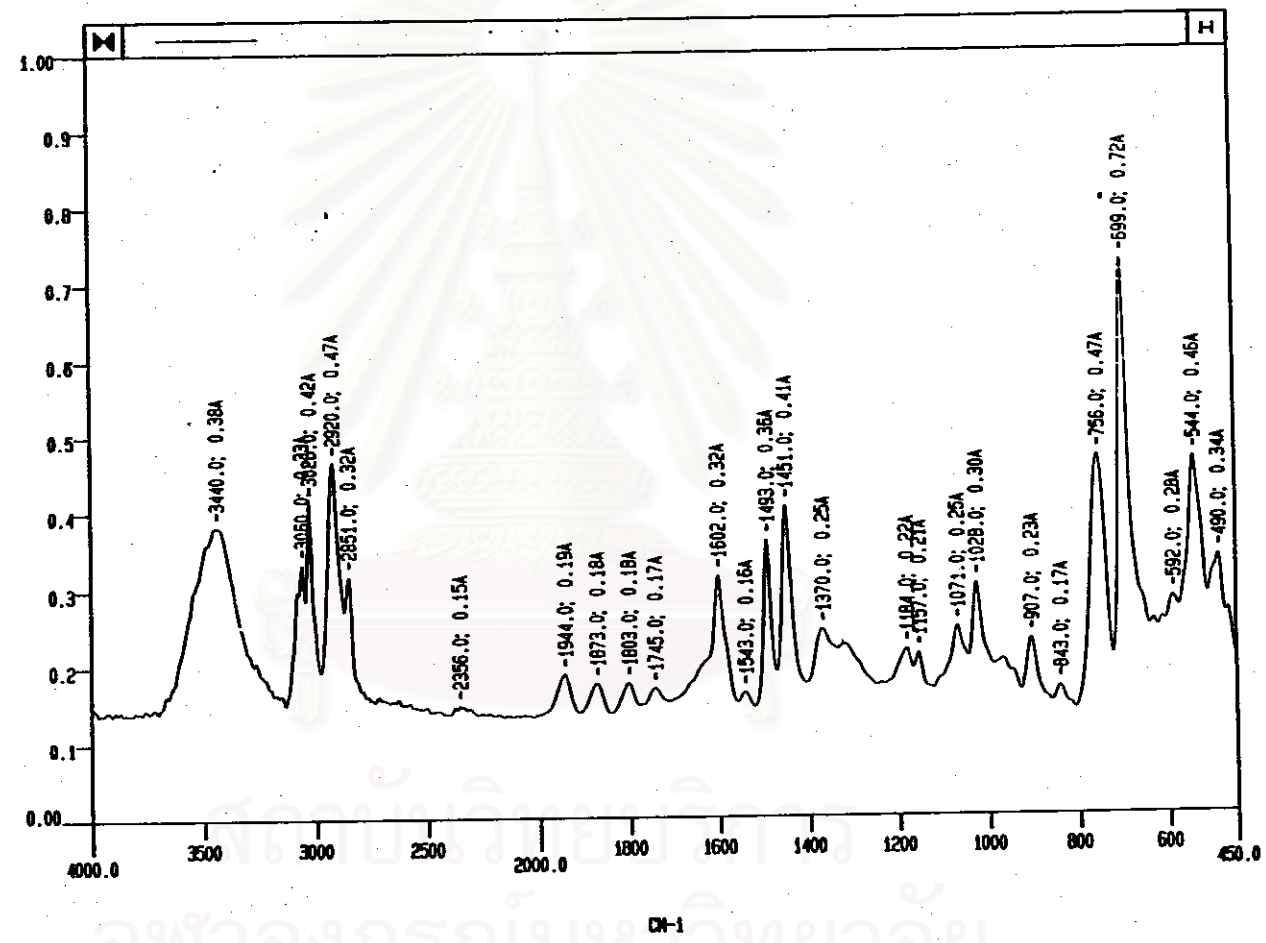

Figure 4.20 Infrared spectrum of Control PS sheet

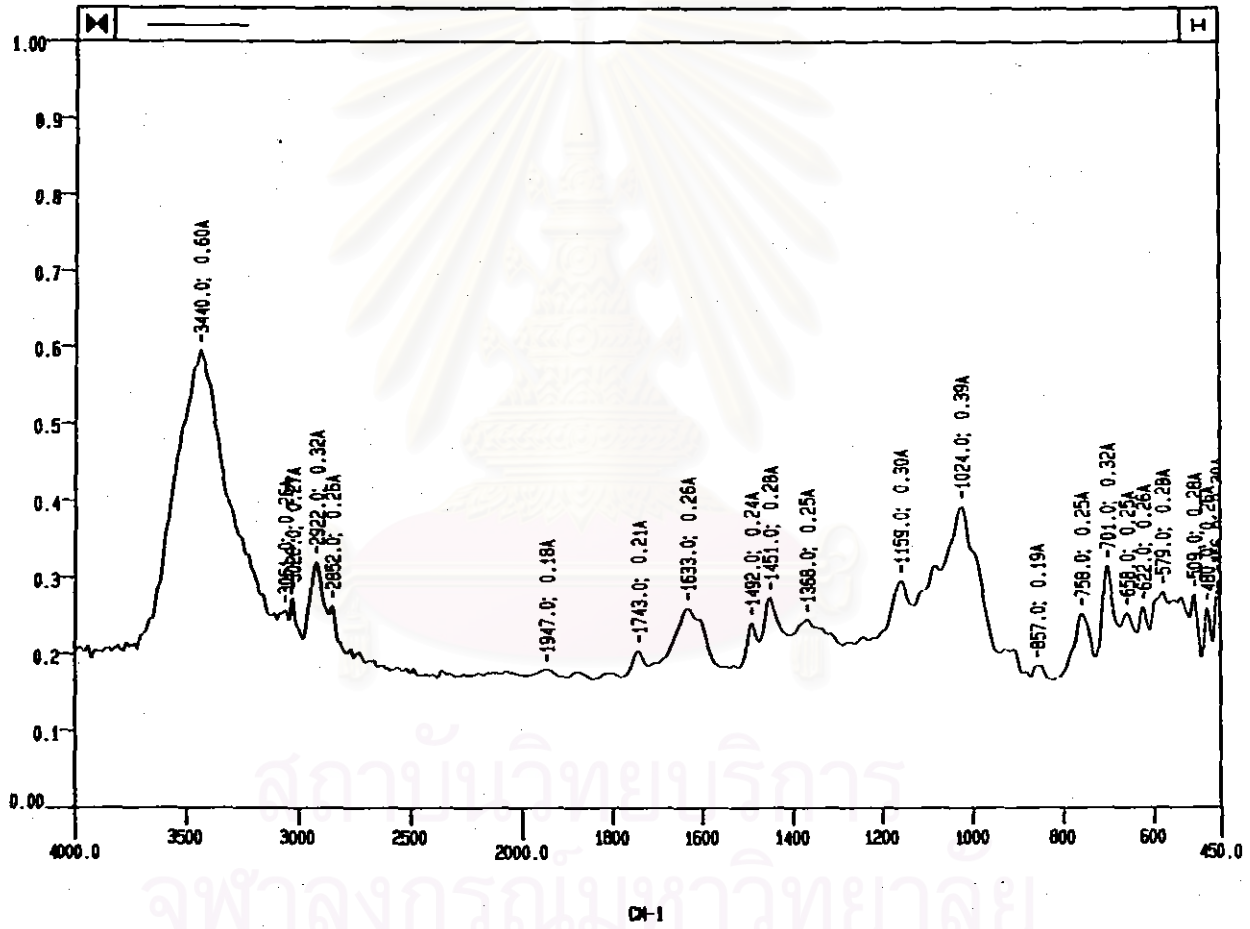

Figure 4.21 Infrared Spectrum of PS sheet at 3-Month Outdoor Exposure

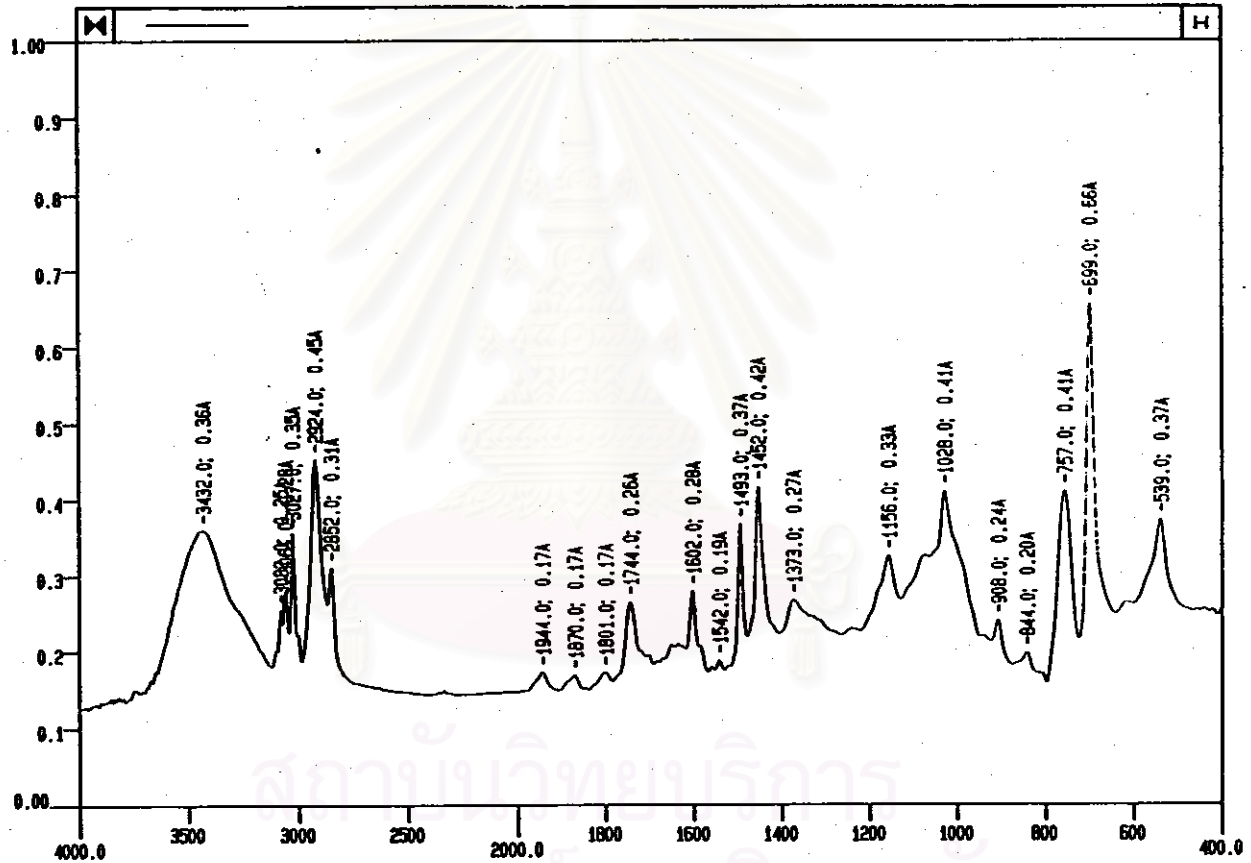

Figure 4.22 Infrared Spectrum of PS sheet at 6-Month Outdoor Exposure

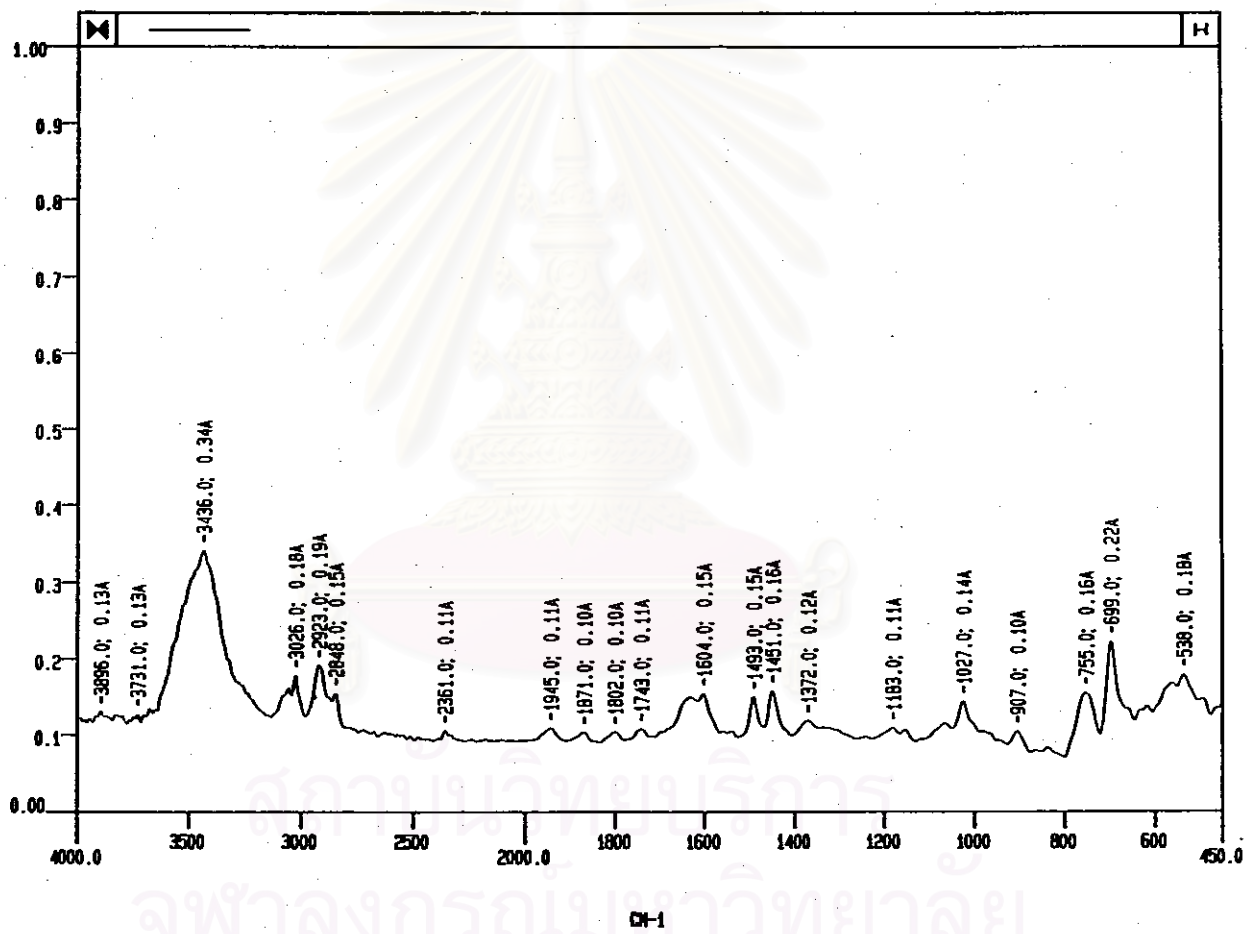

Figure 4.23 Infrared Spectrum of Control PS-G15/36 sheet

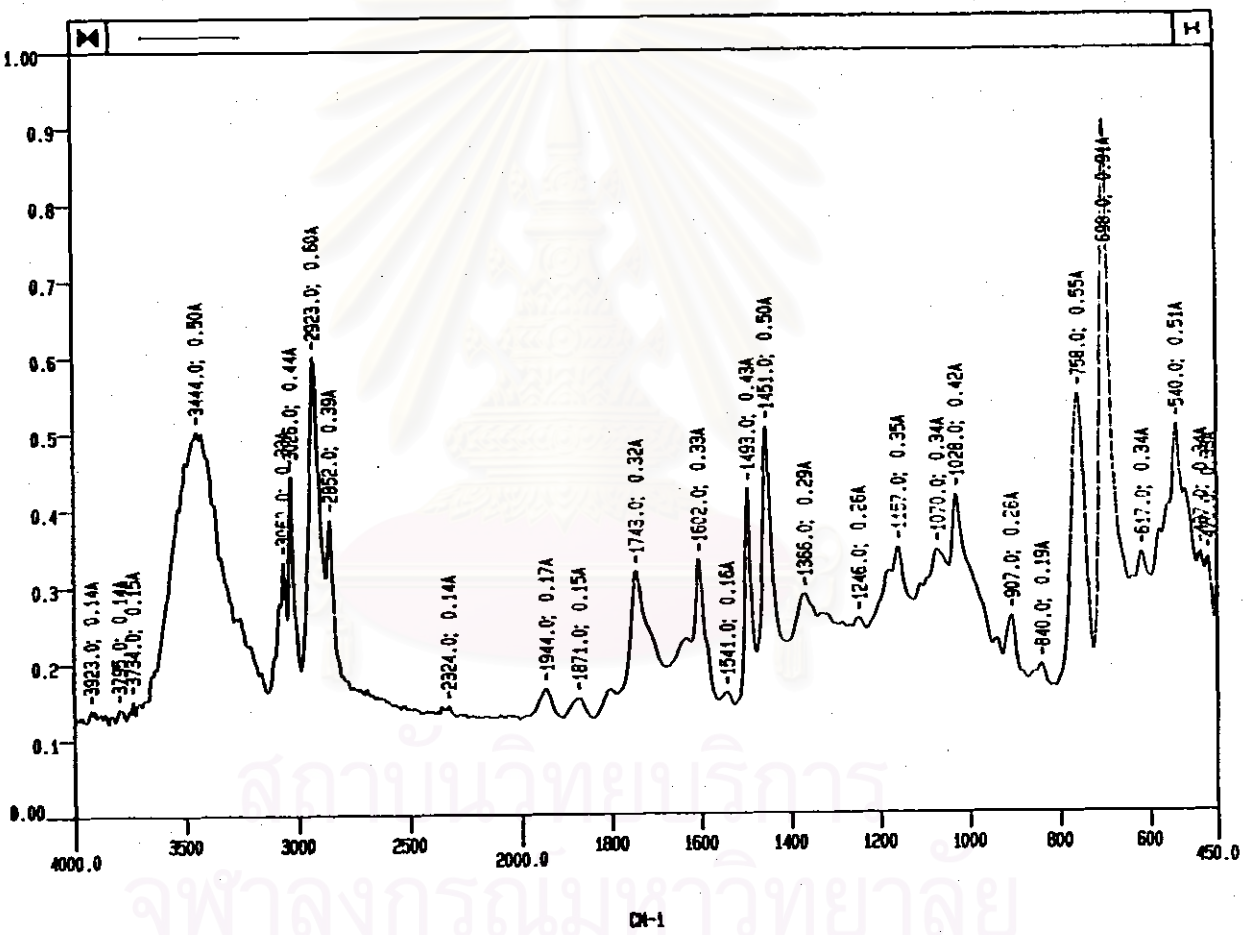

Figure 4.24 Infrared Spectrum of PS-G15/36 sheet at 3-Month Outdoor Exposure

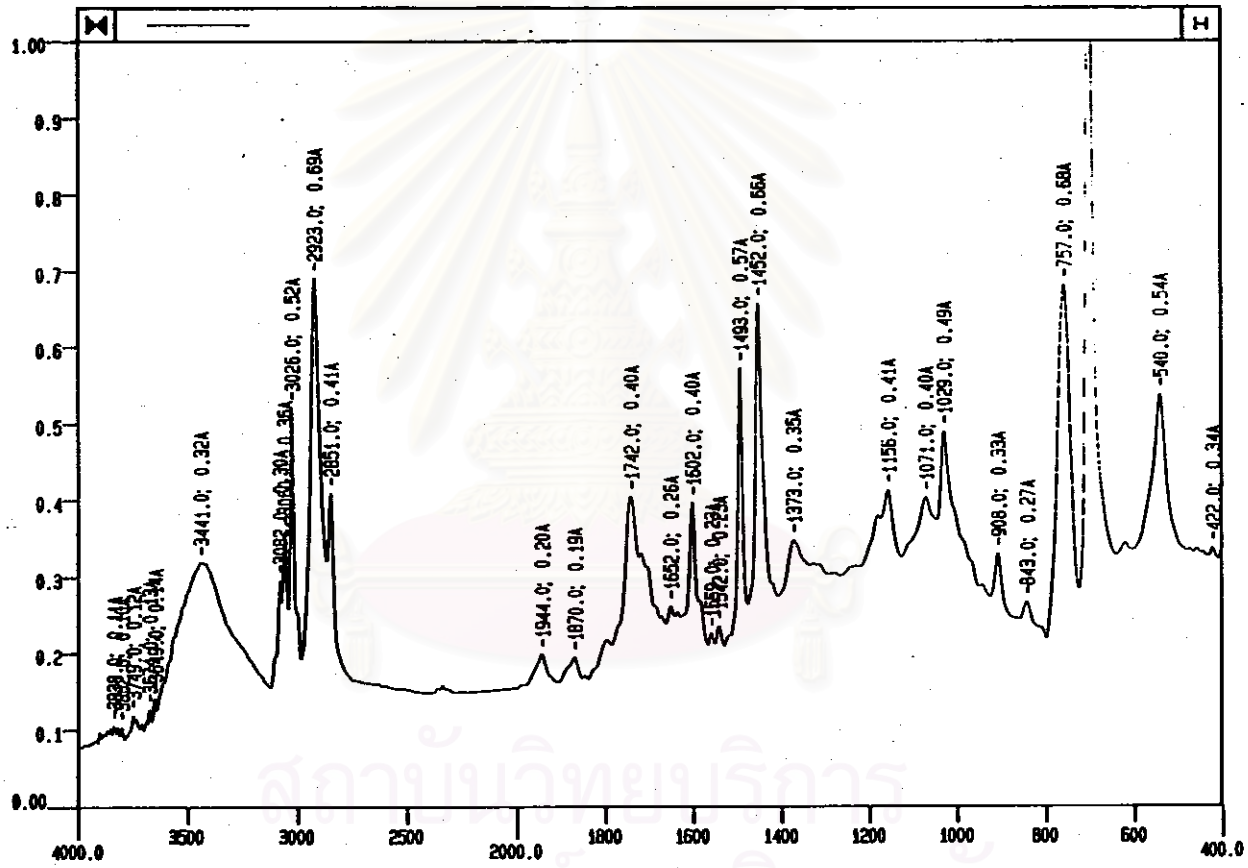

Figure 4.25 Infrared Spectrum of PS-G15/36 sheet at 6-Month Outdoor Exposure

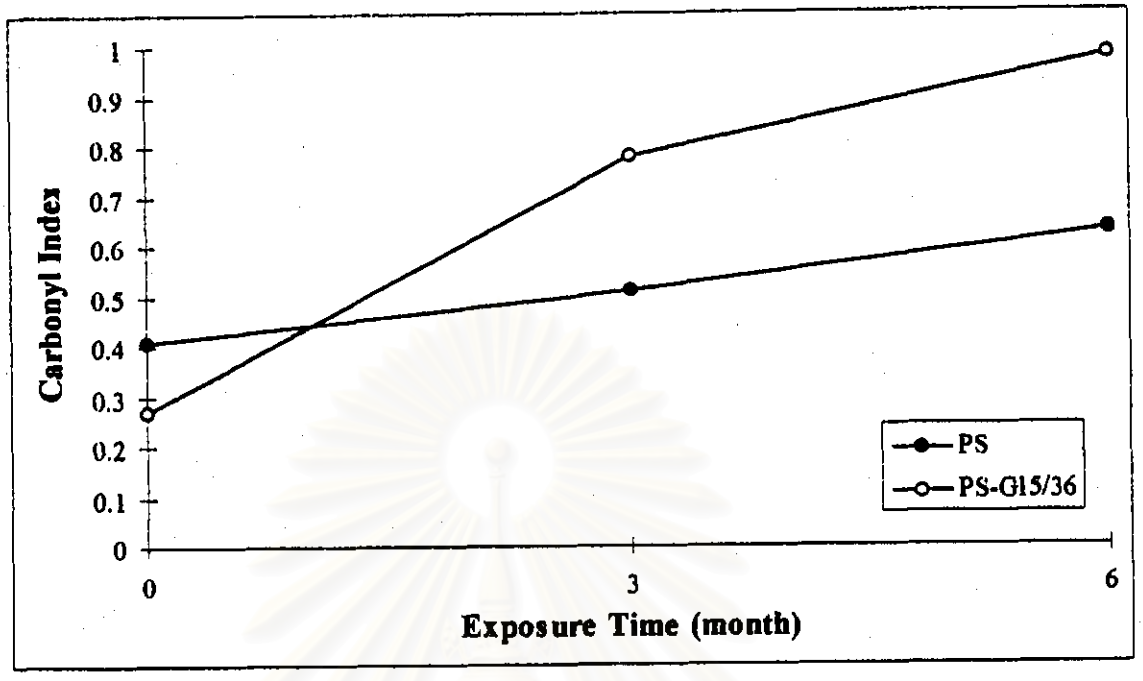

Figure 4.26 The carbonyl indexes of PS and PS-G15/36 sheets during control, 3 and 6-month outdoor exposure

From Table 4.6 and Figure 4.26, it can be seen that the carbonyl indexes of PS and PS-G15/36 sheets increase linearly with increasing exposure time. Particularly, the carbonyl indexes of zinc stearate containing PS-G15/36 sheets are higher than the PS. These can be explained by the photooxidation reaction of PS.

The photodegradation of PS in the presence of air (photooxidation) results in chain scission, some crosslinking, and discoloration (yellowing). Change of chemical structure, molecular weight and various characteristics and mechanical properties of the polymer accompany these reactions. Infrared absorption spectra of polystyrene photoirradiated in air indicate an increase in the absorption band at around 1742-1745 cm^{-1}. The band is attributable to a ketone C=O stretching vibration. This absorption band increases in its intensity with an increase in the exposure time. The increase in the intensity at 1742-1745 cm^{-1} parallels that of the peroxy radical. These results suggest the degradation reaction may proceed via peroxide intermediates and results in the main chain scission of polystyrene, leading to the formation of carbonyl compound. The following mechanism can explain the photooxidation reaction in polystyrene [28].

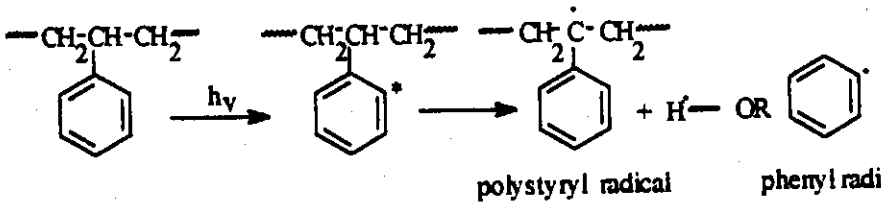

(4.5)

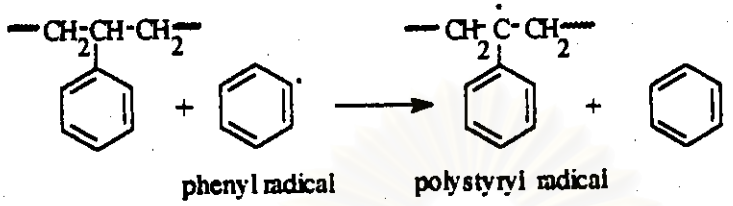

(4.6)

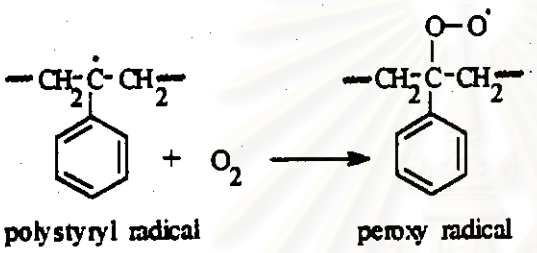

(4.7)

- chain scission via hydroperoxide intermediate

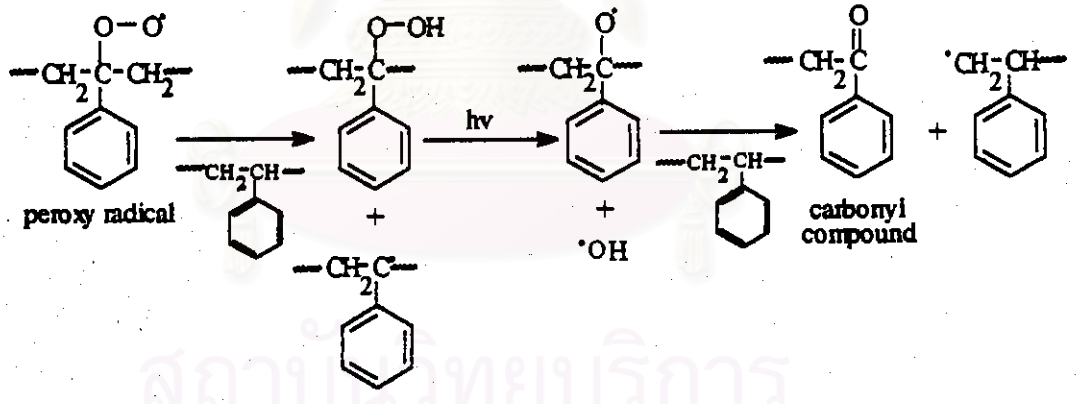

(4.8)

- chain scission

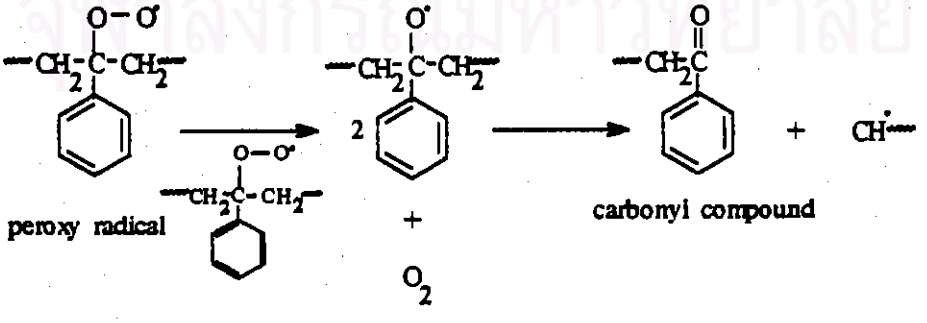

(4.9)

Figure 4.27 Mechanism of photooxidation reaction of polystyrene

The initiation of photochemical reactions is the formation of an electronically excited state. In the case of polystyrene, absorption of radiation wavelength less than 300 nm results in the formation of the excited state of the phenyl groups. The electronically excited state of the polystyrene molecule then dissociated in to polystyryl radical and phenyl radical (eq. 4.5). The phenyl radicals cannot diffuse out and may abstract hydrogen atom from adjacent polymer molecules to form polystyryl radical (eq. 4.6). The polystyryl radicals can react with oxygen (in the presence of air) and results in the formation of peroxy radical (eq. 4.7), that oxygen attack is faster during the early stages of irradiation. The polystyryl radicals thus produced are the important precursors of photoinduced chain scission (eqs. 4.8-4.9), that proceed via peroxide intermediates and leading to the formation of carbonyl compound.

The yellowing of photoirradiated polystyrene has been attributed to the conjugated double bond formation in the polymer backbone. It has also been suggested that the yellowing is due to the fulvene formed by the photoinduced isomerization of benzene rings of polystyrene.

Since the transition metals are usually capable of electron transitions between their outer shells, and the variable valency states render it capable of inducing oxidation reactions in which the zinc stearate acts as a prooxidant to catalyze the oxidation degradation [29]:

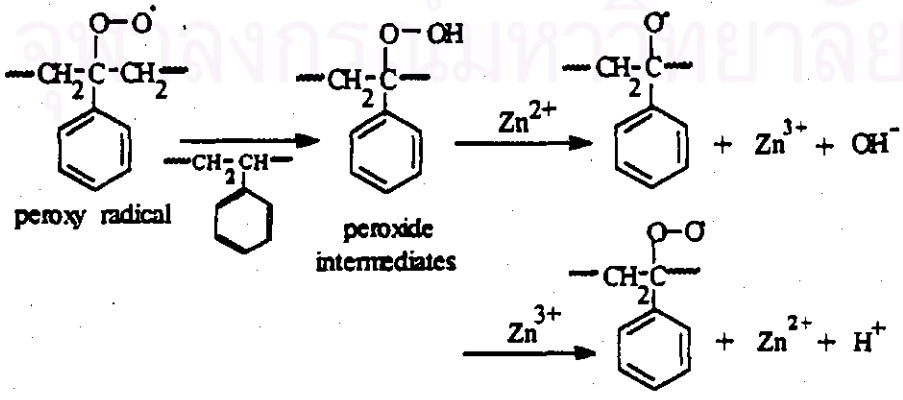

(4.11)

(4.12)

The free radicals are formed and these can react with the polystyrene, forming the polymer radicals. These free polymer radicals are extremely reactive and can further react with oxygen, as shown in the degradation mechanism (Figure 4.27)

4.3.2.3 Molecular Weight Measurements

The average molecular weights of PS and PS-G15/36 sheets were measured by using a GPC (LC-10AD, CTO-10AC, C-R7A plus (SHIMADZU) with a refractive-index detector (RID-6A) and an ultraviolet-visible detector (SPD-10AV) under the following conditions: a pair of Showa Denko columns (K-806 M; 300 mm x 8 mm I.D; packing with styrene-divinylbenzene gels having the number of theoretical plates 17,000), chloroform eluent of a flow rate of 0.017 $cm^3.s^{-1}$, and the working temperature at 25 °C. The calibration curves of GPC analysis were obtained by using a narrow molecular weight distribution polystyrene standards (Shodex standard S-66.0 with molecular weights of 2,400,000, 156,000, 28,500, 2,950, respectively). Polystyrene standards 0.1% each in chloroform (HPLC grade) were prepared and the injection volume, 70 µl, of each standard was injected. For PS and PS-G15/36, 0.1% solution of dried sample was prepared in chloroform (HPLC grade). The solutions were then filtered using a 0.45 µm membrane filter, and 70 µl of the filtered polymer solution was then injected into GPC for analysis.

The calibration data of Shodex polystyrene standard S-66.0 are shown in Table 4.7 and Figure 4.28, respectively. The average molecular weights and molecular weight distribution of PS and PS-G15/36 were measured after setting up of a basic calculation of parameters and the retention times of polystyrene standard were completed.

Table 4.7 The calibration data of Shodex polystyrene standard S-66.0

Sample Number	Average Molecular Weights	Retention Times, min.
1	2,400,000	15.317
2	156,000	17.302
3	28,500	19.203
4	2,950	21.148

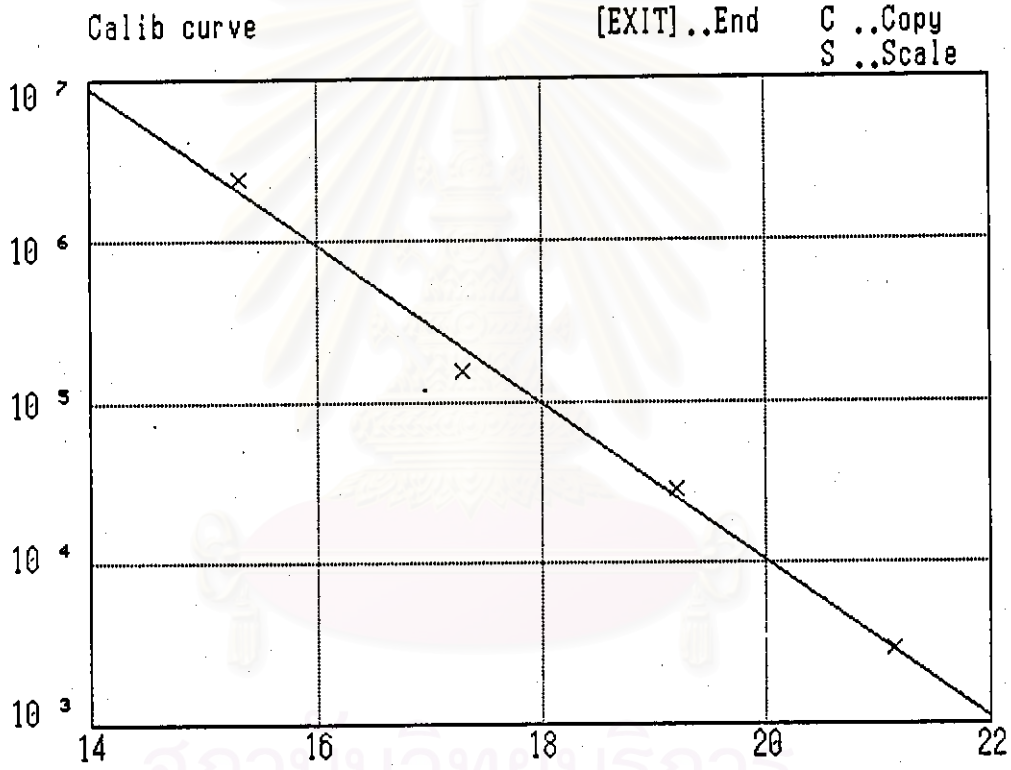

Figure 4.27 The calibration curve of Shodex polystyrene standard S-66.0

The data of average molecular weights and molecular weight distribution of PS and PS-G15/36 sheets during outdoor exposure are shown in Table 4.8 and Figure 4.29, respectively.

Table 4.8 Average molecular weights and molecular weight distribution of PS and PS-G15/36 sheets during outdoor exposure

a) PS sheet

Data	Samples Exposure Time		
	Control	3 months	6 months
$\overline{M}w$	484,040	425,695	398,238
$\overline{M}n$	10,754	6,701	1,075
$\overline{M}z$	1,171,640	1,234,395	976,601
$\overline{M}v$	424,063	363,817	342,731
$\overline{M}w / \overline{M}n$	45.01	63.52	370.32
$\overline{M}z / \overline{M}w$	2.42	2.90	2.45
$\overline{M}v / \overline{M}n$	39.43	54.29	318.71
I. VISC	14,376.74	12,796.30	12,228.63

b) PS-G15/36 sheet

Data	Samples Exposure Time		
	Control	3 months	6 months
$\overline{M}w$	395,008	362,744	277,292
$\overline{M}n$	6,823	3,671	3,451
$\overline{M}_z$	924,450	988,583	929,792
$\overline{M}v$	344,981	311,730	231,510
$\overline{M}w / \overline{M}n$	57.90	98.81	80.34
$\overline{M}z / \overline{M}w$	2.34	2.72	3.35
$\overline{M}v / \overline{M}n$	50.56	84.92	67.08
I. VISC	12,289.58	11,378.50	9,075.81

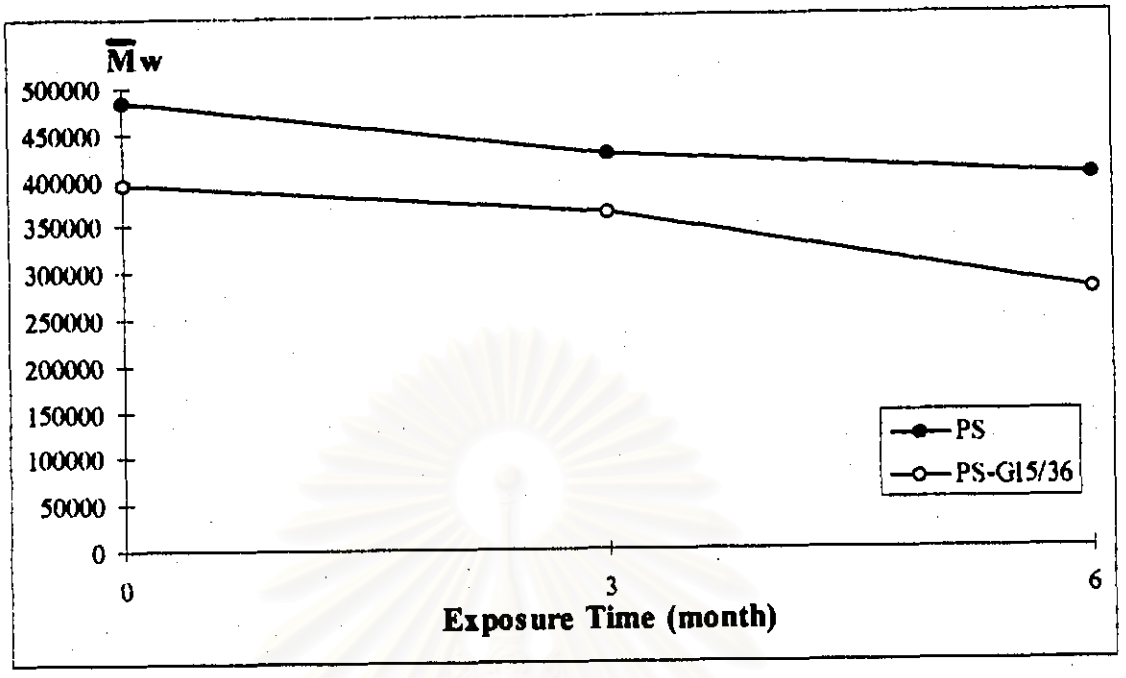

Figure 4.29 Weight-average molecular weights of PS and PS-G15/36 sheets during outdoor exposure

The changes of weight-average molecular weight of PS and PS-G15/36 sheets at various exposure times are shown in Figure 4.29. From these Figures, it can be seen that the molecular weight of PS sample decreases slower than that of PS-G15/36 sheet, corresponding to a sharp drop of tensile strength. The initial molecular weight of PS sheet was 484,040, after 6-month exposure, the molecular weight of PS sheet became 398,238. The molecular weight of PS-G15/36 sample decreases rapidly with time, i.e. the initial molecular weight of PS-G15/36 sheet was 395,008, after 6-month exposure, the molecular weight became 277,292. The decreasing of molecular weight can be described by the oxidative degradation as in FTIR absorption measurements. In addition, the molecular weight distribution of $\overline{M}w/\overline{M}n$ of PS sheet is broader than of the PS-G15/36 sheet. This implies that the degradation products of PS sheet are more polydispersed and of more variety.

4.3.2.4 Thermal Property Measurements

The thermal properties of PS and PS-G15/36 at various outdoor exposures were measured by Thermogravimetric analysis (TGA, Perkin-Elmer, model 7) at a heating rate of 10°C.min^{-1}, and the temperature between 30°C to 500°C in the nitrogen atmosphere. TGA technique is used to determine percent weight loss (%wt) and decomposition temperature (T_d) of the polymer.

Figures 4.30 through 4.33 show the TGA thermograms of PS and PS-G15/36 sheets of the control and 6-month outdoor exposure. The percent weight loss of control PS sheet was 99.95%, after 6-month outdoor exposure, the percent weight loss became 99.78%. It was found that percent weight loss of PS sheet changed slightly or even unchanged under outdoor exposure, which indicated that PS sheet degraded very slowly under outdoor exposure. The TGA thermogram of control PS sheet showed no weight loss at the temperatures below 393.5°C and decomposed completely at the temperature of 445.3°C. The values of the initial decomposition temperature are very important since they would indicate which of them would be the processing and manufacturing without continuing or initiating a process of decomposition, specially in the blends of recycled material. The TGA thermograms of control PS-G15/36 sheet show two steps of weight loss, the first one involving the decompose of cassava starch at the decomposition temperature of 307°C [30]. Pyrolytic decomposition of starch and its fractions sets in at temperatures higher than 220°C, the decomposition products include carbon dioxide, carbon monoxide, water, volatile organic compounds, and a carbonaceous residue. The second involving the decompose of polystyrene plastic at the decomposition temperature of 403.7°C and decomposed completely at the temperature of 446.9°C. The percent weight loss of control PS-G15/36 sheet was 97.63%, after 6-month outdoor exposure, the percent weight loss became 95.44%. The result indicates that PS-G15/36 sheet degrades rapidly than that of PS sheet under outdoor exposure.

The differential method of Freeman and Carroll is used to determine the kinetic data of a thermogravimetric curve by the following equation [31]:

$$[\Delta \ln (dW_r/dt)] / [\Delta \ln W_f] = n - [E/R] \cdot [\Delta(1/T)] / [\ln W_f] \qquad (4.13)$$

Where

W_r = The weight of the reactive portion which remains at time t

W_f = The total weight-loss for the particular reaction step

T = Temperature (K)

E = The activation energy ($kJ.mol^{-1}$)

R = Gas constant ($8.314\ J.mol^{-1}K^{-1}$)

n = Reaction order

Thus, a plot of $[\Delta \ln (dW_r/dt)] / [\Delta \ln W_f]$ against $[\Delta(1/T)] / [\ln W_f]$ is a straight line of the slope –E/R and an intercept n. From the slope, the initial activation energy of PS sheet was 201.3 $kJ.mol^{-1}$, after 6-month outdoor exposure, the activation energy became 166.3 $kJ.mol^{-1}$. The activation energy of PS-G15/36 sheet is lower than that of the polystyrene sheet. The initial activation energy of PS-G15/36 sheet was 97.8 $kJ.mol^{-1}$, after 6-month exposure, the activation energy became 92.7 $kJ.mol^{-1}$. This confirms that the PS-G15/36 sheet decompose quickly than PS sheet, because the former requires less activation energy to start the decomposition process. The presence of starch grafted polystyrene, zinc stearate and soya oil may be the attribute to ease the decomposition process. In addition, one has to consider bond dissociation energies of the ingredients concerned in the composite. According to the bond dissociation energies, the breakages of C=C, C-C, C-H and RO-OH (hydroperoxide) linkages require 733; 348, 338, and 188.2 $kJ.mol^{-1}$, respectively [32]. It was thus found that the bond dissociation energy of oxygen-oxygen bond of hydroperoxide is much weaker than that other bonds. This concludes that thermal degradation of polystyrene plastic proceeds much easier through the breakage of oxygen-oxygen bond of hydroperoxides to give alkoxy radicals, which initiates the degradation reactions.

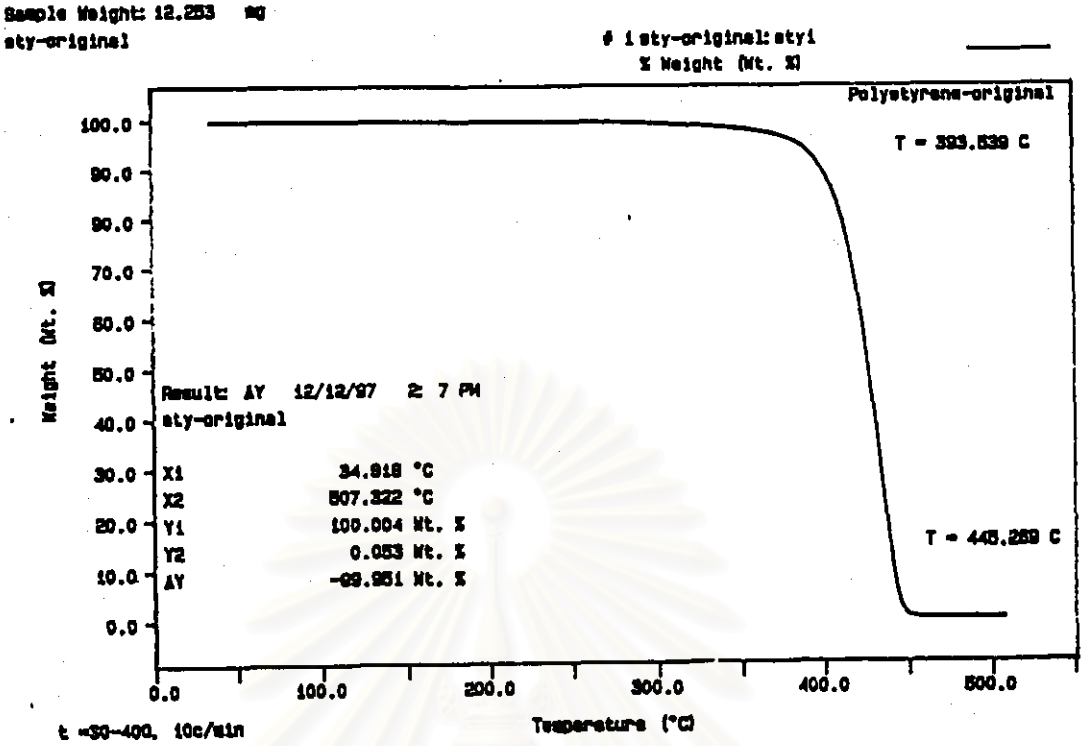

Figure 4.30 TGA thermogram of control PS sheet

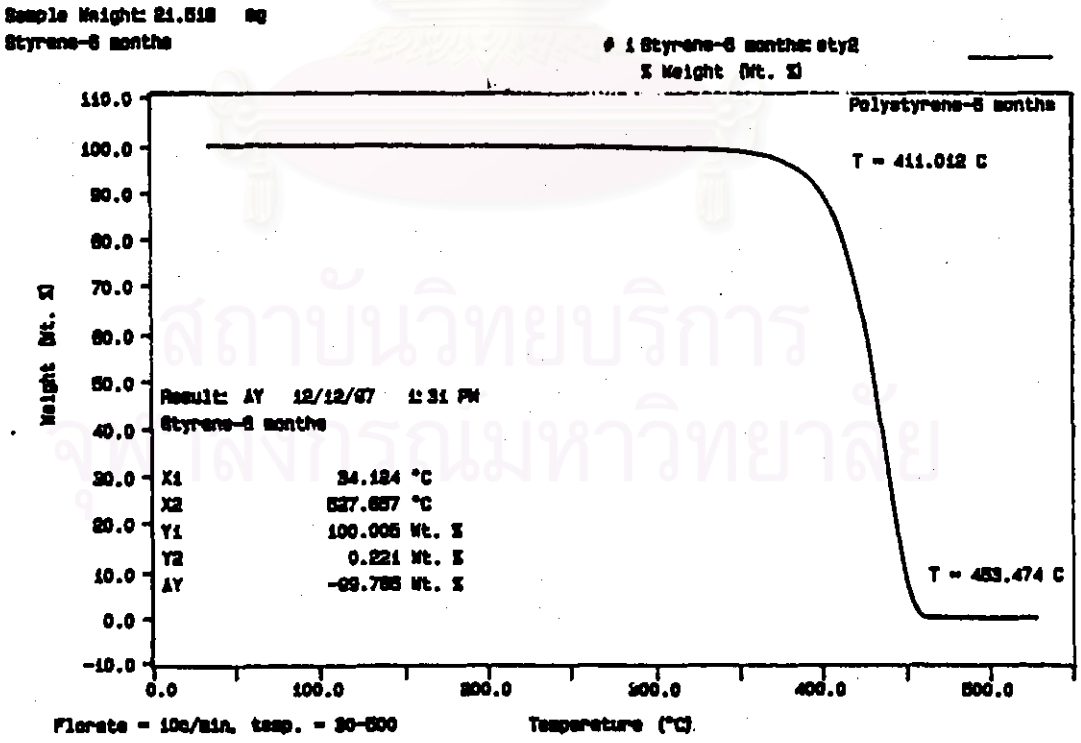

Figure 4.31 TGA thermogram of PS sheet after 6-month outdoor exposure

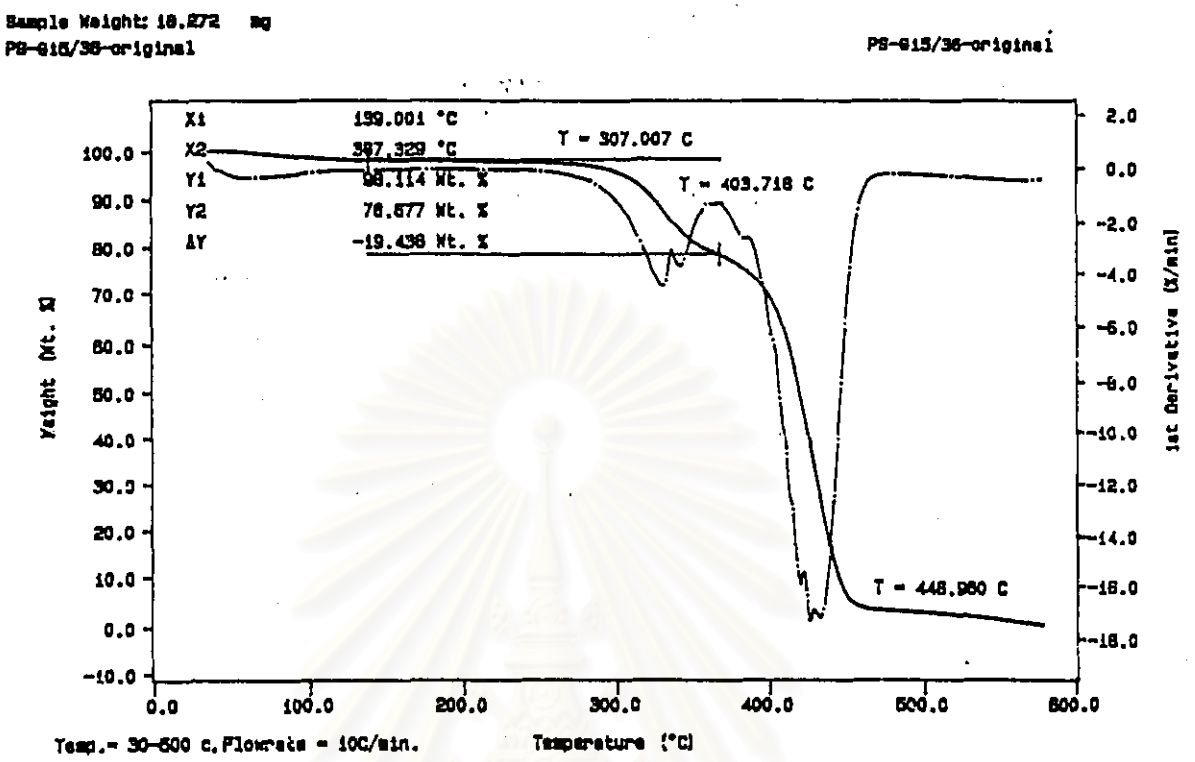

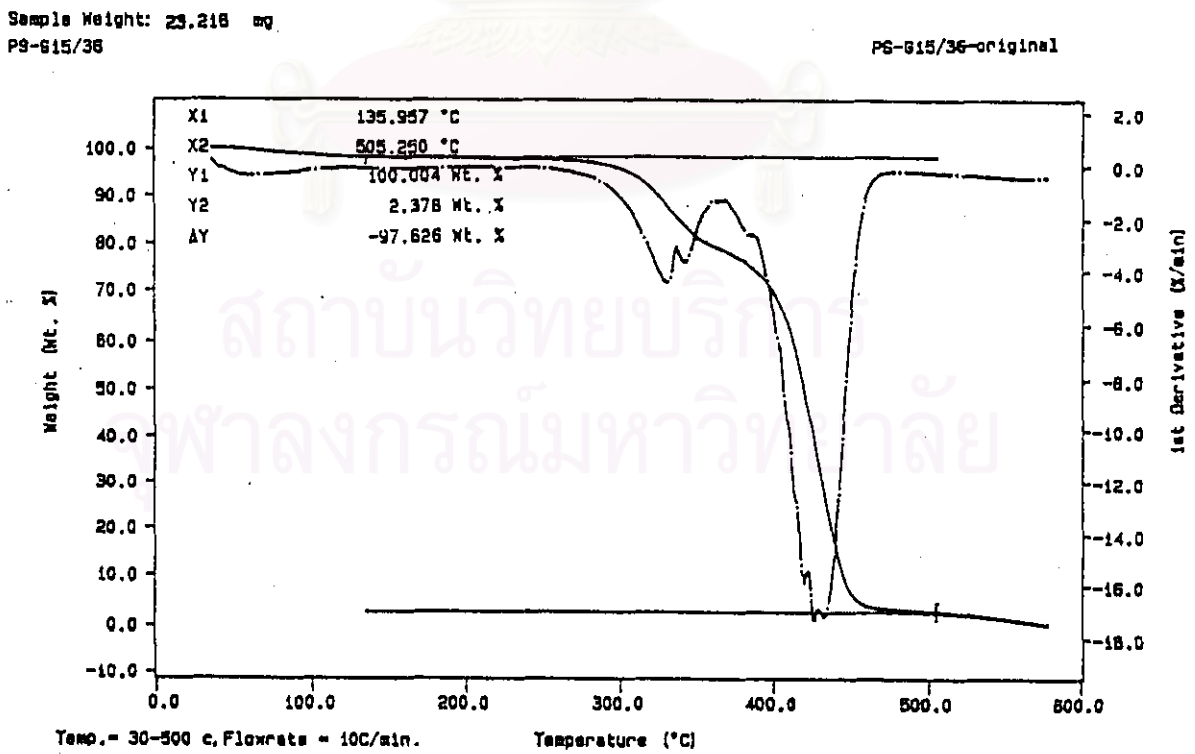

Figure 4.32 TGA thermograms of control PS-G15/36 sheet

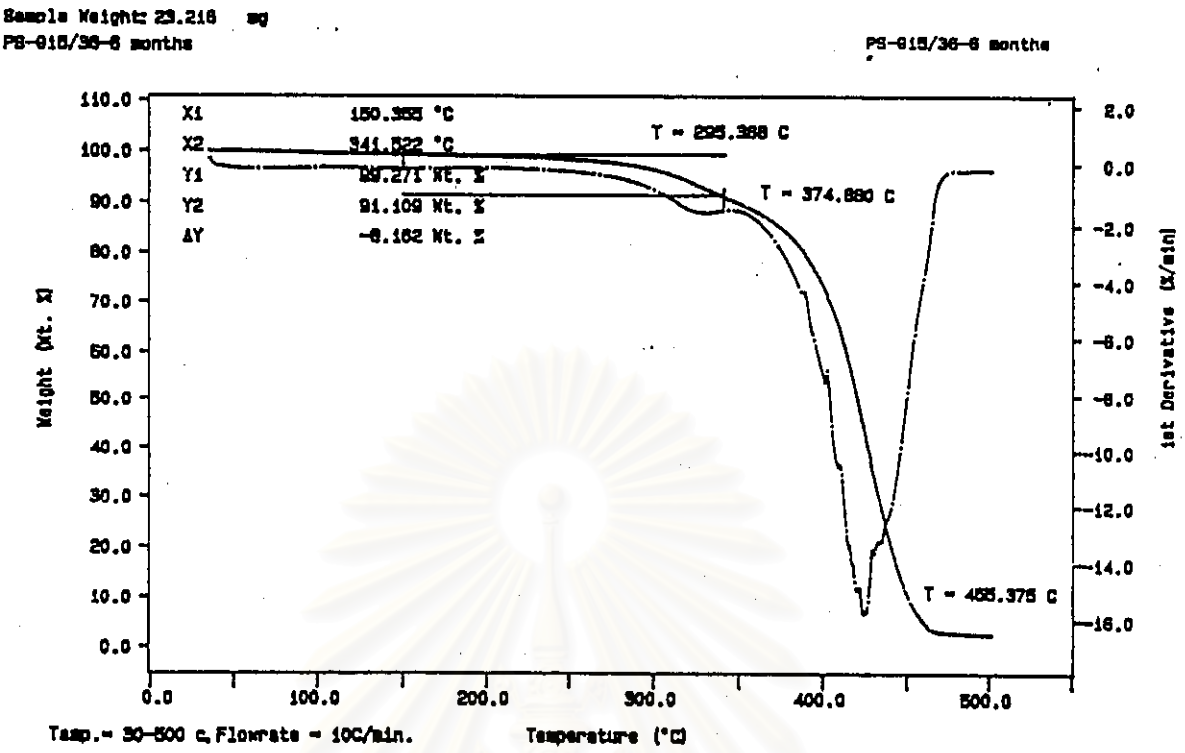

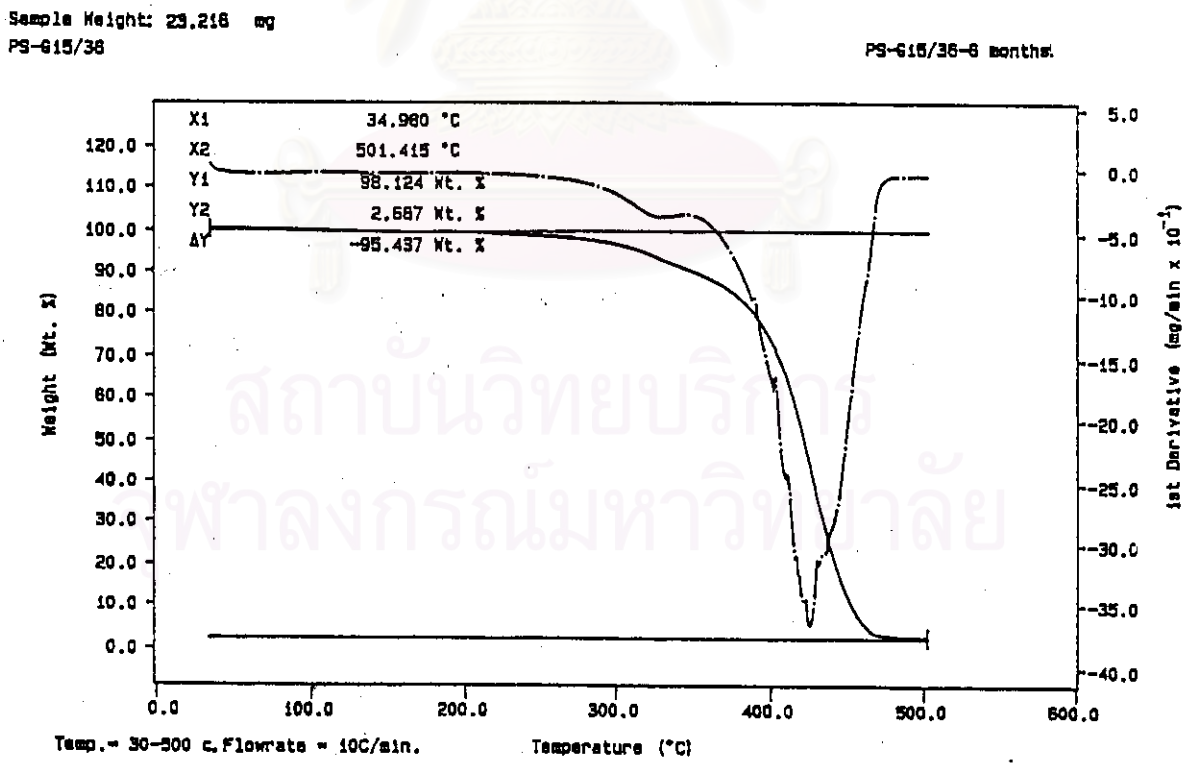

Figure 4.33 TGA thermograms of PS-G15/36 sheet after 6-month outdoor exposure

4.3.3 Soil Burial Test

4.3.3.1 Tensile Property Measurements

The PS and composite PS sheets were buried in soil for 6 months and removed every month for evaluating the effect of soil burial test on mechanical properties of the plastic. After removal, the composite PS sheets have many dark spots on the surface and on some sheets with various sizes of small holes, indicating the removal of starch from the plastics. The typical effects of soil burial on the tensile property of PS and composite PS sheets are shown in Table 4.9, Figures 4.34 through 4.37.

From Table 4.9 and Figure 4.38, it was found that the tensile strength of PS sheet decreases by a low rate. An initial tensile strength and elongation at break of PS sheet were 43.0 MPa and 5%, respectively. After 6 months, tensile strength of PS sheet was 33.9 MPa and elongation at break was 3%. It shows that the soil burial had a week effect on tensile property of PS sheet. The tensile strength of composite PS sheets decreases rapidly than that PS sheet, particularly for the tensile strength of PS-G15/36 sheet. For example, the initial tensile strength of PS-G15/36 sheet was 20.0 MPa, after 6-month soil burial test, the tensile strength of PS-G15/36 sheet became 3.3 MPa. The decrease in tensile strength of PS-G15/36 sheet after 6-month soil burial test can be caused by the starch-*g*-polystyrene embedded in the PS matrix, which can easily absorb moisture in its surrounding and decreased the tensile property of the plastic. Furthermore, the starch portion can be attacked by microorganisms such as fungi or bacteria, which leads to increased porosity and void formation. The biodegradation of plastics can be produced from microorganisms through fermentation, from plant produces or through synthetic polymer products. The chemical linkages between the monomers in the polymer chain and pendant groups attached to the polymer greatly influence biodegradability by altering chain flexibility and polymer crystallinity, which can influence enzyme and water access to polymer [33]. From Figure 4.39, it was found that the amount of zinc stearate has a rather week effect on tensile strength of PS-G15 sheets.

Table 4.9 Tensile properties of PS and composite PS sheets during soil burial test.

a) Tensile strength (MPa)

Sample	Sample Exposure Time						
	Control	1 month	2 months	3 months	4 months	5 months	6 months
PS	43.0	41.2	40.0	39.2	37.6	35.4	33.9
PS-S5-G5/1	31.2	29.6	28.2	26.8	24.9	22.4	20.4
PS-S5-G5/2	30.0	27.9	26.4	24.6	22.4	21.0	19.2
PS-S5-G5/3	27.6	24.8	22.3	20.8	20.4	19.9	18.4
PS-S5-G5/4	30.2	27.9	26.1	25.6	24.2	22.4	20.0
PS-S5-G5/5	28.4	25.4	24.6	22.6	20.2	20.2	19.1
PS-S5-G5/6	26.0	24.1	22.8	20.4	18.8	17.9	16.4
PS-S5-G5/7	29.7	24.0	20.2	19.9	18.6	17.4	16.0
PS-S5-G5/8	27.9	22.4	18.6	17.4	16.3	15.6	14.8
PS-S5-G5/9	24.6	20.2	16.8	15.8	15.2	14.9	14.1
PS-S5-G10/10	23.7	18.5	16.5	15.5	13.5	12.7	10.6
PS-S5-G10/11	22.1	17.4	15.0	13.6	12.6	11.5	10.4
PS-S5-G10/12	20.1	14.6	13.6	12.7	11.6	11.0	9.6
PS-S5-G10/13	22.0	15.9	14.6	12.6	11.3	10.9	10.0
PS-S5-G10/14	21.7	14.8	11.5	11.0	10.3	9.5	8.3
PS-S5-G10/15	20.0	13.0	10.3	10.2	9.2	8.1	7.3
PS-S5-G10/16	20.2	15.7	14.3	12.4	10.9	9.4	8.1
PS-S5-G10/17	19.2	14.2	12.5	11.7	9.7	8.3	7.2
PS-S5-G10/18	18.2	12.0	9.5	8.3	7.6	6.2	5.2
PS-S15/19	26.4	23.2	22.6	21.4	21.2	18.7	17.6
PS-S15/20	25.4	17.6	16.8	15.6	14.3	13.7	12.6
PS-S15/21	23.2	16.8	16.1	14.1	13.8	12.3	11.6
PS-S15/22	25.8	22.6	20.7	19.7	17.8	15.2	14.5
PS-S15/23	24.7	17.2	16.3	15.8	13.5	12.3	11.2
PS-S15/24	22.4	17.1	15.1	14.4	12.2	11.2	10.8
PS-S15/25	24.9	19.8	19.2	18.5	17.1	15.1	14.2
PS-S15/26	23.7	17.8	16.9	15.6	13.4	12.2	11.0
PS-S15/27	21.0	15.4	14.1	13.0	10.9	10.1	9.6
PS-G15/28	20.2	13.7	12.3	11.3	10.6	9.5	9.0
PS-G15/29	20.1	13.3	11.7	10.3	9.3	8.4	7.5
PS-G15/30	20.0	10.3	9.1	8.9	8.8	7.4	6.5
PS-G15/31	20.0	12.5	11.4	10.7	9.4	9.4	7.2
PS-G15/32	20.1	12.2	10.0	9.7	8.0	7.3	6.4
PS-G15/33	20.2	10.1	9.8	8.7	6.9	5.8	5.4
PS-G15/34	20.0	12.0	9.6	9.3	8.9	7.1	6.1
PS-G15/35	21.0	10.7	9.7	8.7	7.6	6.8	6.0
PS-G15/36	20.0	9.2	7.2	6.5	5.2	4.4	3.3

Table 4.9 (continued)

b) Elongation at break (%)

Sample	Sample Exposure Time						
	Control	1 month	2 months	3 months	4 months	5 months	6 months
PS	5	4	4	4	4	4	3
PS-S5-G5/1	4	4	4	4	4	3	3
PS-S5-G5/2	4	4	4	4	3	3	3
PS-S5-G5/3	4	4	3	3	3	3	3
PS-S5-G5/4	4	4	4	4	4	4	2
PS-S5-G5/5	4	4	4	4	3	3	3
PS-S5-G5/6	4	4	4	3	3	3	3
PS-S5-G5/7	4	4	4	3	3	3	3
PS-S5-G5/8	4	4	4	3	3	3	3
PS-S5-G5/9	4	4	3	3	3	3	3
PS-S5-G10/10	4	3	4	3	3	3	3
PS-S5-G10/11	3	3	3	3	3	3	3
PS-S5-G10/12	3	3	3	3	2	2	2
PS-S5-G10/13	3	3	3	3	3	3	3
PS-S5-G10/14	3	3	3	3	3	2	2
PS-S5-G10/15	3	3	3	3	2	2	2
PS-S5-G10/16	3	3	3	3	2	2	2
PS-S5-G10/17	3	3	3	2	2	2	2
PS-S5-G10/18	3	3	3	2	2	2	2
PS-S15/19	4	4	4	4	4	4	3
PS-S15/20	4	4	4	4	3	3	3
PS-S15/21	4	3	3	3	3	2	2
PS-S15/22	4	4	4	4	4	3	3
PS-S15/23	4	4	4	4	3	3	3
PS-S15/24	3	3	3	3	3	2	2
PS-S15/25	4	4	4	3	3	3	3
PS-S15/26	4	4	3	3	3	3	3
PS-S15/27	3	3	3	3	3	2	2
PS-G15/28	3	3	4	3	3	3	3
PS-G15/29	3	3	3	2	2	2	2
PS-G15/30	3	3	2	2	2	2	2
PS-G15/31	3	3	3	3	3	2	2
PS-G15/32	3	3	2	2	2	2	2
PS-G15/33	2	2	2	2	2	2	2
PS-G15/34	3	3	3	3	2	2	2
PS-G15/35	2	2	2	2	2	2	2
PS-G15/36	2	2	2	2	2	2	2

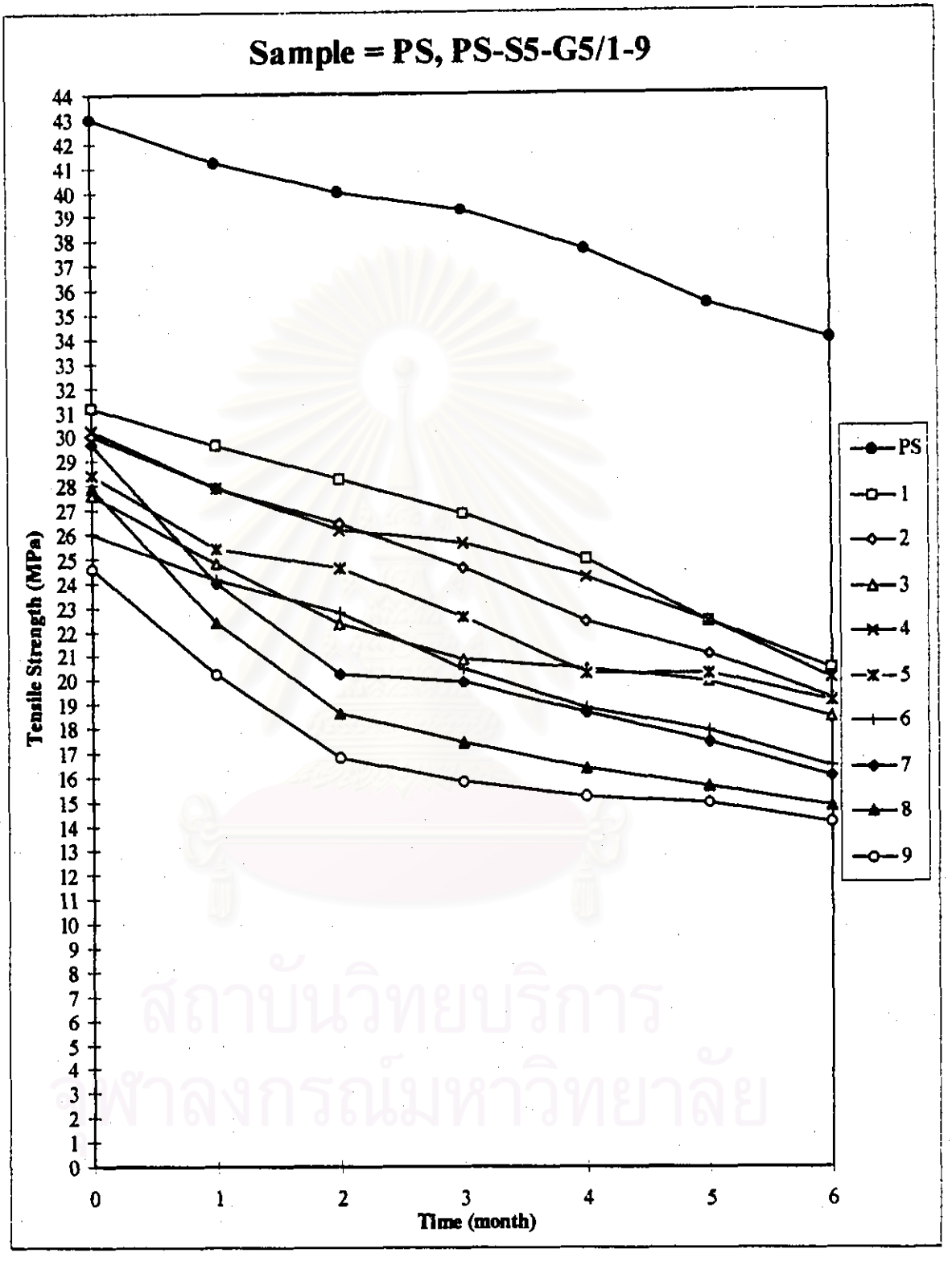

Figure 4.34 Tensile strength of PS and PS-S5-G5/1-9 sheets during soil burial test.

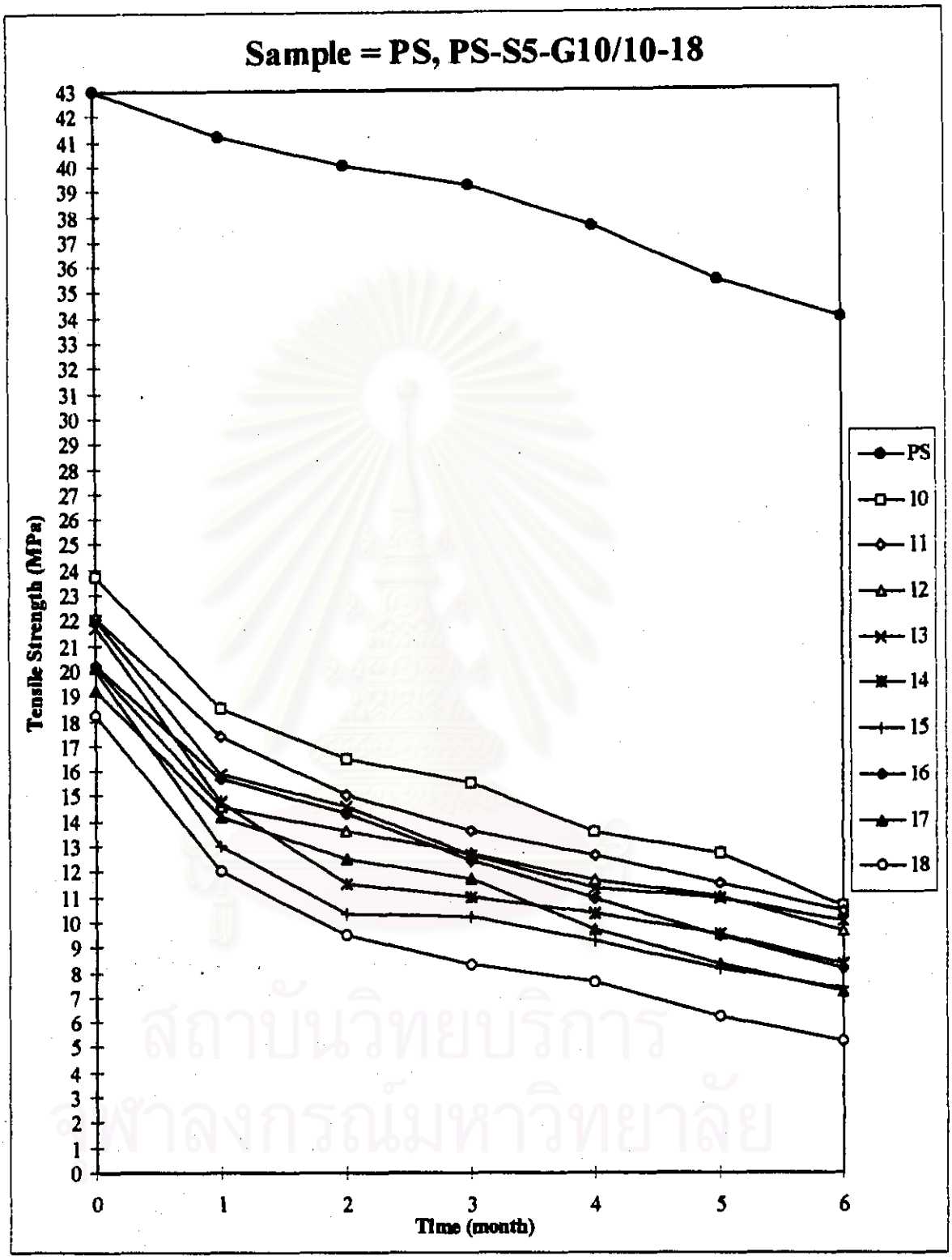

Figure 4.35 Tensile strength of PS and PS-S5-G10/10-18 sheets during soil burial test.

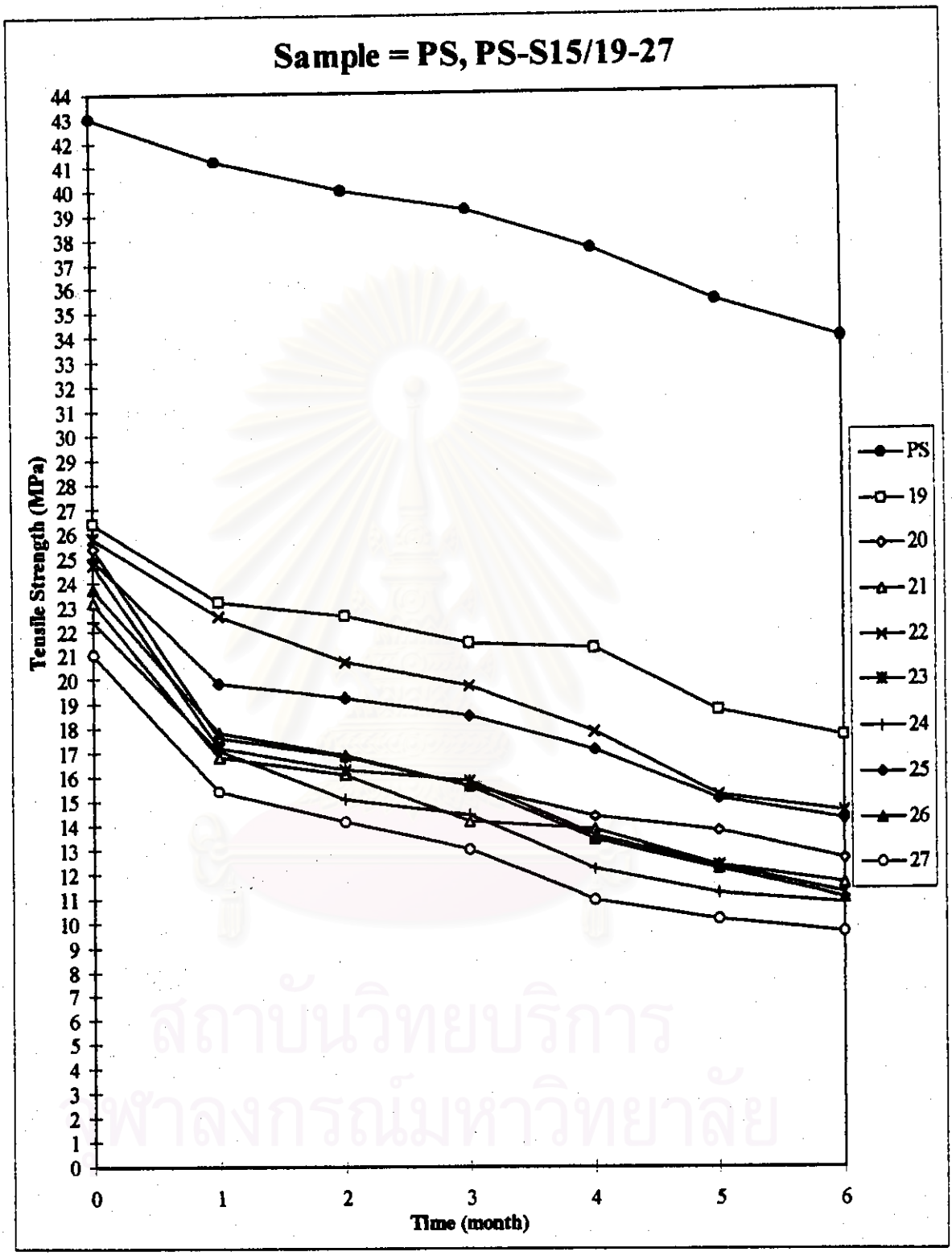

Figure 4.36 Tensile strength of PS and PS-S15/19-27 sheets during soil burial test.

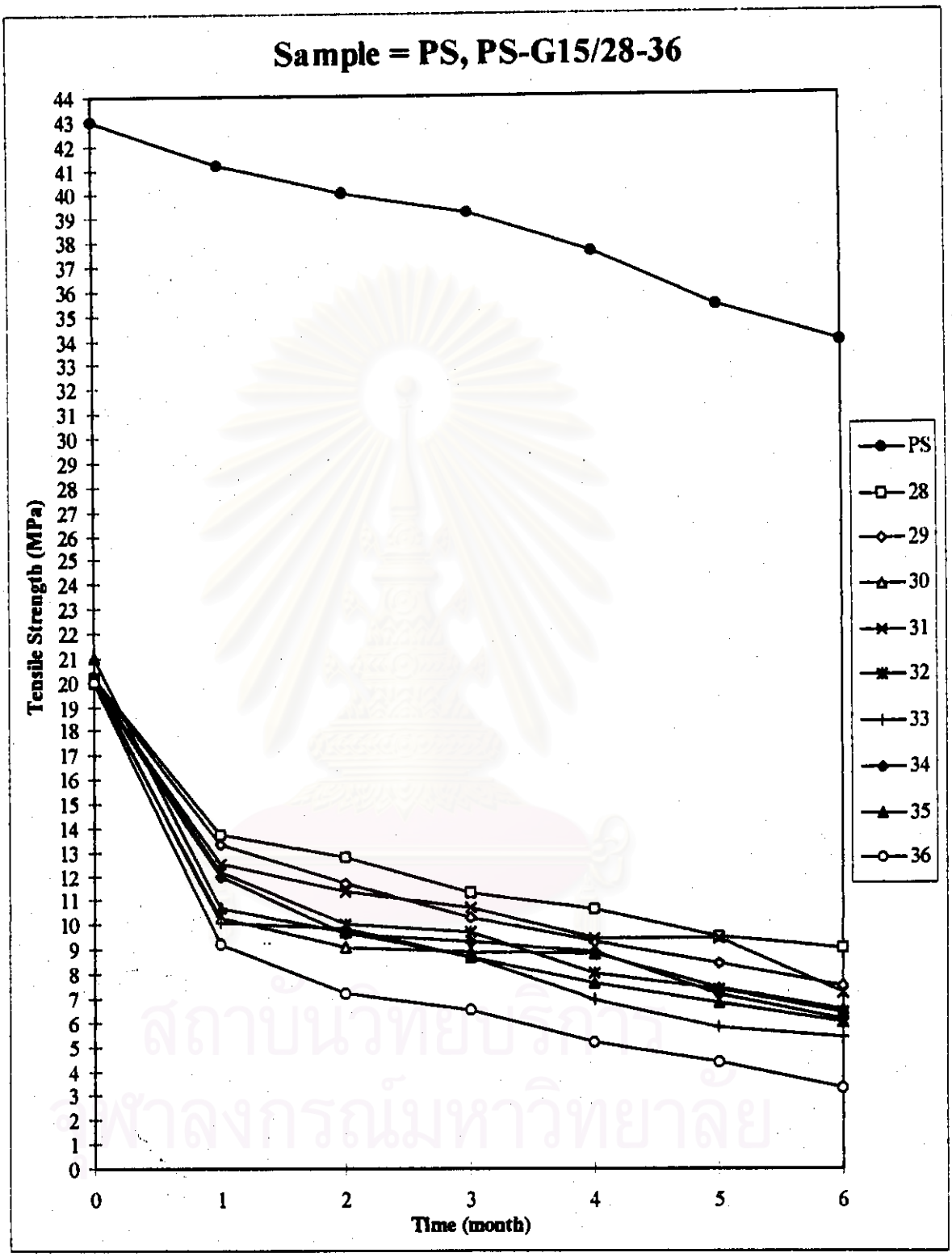

Figure 4.37 Tensile strength of PS and PS-G15/28-36 sheets during soil burial test.

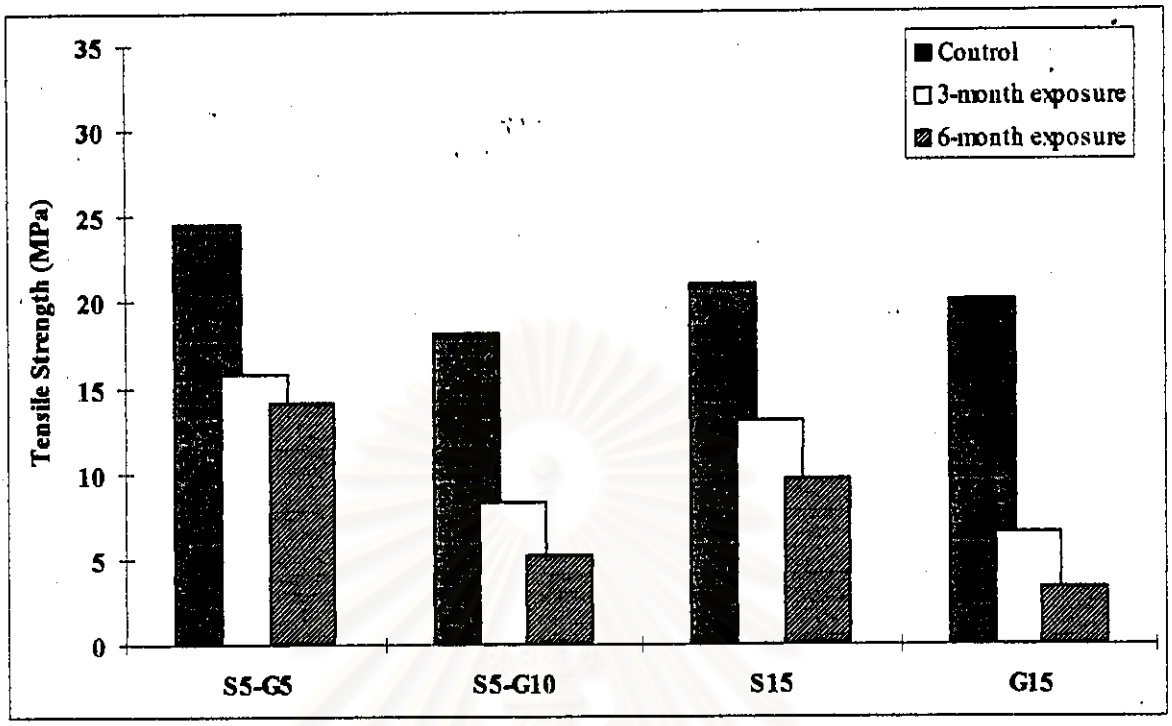

Figure 4.38 Effect of starch and graft copolymer content on tensile strength of composite PS sheets at 8% of soya oil and 0.4% of zinc stearate for soil burial test.

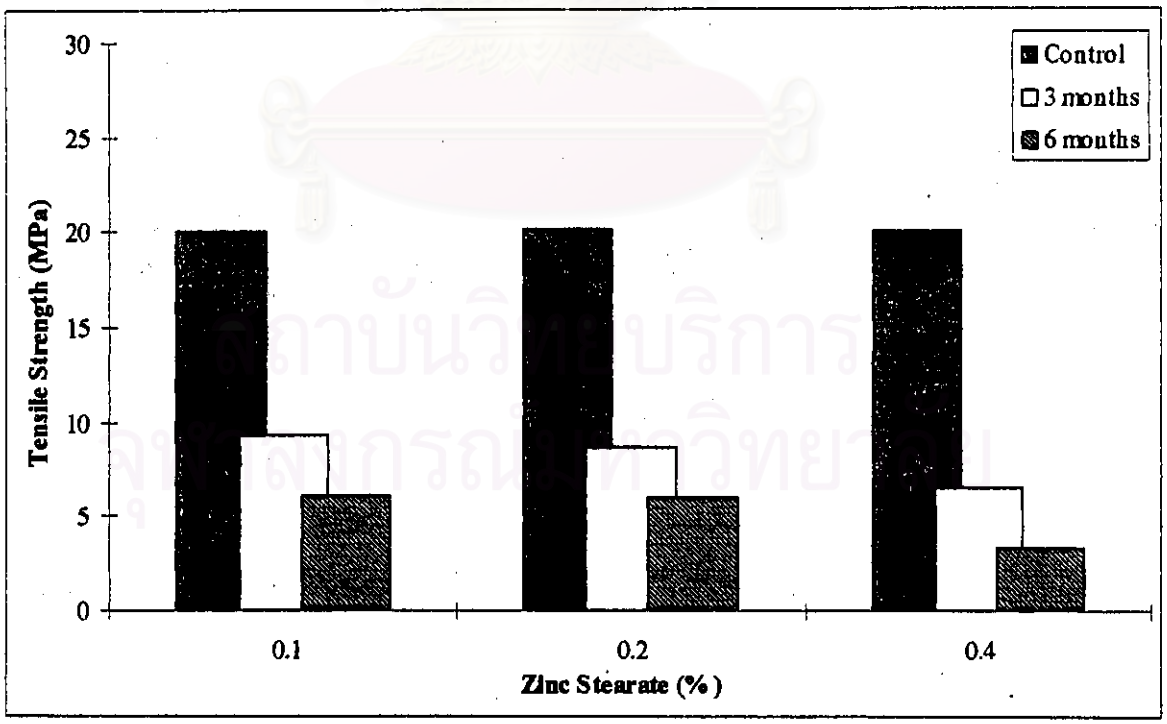

Figure 4.39 Effect of zinc stearate content on tensile strength of PS-G15 sheets at 8% of soya oil for soil burial test.

4.3.3.2 Surface Morphology of PS and Composite PS sheet

A Scanning Electron Microscope (JEOL, model JSM-5410LV) was used to study surface morphology of PS and composite PS sheet at control and 6-month soil burial test (Figures 4.40 through 4.45)

Figures 4.40 and 4.41 show electron micrographs of the surface morphology of PS sheets before and after soil burial test for 6 months. It was seen that the control PS sheet has a smooth surface, the PS sheet of after 6-month soil burial test has a rough surface. Figures 4.42 to 4.45 show electron micrographs of the surface morphology of composite PS sheets at 6-month soil burial test. It was found that the composite PS sheet has many holes throughout the plastic surface, indicating the occurrence of degradation, which enables the removal of starch products by microorganisms. Some more interesting features are also observed on the micrographs. Increasing the concentrations of starch and its graft copolymers seems to give more holes. In addition, external influences of underground water and rainfalls enhance the leaching of the destroyed surface caused by the microorganisms in soil.

Figure 4.40 SEM micrograph of control PS sheet

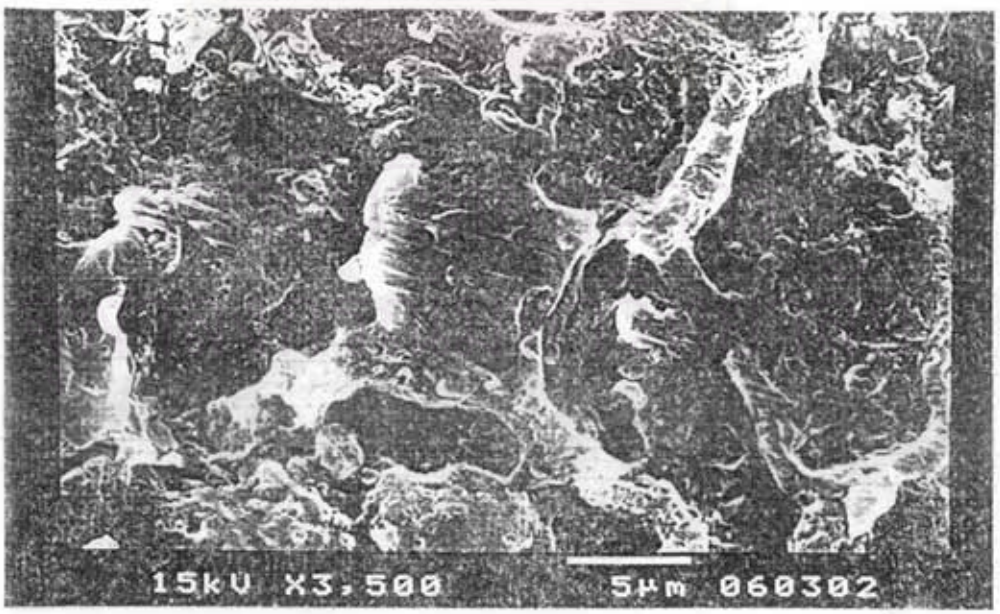

Figure 4.41 SEM micrograph of PS sheet at 6-month soil burial test

Figure 4.42 SEM micrograph of PS-S5-G5/9 at 6-month soil burial test

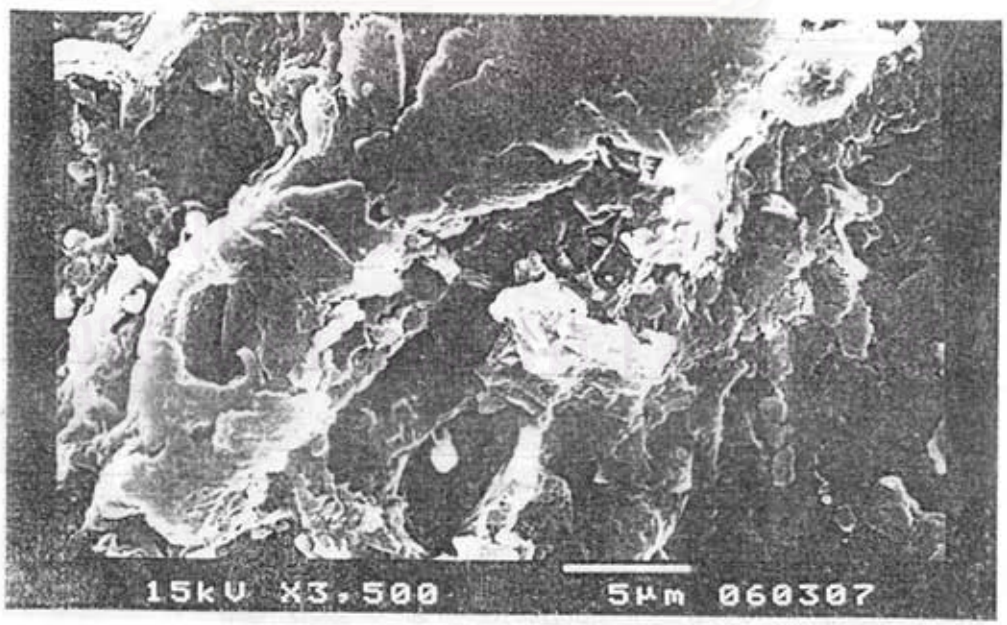

Figure 4.43 SEM micrograph of PS-S5-G10/18 sheet at 6-month soil burial test

Figure 4.44 SEM micrograph of PS-S15/27 sheet at 6-month soil burial test

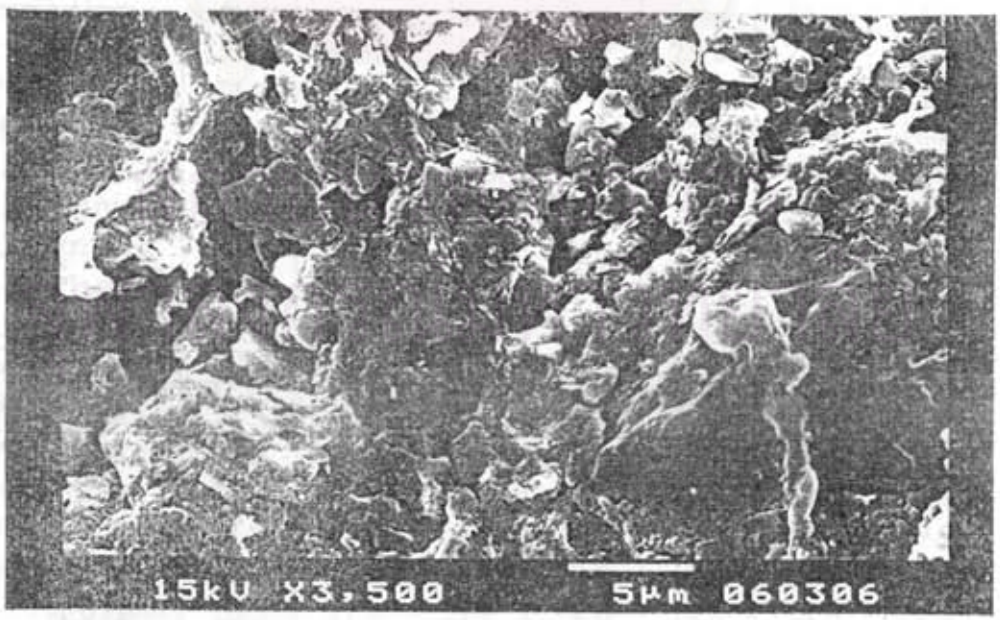

Figure 4.45 SEM micrograph of PS-G15/36 sheet at 6-month soil burial test

4.3.4. Gamma Irradiation Test

4.3.4.1 Tensile Property Measurements

The PS and composite PS sheets were irradiated under gamma rays at a fixed dose rate of 2.5×10^{-3} kGy/sec to various quantities of total dose of 50, 100, 150, 200, 250, and 300 kGy. After irradiation, it was found that the color of the plastic becomes yellow; it thus indicated the formation of conjugated double bonds in polymer chains. A typical study of the effect of gamma radiation on the tensile strength and elongation at break of both PS and composite PS sheets is shown in Table 4.10 and Figures 4.46 through 4.47.

Table 4.10 Tensile properties of PS and composite PS sheets during gamma irradiation

a) Tensile strength (MPa)

Sample	Tensile Strength (MPa) of Sample Absorbed Dose						
	Control	50 kGy	100 kGy	150 kGy	200 kGy	250 kGy	300 kGy
PS	43.0	43.0	44.6	43.6	42.0	41.1	38.2
PS-S5-G5/3	27.6	28.4	29.2	28.5	27.3	25.0	24.7
PS-S5-G5/6	26.0	28.0	30.8	28.6	26.4	24.6	23.4
PS-S5-G5/7	29.7	30.4	32.1	28.3	25.8	23.4	22.1
PS-S5-G5/8	27.9	28.0	29.8	27.0	25.2	24.1	20.3
PS-S5-G5/9	24.6	25.9	27.9	23.9	22.4	20.8	18.8
PS-S5-G10/12	20.1	22.5	23.8	22.6	20.5	20.0	19.6
PS-S5-G10/15	20.0	22.5	26.7	24.2	21.4	20.4	19.4
PS-S5-G10/16	20.2	23.4	26.4	23.4	22.5	21.4	20.6
PS-S5-G10/17	19.2	23.2	25.7	22.0	21.6	20.6	19.2
PS-S5-G10/18	18.2	20.9	23.0	21.0	19.3	18.5	18.0
PS-S15/21	23.2	28.3	29.8	24.4	22.5	21.2	20.4
PS-S15/24	22.4	27.4	28.6	24.2	22.3	21.0	20.2
PS-S15/25	24.9	28.2	29.4	26.0	23.1	21.4	20.2
PS-S15/26	23.7	24.1	26.3	23.6	21.0	20.9	20.2
PS-S15/27	21.0	21.9	23.1	20.8	20.2	20.1	19.9
PS-G15/30	20.0	22.0	25.1	20.0	17.9	15.2	14.6
PS-G15/33	20.2	21.4	22.8	18.6	16.4	14.6	12.9
PS-G15/34	20.0	21.0	22.0	17.9	15.8	13.9	10.8
PS-G15/35	20.1	21.0	22.9	18.7	14.6	12.5	8.3
PS-G15/36	20.0	21.0	22.1	16.5	12.1	9.1	7.4

Table 4.10 (continued)

b) Elongation at break (%)

Sample	Sample Absorbed Dose						
	Control	50 kGy	100 kGy	150 kGy	200 kGy	250 kGy	300 kGy
PS	5	5	5	4	4	4	4
PS-S5-G5/3	4	4	4	4	4	4	3
PS-S5-G5/6	4	4	4	4	4	4	3
PS-S5-G5/7	4	4	4	4	4	4	3
PS-S5-G5/8	4	4	4	4	4	4	3
PS-S5-G5/9	4	4	4	3	3	3	3
PS-S5-G10/12	3	3	3	3	3	3	3
PS-S5-G10/15	3	3	3	3	3	3	3
PS-S5-G10/16	3	3	3	3	3	3	3
PS-S5-G10/17	3	3	3	3	3	3	3
PS-S5-G10/18	3	3	3	3	3	3	3
PS-S15/21	4	3	3	3	3	3	3
PS-S15/24	3	3	3	3	3	3	3
PS-S15/25	4	4	4	4	3	3	3
PS-S15/26	4	4	4	4	3	3	3
PS-S15/27	3	3	3	3	3	3	3
PS-G15/30	3	3	3	3	3	3	3
PS-G15/33	2	2	2	2	2	2	2
PS-G15/34	3	3	3	2	2	2	2
PS-G15/35	2	2	2	2	2	2	2
PS-G15/36	2	2	2	2	2	2	2

With increasing requirements for polymer wastes management, much attention has been paid to the conversion of macromolecules into small molecules for reuse in polymerization or other petrochemical processes. Pyrolysis is the currently used method for this conversion. Catalysts are often used to promote the degradation efficiency as well as to modify the product's selectivity. On the other hand, high energy irradiations have been applied for both polymer modification and catalyst-treatment. Radiation induced chain scission leads to less thermal stability of some polymers, which is expected to enhance the conversion of polymers to low molecular weight compounds. Additionally, irradiation reduces molecular weights and forms polar

groups in some macromolecular chains. These two effects may allow macromolecules better access to the active sites of the catalyst such as zinc stearate. For our present studies, it seems that the presence of starch and starch-*g*-polystyrene exerts an overwhelming effect over the zinc stearate on promoting degradation. From Table 4.10 and Figures 4.48-4.49, the tensile strength of PS and composite PS sheets are the highest at the total irradiation dose of 100 kGy and decreased with increasing total dose higher than 100 kGy. At total irradiation dose of 100 kGy, it may be attributed that the important effects of gamma rays on PS and composite PS sheets are crosslinking due to their inherent nature, which is analogous to the dimerization of adjacent free radicals to obtain another C-C bond [34]. When an absorbed doses are higher than 100 kGy, tensile strength decreased with increasing total dose. It then suggests that the decreasing of tensile strength be due to the formation of degradation reaction, which is analogous to randomly main chain scission.

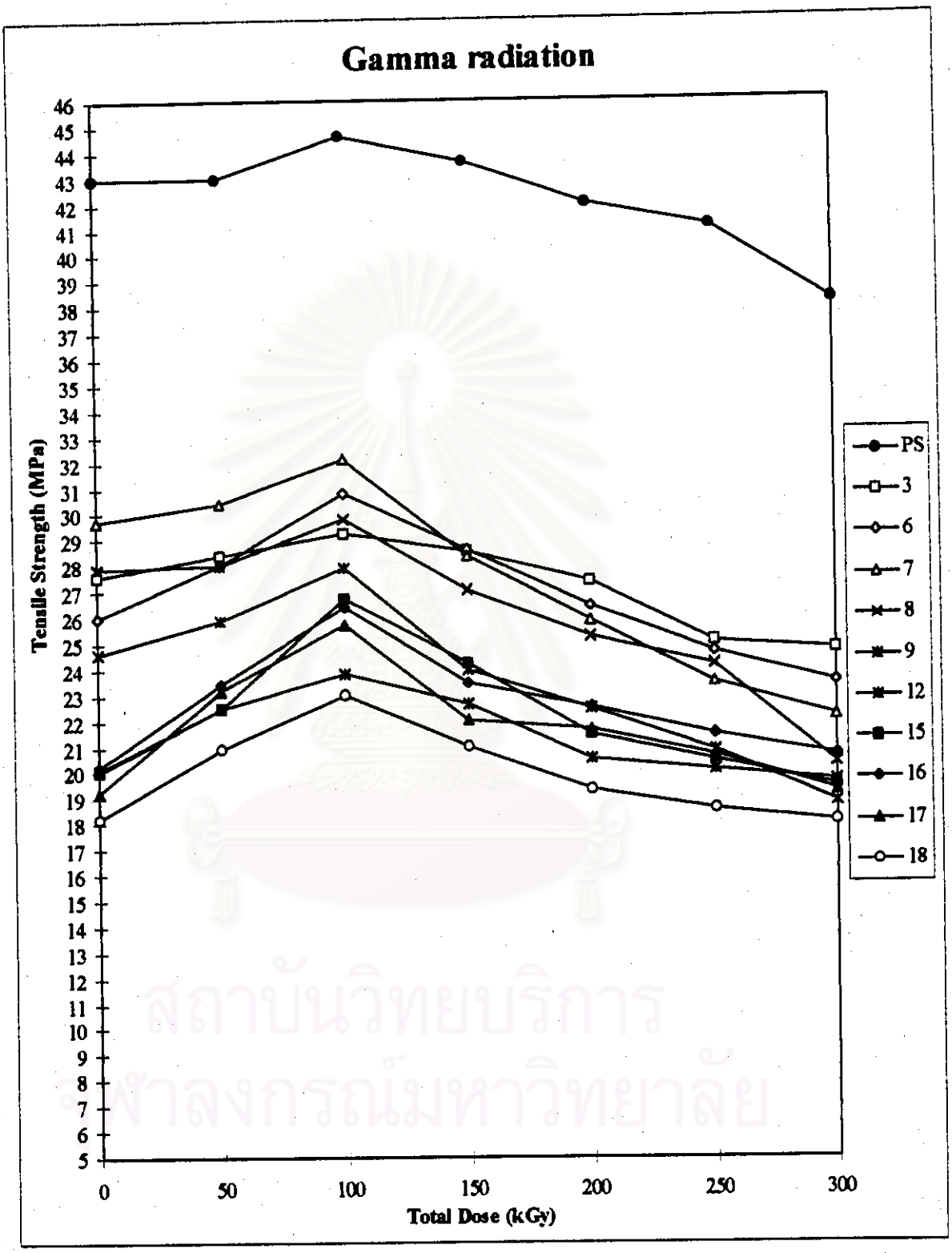

Figure 4.46 Tensile strength of PS, PS-S5-G5 and PS-S5-G10 sheets during gamma irradiation

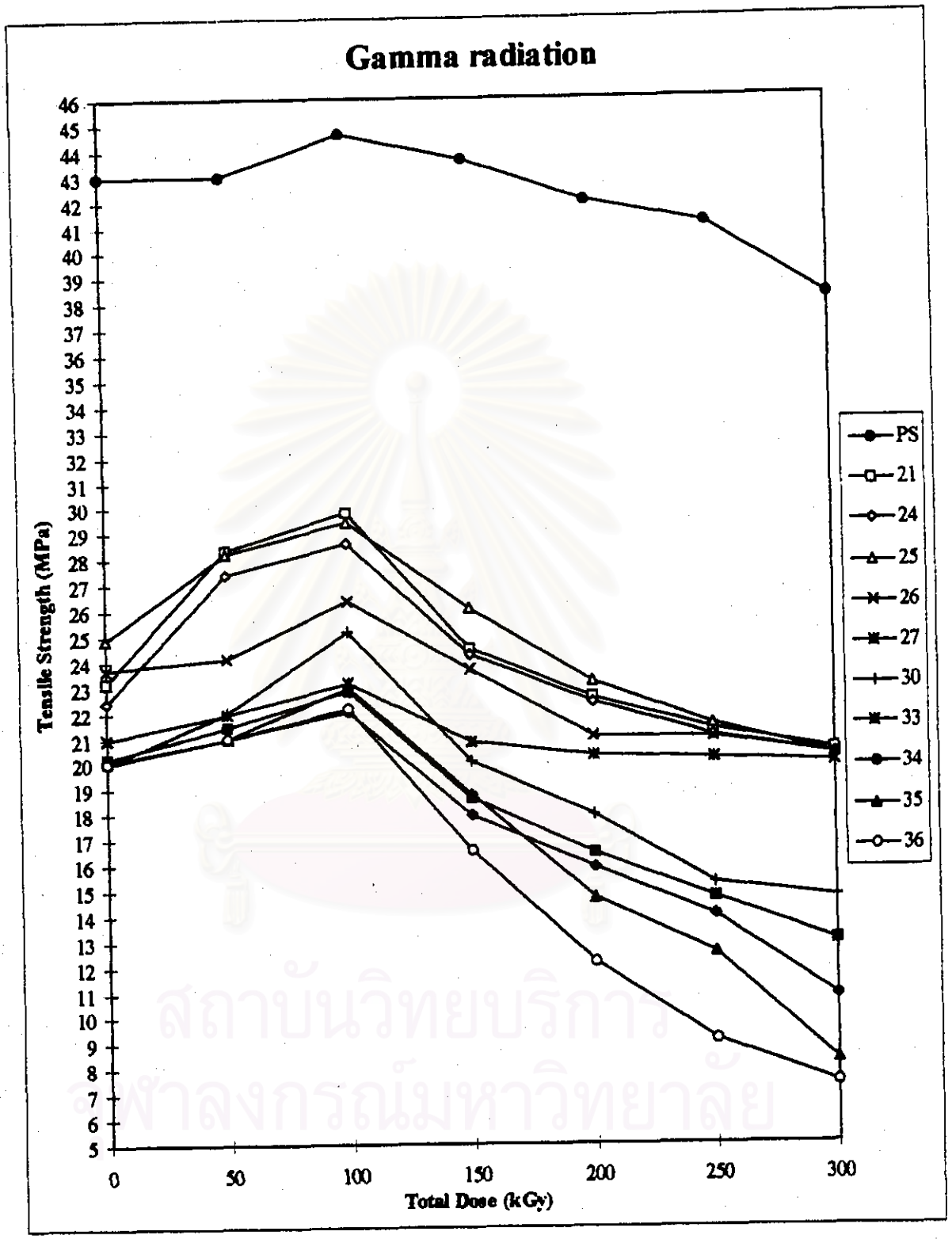

Figure 4.47 Tensile strength of PS, PS-S15 and PS-G15 sheets during gamma irradiation

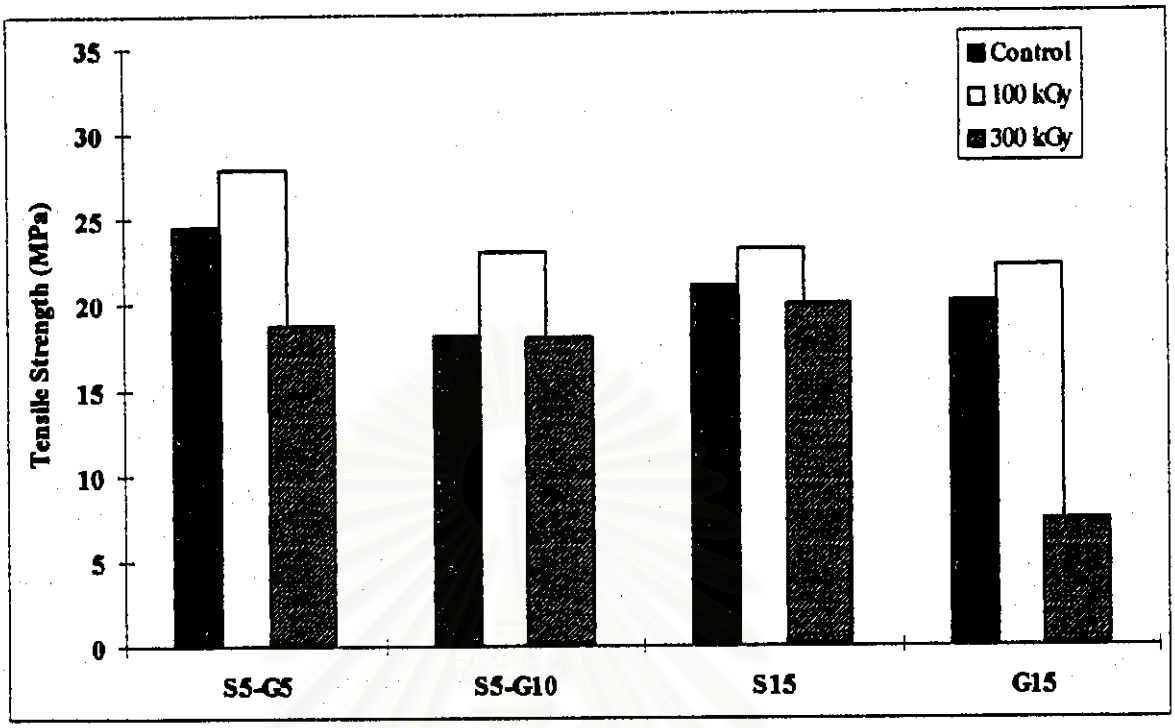

Figure 4.48 Effect of starch and graft copolymer content on tensile strength of composite PS sheets at 8% of soya oil and 0.4% of zinc stearate of gamma irradiation.

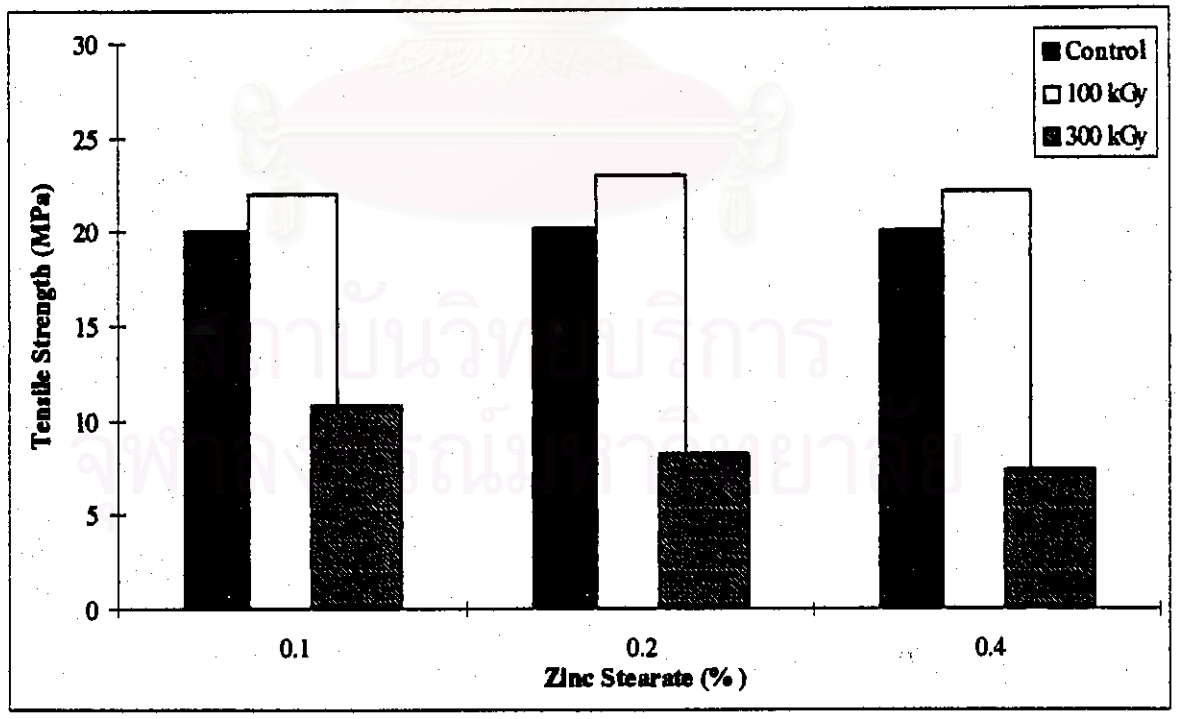

Figure 4.49 Effect of zinc stearate content on tensile strength of PS-G15 sheets at 8% of soya oil of gamma irradiation.

4.3.4.2 Hardness Property Measurements

Shore A hardness measurement for the gamma irradiated PS and PS-G15/36 sheets are shown in Table 4.11 and Figure 4.50.

Table 4.11 Shore A hardness measurements of PS and PS-G15/36 sheets

Sample	Hardness Shore A	
Absorbed Dose*(kGy)	PS	PS-G15/36
Control	40.2	39.5
50	40.3	39.8
100	40.5	40.0
150	38.6	36.2
200	38.4	35.6
250	38.2	35.4
300	38.2	35.2

* At a fixed dose rate of 2.5×10^{-3} kGy/sec.

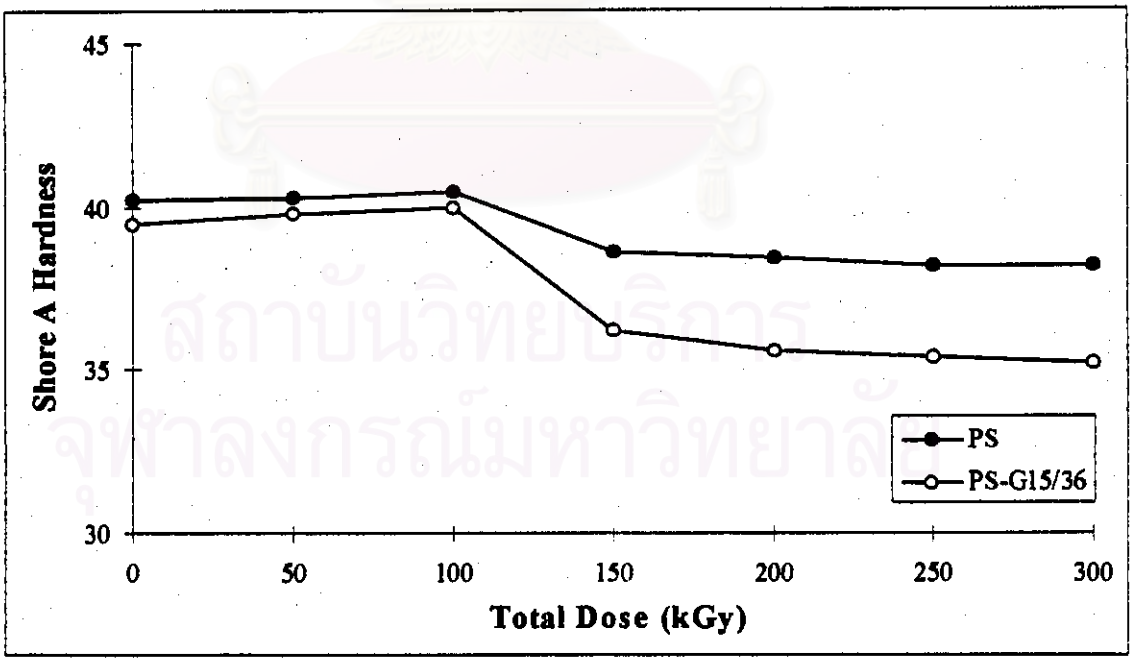

Figure 4.50 Shore A hardness measurements as a function of total irradiation dose for PS and PS-G15/36 sheets

Table 4.11 and Figure 4.50 show that the shore A hardness of PS and PS-G15/36 sheets changes slightly or remains constant at the total irradiation doses of 50-100 kGy. When the total dose is higher than 100 kGy, shore A hardness of PS and PS-G15/36 sheets decreased with increasing total dose, particularly, shore A hardness of PS sheet decreases less than that of PS-G15/36 sheet. The decreasing of hardness beyond the total irradiation dose of 100 kGy, can be explained by the formation of degradation reactions, which is analogous to main chain scission. On the other words, PS-G15/36 degrades more to give a soften plastics or a lower Shore A hardness.

4.3.4.3 Fourier Transform Infrared Absorption Measurements

The FTIR spectra of the PS and PS-G15/36 sheets are given in Figures 4.51 through 4.56. The carbonyl indexes of the samples are shown in Table 4.12 and Figure 4.57.

Table 4.12 Change in the carbonyl indexes of PS and PS-G15/36 sheets at control, 100 and 300 kGy total irradiation dose.

Samples Absorbed Dose* (kGy)	Carbonyl Index (I_{co})	
	PS	PS-G15/36
Control	0.41	0.27
100	0.56	0.29
300	0.61	0.68

* At a fixed dose rate of 2.5×10^{-3} kGy/sec.

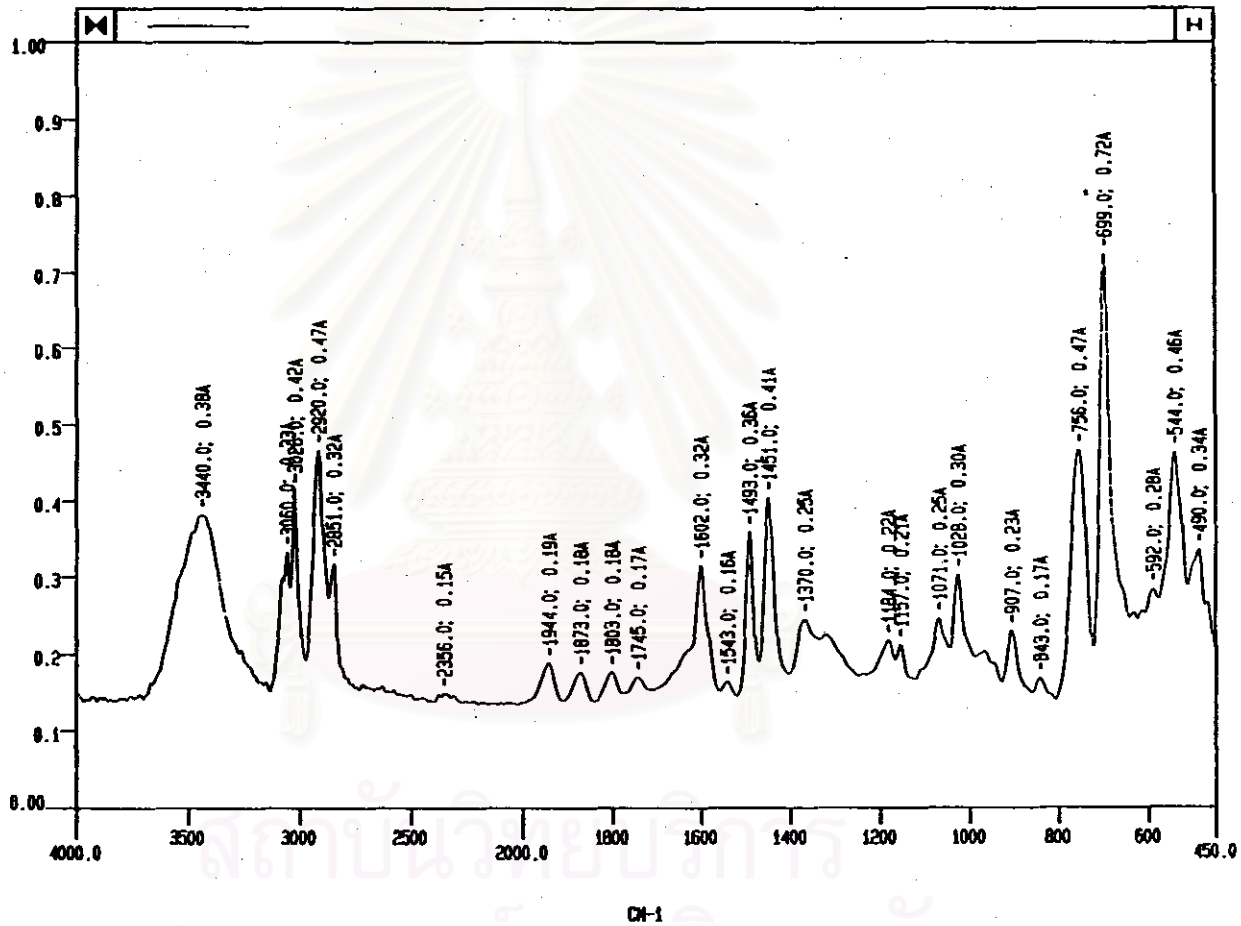

Figure 4.51 Infrared spectrum of Control PS sheet

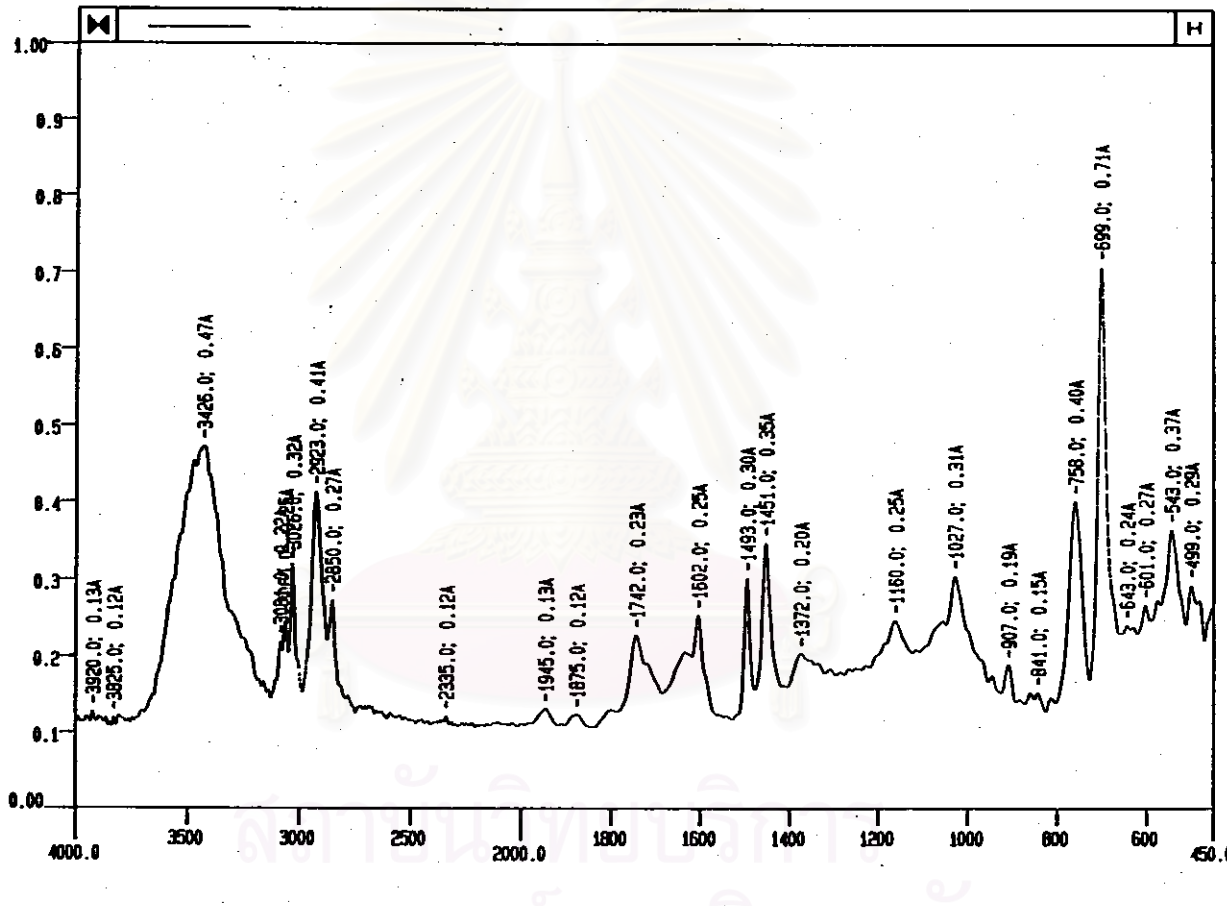

Figure 4.52 Infrared Spectrum of PS sheet at 100 kGy Absorbed Dose

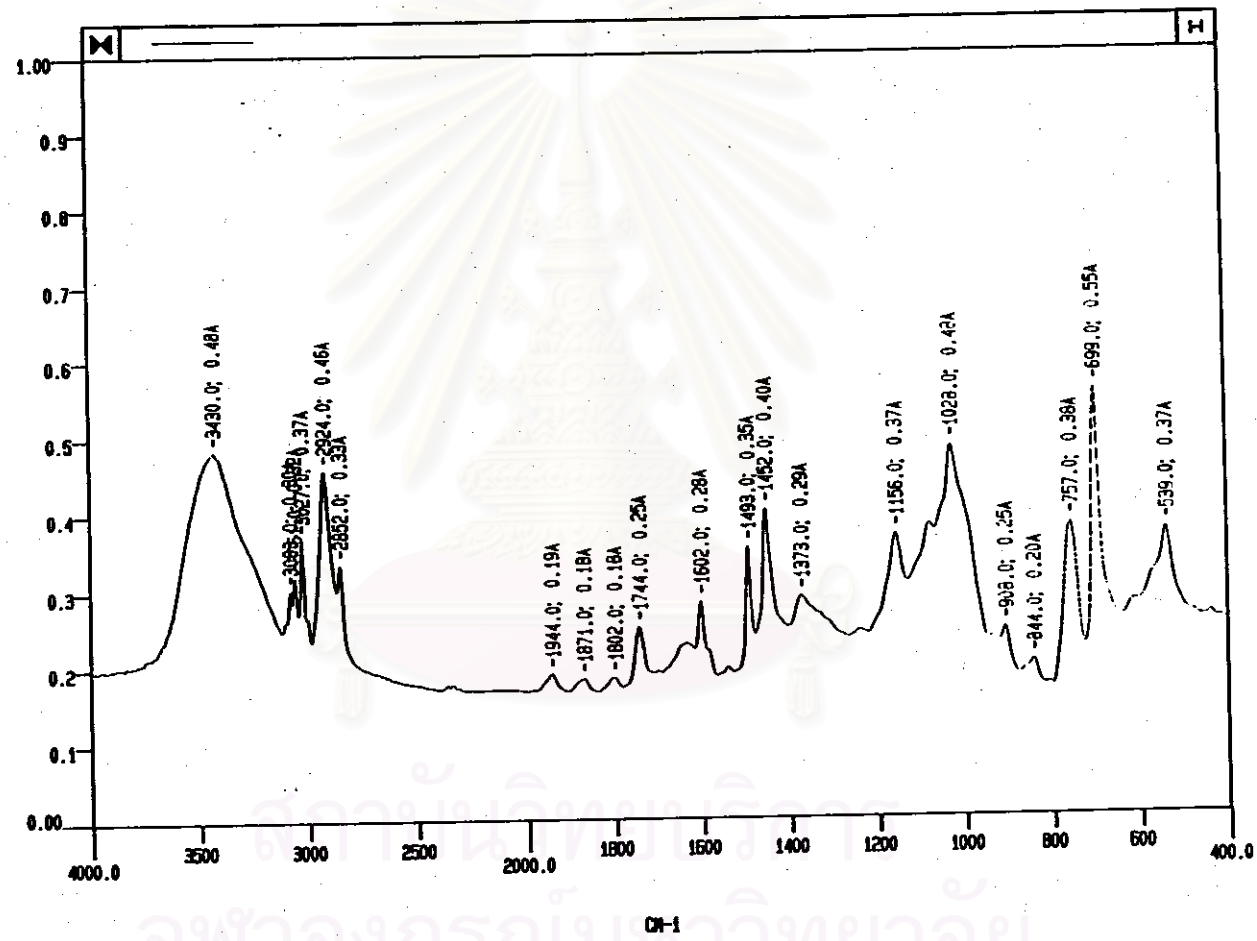

Figure 4.53 Infrared Spectrum of PS sheet at 300 kGy Absorbed Dose

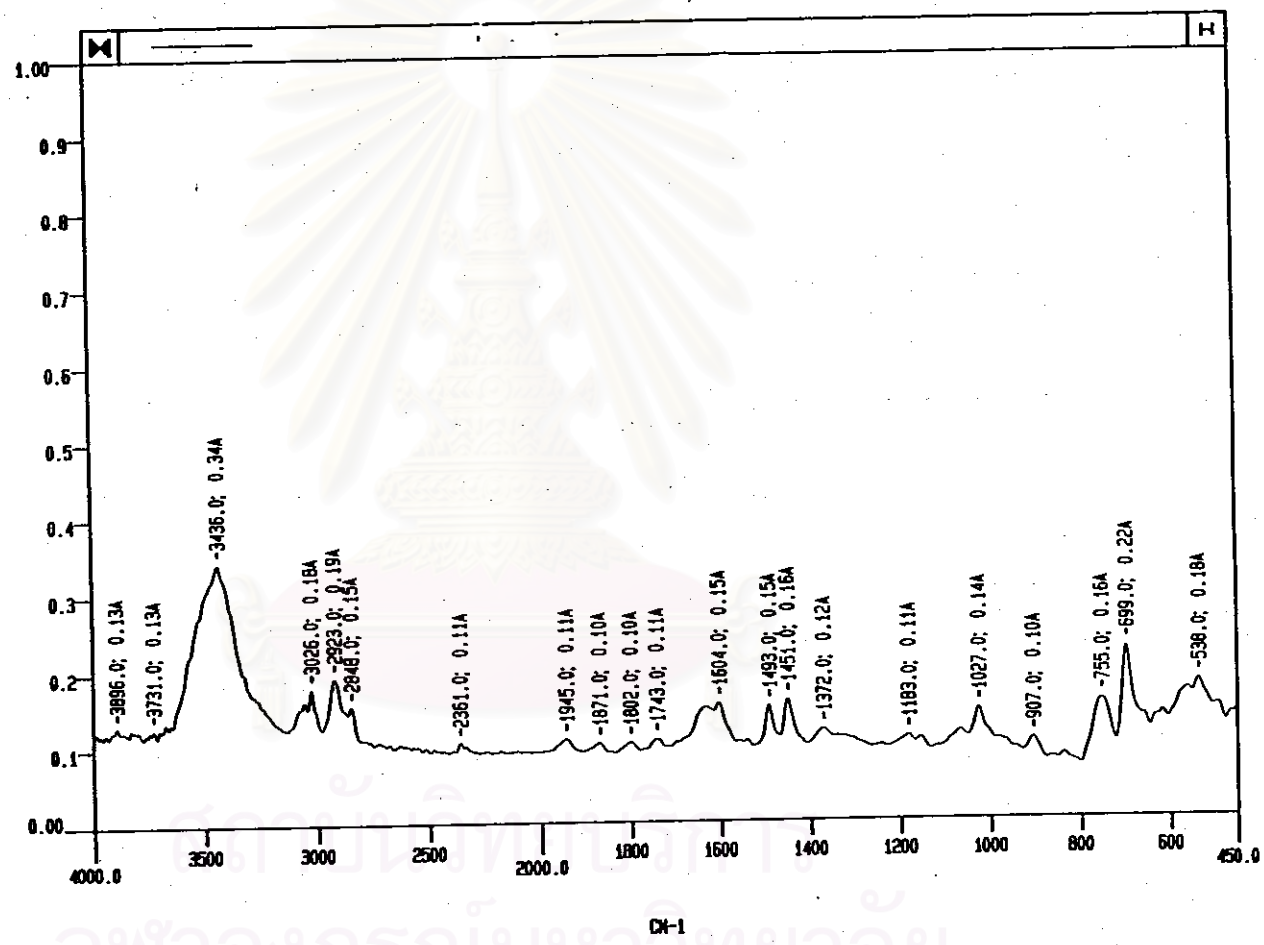

Figure 4.54 Infrared Spectrum of Control PS-G15/36 sheet

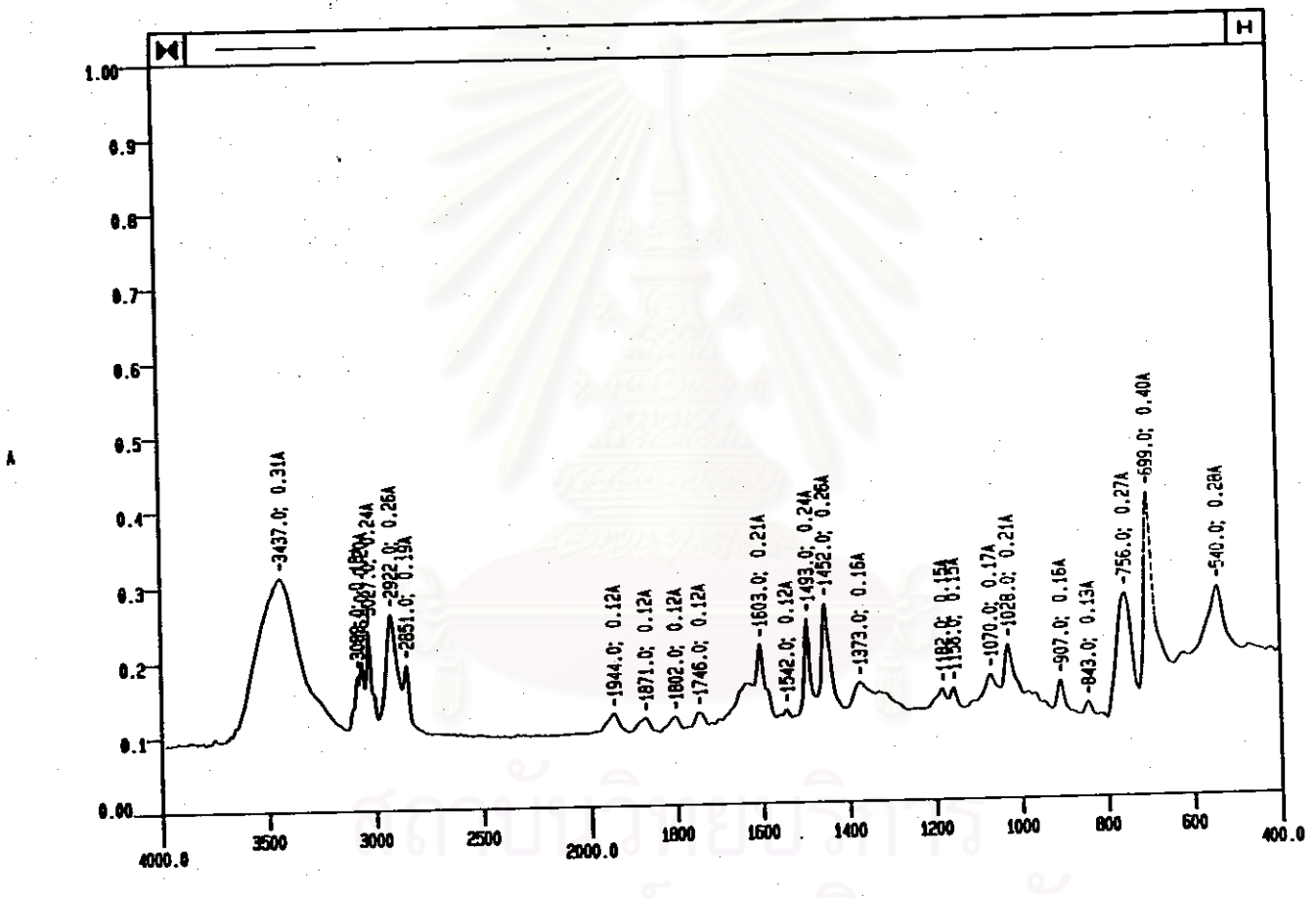

Figure 4.55 Infrared Spectrum of PS-G15/36 sheet at 100 kGy Absorbed Dose

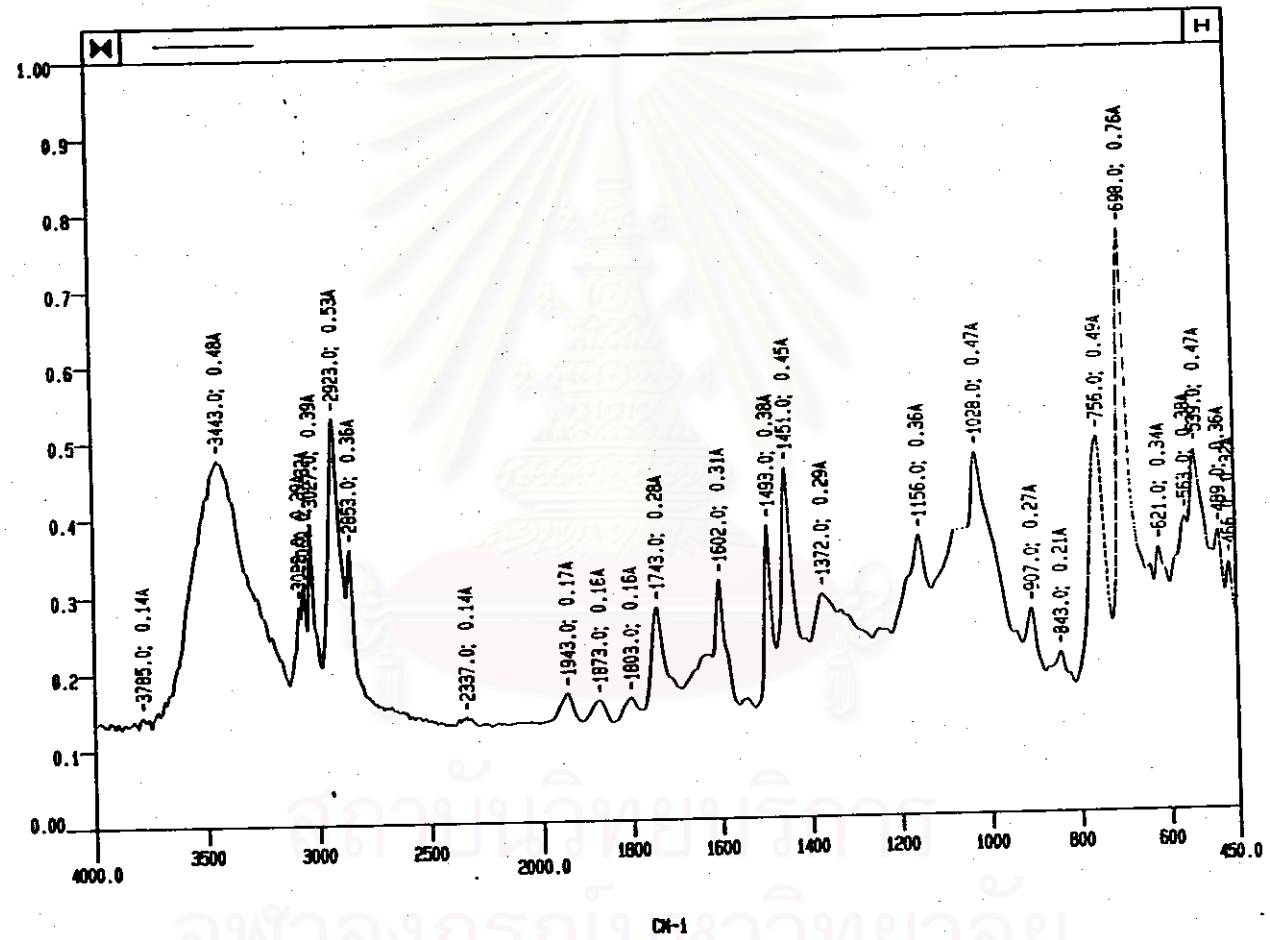

Figure 4.56 Infrared Spectrum of PS-G15/36 sheet at 300 kGy Absorbed Dose

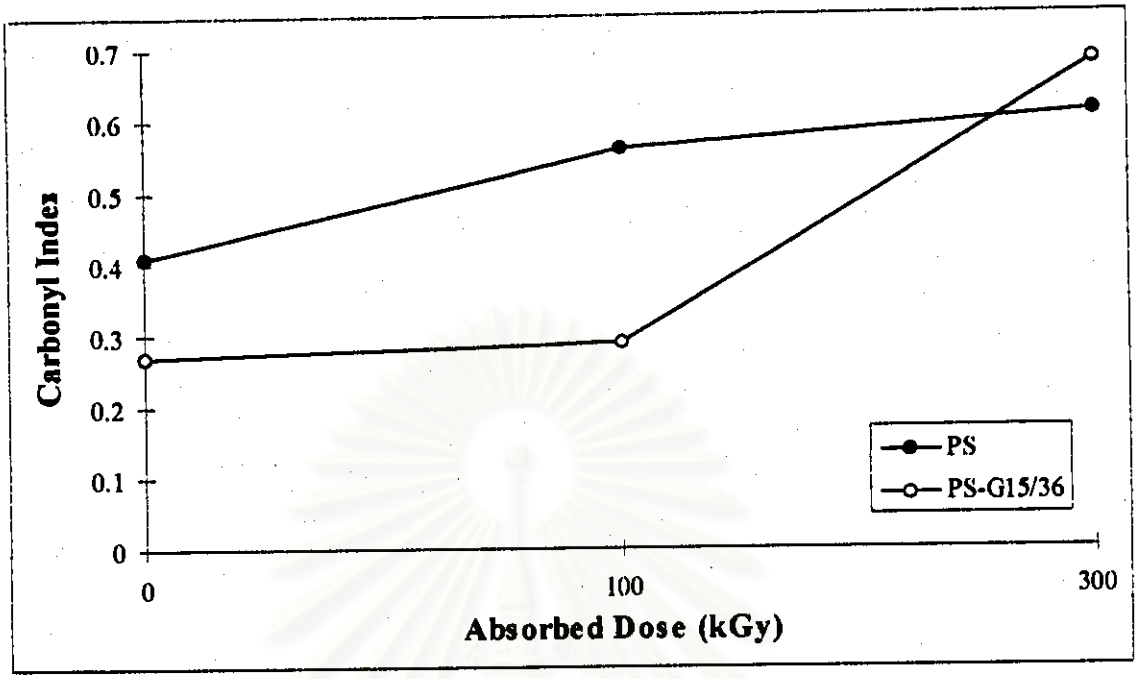

Figure 4.57 The carbonyl indexes of PS and PS-G15/36 sheets at control, 100 and 300 kGy absorbed dose

From Table 4.12 and Figure 4.57, It can be seen that the carbonyl indexes of PS and PS-G15/36 sheets increase linearly with increasing absorbed dose. Particularly, the carbonyl indexes of zinc stearate containing PS-G15/36 sheets are higher than PS sheets. These can be explained by the formation of degradation reaction (see eqs 4.5-4.12), which results in the main chain scission, leading to the formation of carbonyl compound.

4.3.4.4 Molecular Weight Measurements

The data of average molecular weights and molecular weight distribution of PS and PS-G15/36 sheets during gamma radiation are shown in Table 4.13 and Figure 4.58, respectively.

Table 4.13 Average molecular weights and molecular weight distribution of PS and PS-G15/36 sheets during gamma irradiation

a) PS sheet

Data	Samples Absorbed Dose*		
	Control	100 kGy	300 kGy
$\overline{M}w$	484,040	435,568	425,319
$\overline{M}n$	10,754	2,993	3,598
$\overline{M}z$	1,171,640	28,245,110	1,955,141
$\overline{M}v$	424,063	241,812	334,452
$\overline{M}w / \overline{M}n$	45.01	145.52	118.20
$\overline{M}z / \overline{M}w$	2.42	64.85	4.60
$\overline{M}v / \overline{M}n$	39.43	80.79	92.94
I. VISC	14,376.74	9,381.16	12,003.46

b) PS-G15/36 sheet

Data	Samples Absorbed Dose*		
	Control	100 kGy	300 kGy
$\overline{M}w$	395,008	377,263	328,835
$\overline{M}n$	6,823	6,159	1,567
$\overline{M}_z$	924,450	897,600	23,607,450
$\overline{M}v$	344,981	328,340	190,372
$\overline{M}w / \overline{M}n$	57.90	61.25	209.80
$\overline{M}z / \overline{M}w$	2.34	2.38	71.79
$\overline{M}v / \overline{M}n$	50.56	53.31	121.46
I. VISC	12,289.58	11,836.37	7,821.90

*At a fixed dose rate of 2.5×10^{-3} kGy/sec.

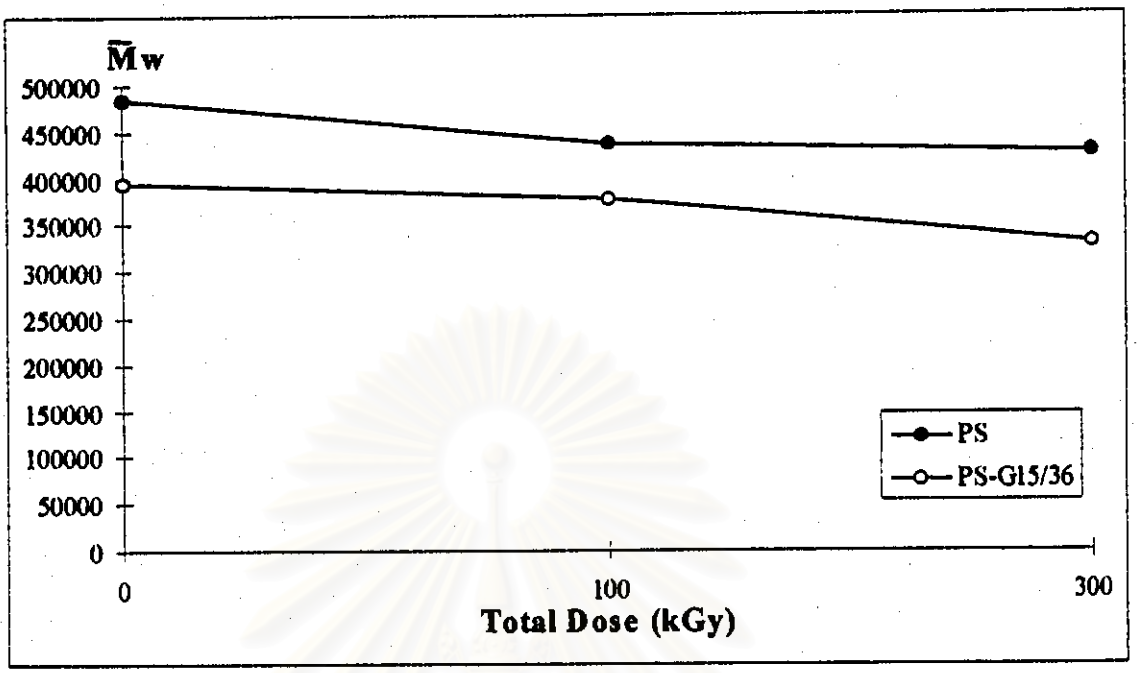

Figure 4.58 Weight-average molecular weights of PS and PS-G15/36 sheets during gamma irradiation

The changes of weight-average molecular weight of PS and PS-G15/36 sheets at various total irradiation doses (at a fixed dose rate of 2.5×10^{-3} kGy/sec) are shown in Figure 4.58. At lower total irradiation doses than 100 kGy, it can be seen that the molecular weight of PS and PS-G15/36 sheets decrease with as low rate. Beyond the absorbed dose of 100 kGy, the molecular weights of all samples decrease rapidly with absorbed dose, especially the molecular weights of PS sample decreases slower than that PS-G15/36 sample. The decreasing of molecular weight can be described by the oxidative degradation of the sample as in agreement with the FTIR absorption measurements. Considering the values of $\bar{M}w/\bar{M}n$ of the PS control sheet and PS-G15/36 sheet, the latter has a wider polydispersity ($\bar{M}w/\bar{M}n$ = 209.8 vs 118.2). In comparison with those of the outdoor exposure, gamma irradiation imposes more effect on PS-G15/36 sheet because it contains all the degradation promoters.

4.3.4.5 Thermal Property Measurements

Figures 4.59-4.62 show the TGA thermograms of PS and PS-G15/36 sheet at various total irradiation doses. The initial percent weight loss of PS sheet was 99.95%, at 300 kGy total irradiation dose, the percent weight loss became 99.58%. The TGA thermograms of PS-G15/36 sheet as a control and 300 kGy total irradiation dose show two steps of weight loss, the first one involving the decomposition of cassava starch and the second one for polystyrene plastic. The percent weight loss of control PS-G15/36 sheet was 97.63%, but at 300 kGy total irradiation dose, the percent weight loss became 97.14%. It was found that percent weight loss of PS and PS-G15/36 sheet changed slightly or even unchanged under gamma irradiation and the result indicates that PS and PS-G15/36 sheet degrades slowly under gamma irradiation.

From equation 4.13, the initial activation energy of PS sheet was 201.3 $kJ.mol^{-1}$, at 300 kGy total irradiation dose, the activation energy became 239.0 $kJ.mol^{-1}$. For PS-G15/36 sheet, the initial activation energy was 97.8 $kJ.mol^{-1}$, at 300 kGy total irradiation dose, the activation energy became 104.8 $kJ.mol^{-1}$. It was found that the activation energies of PS and PS-G15/36 sheets at 300 kGy irradiation dose are higher than that of the PS and PS-G15/36 sheets at control, it may be attributed that the important effects of gamma rays on PS and PS-G15/36 sheets are crosslinking.

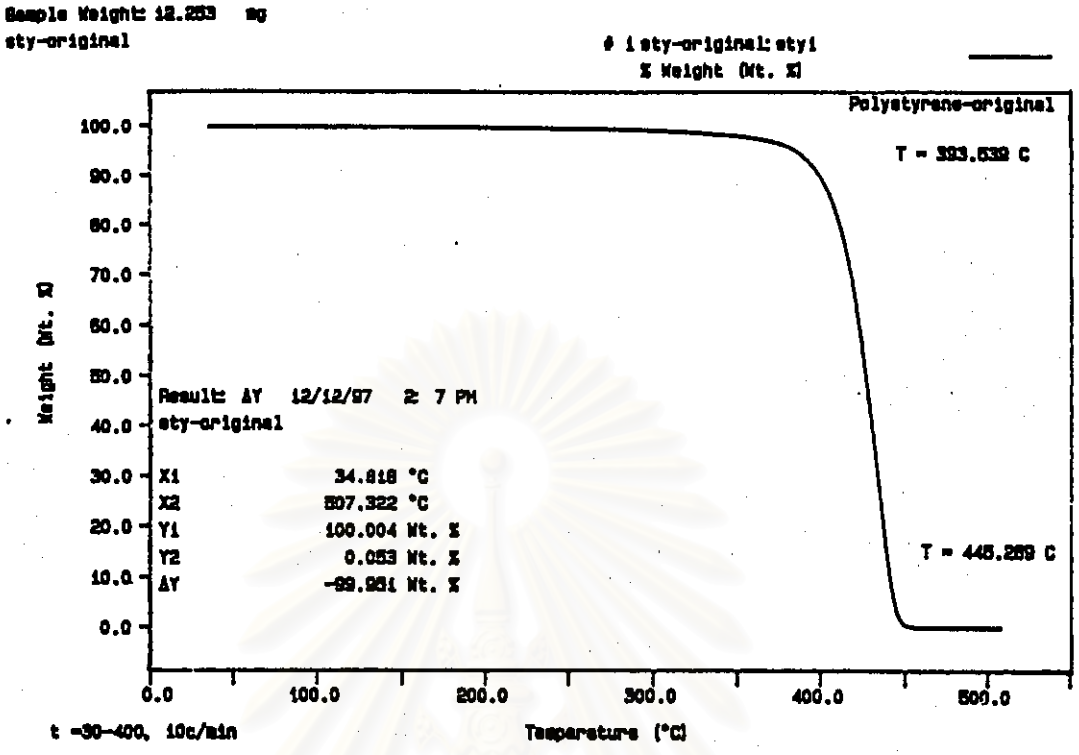

Figure 4.59 TGA thermogram of control PS sheet

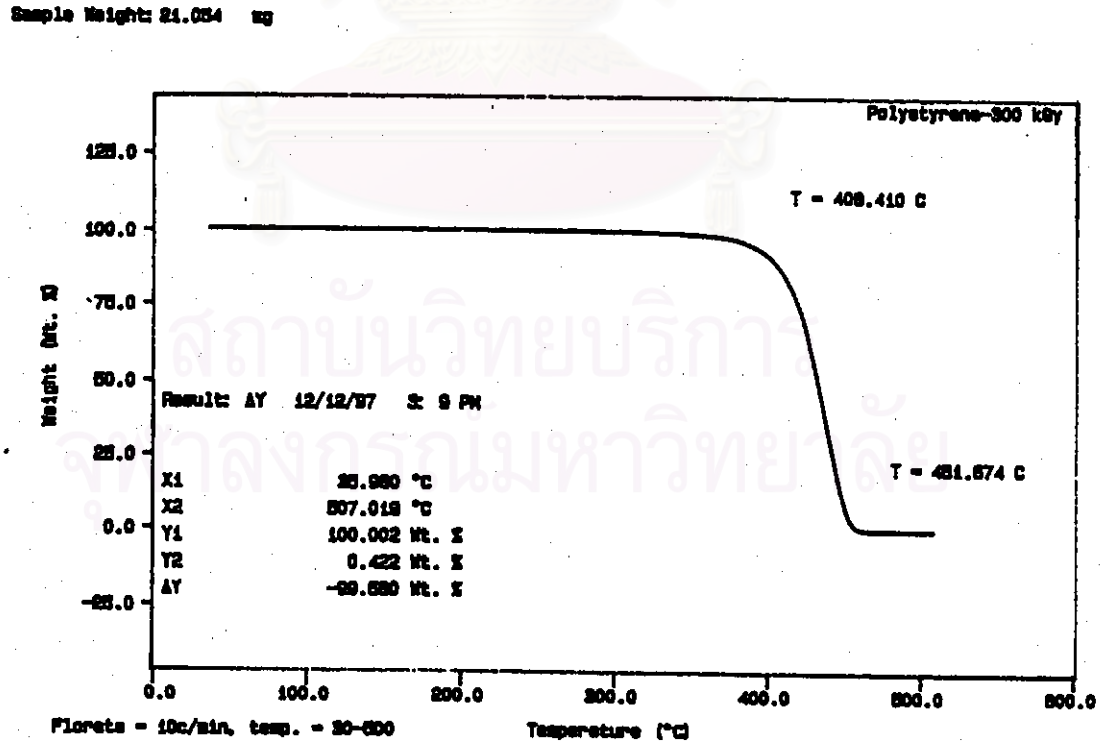

Figure 4.60 TGA thermogram of PS sheet at 300 kGy absorbed dose

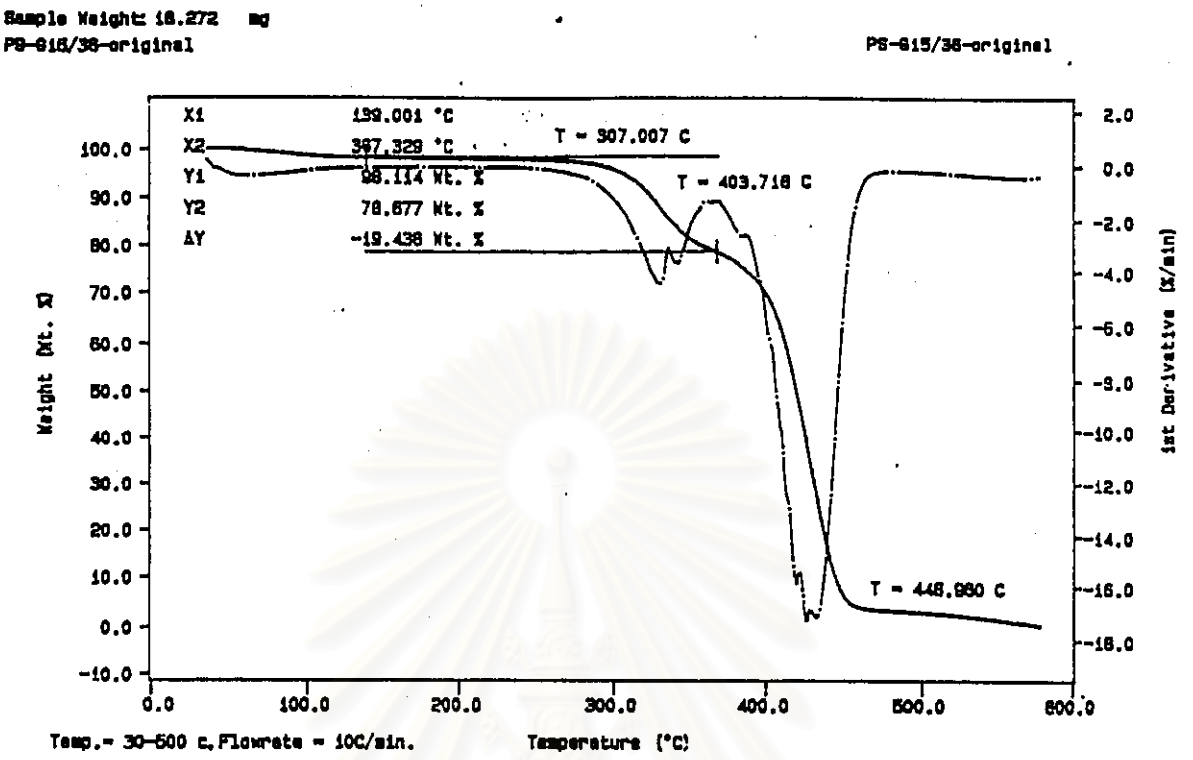

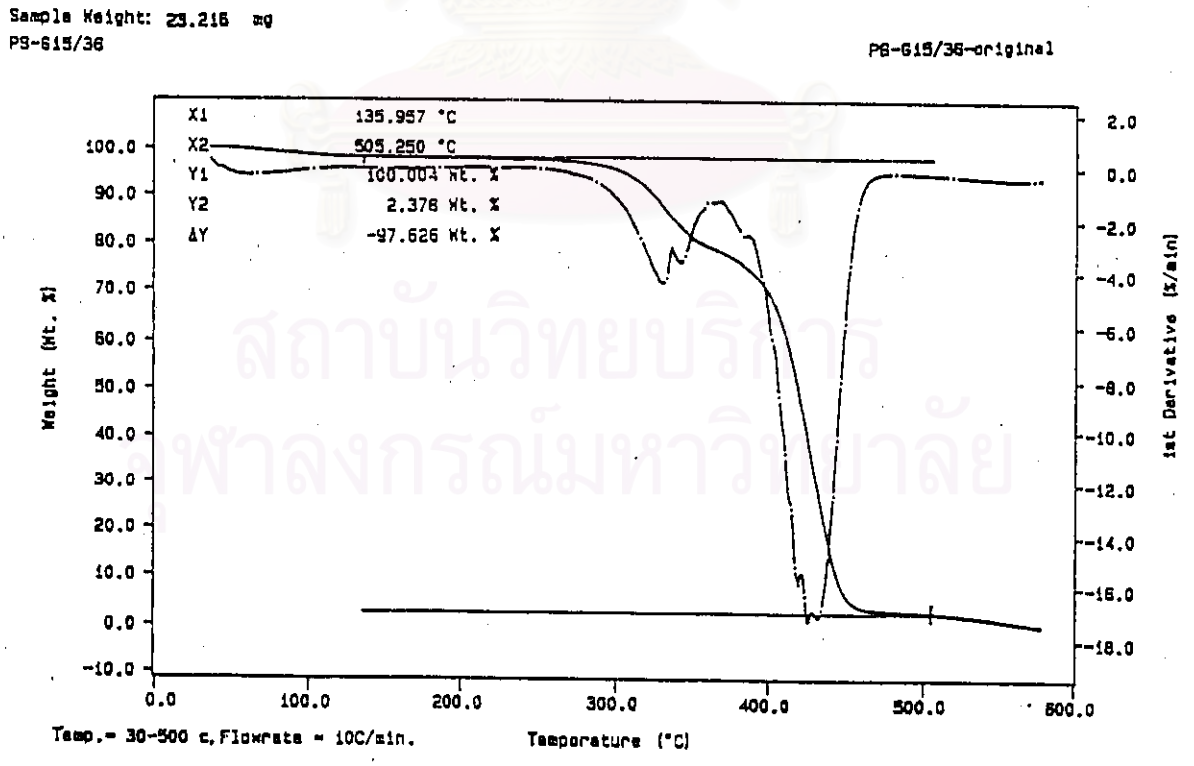

Figure 4.61 TGA thermograms of control PS-G15/36 sheet

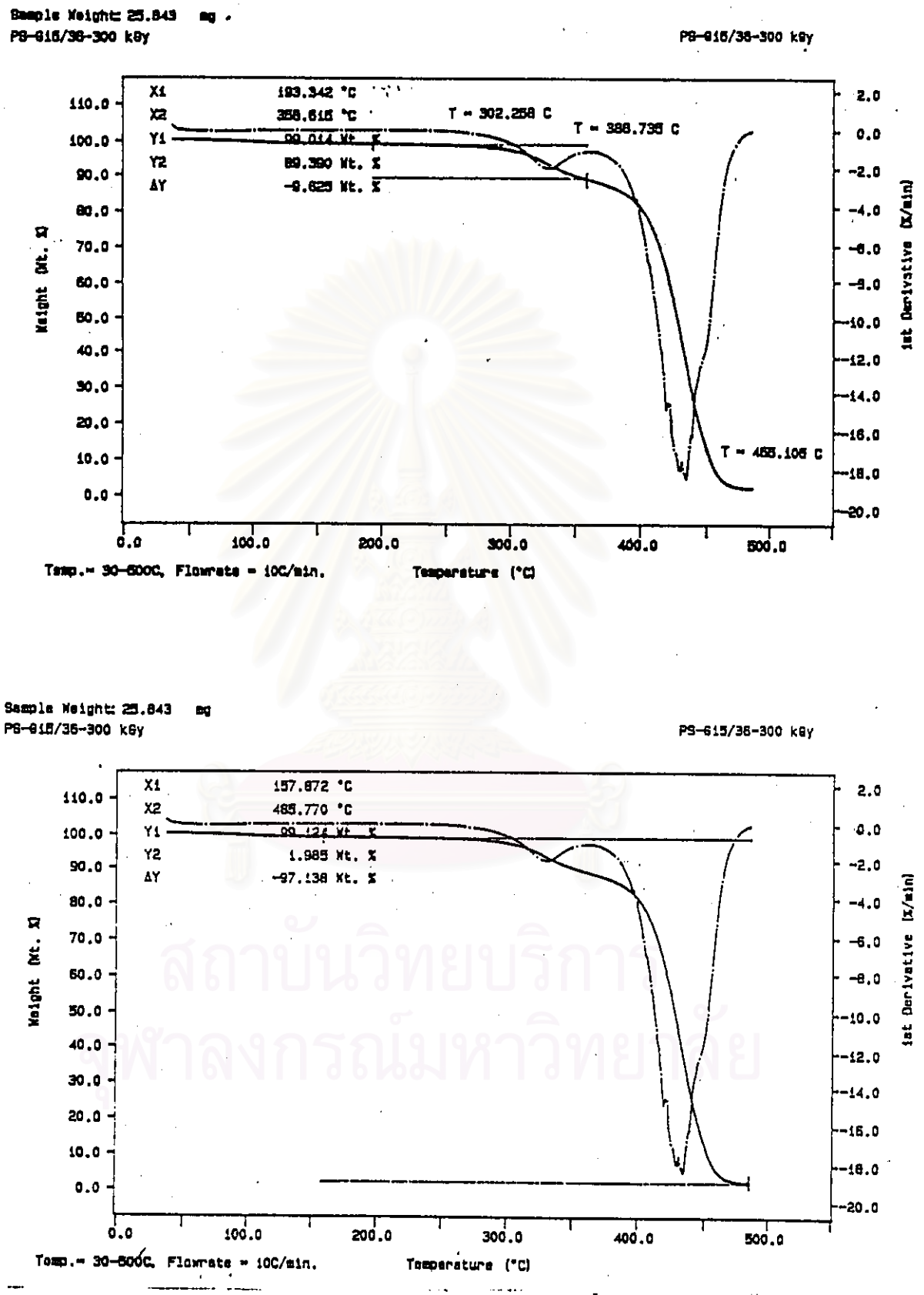

Figure 4.62 TGA thermograms of PS-G15/36 sheet at 300 kGy absorbed dose

4.3.5 UV Irradiation Test

4.3.5.1 Hardness Property Measurements

Shore A hardness measurements for the UV irradiation of the PS and PS-G15/32 sheets are shown in Table 4.14 and Figure 4.63.

Table 4.14 Shore A hardness measurements of the PS and PS-G15/36 sheets

Sample Irradiation Time (hours)	Total Dose* (MJ/m^2)	Hardness Shore A	
		PS	PS-G15/36
0	0	40.2	39.5
0.5	0.03	39.6	37.6
5	0.32	36.8	36.2
10	0.63	36.0	34.0
21	1.32	36.0	32.0

* Measured by EIT radiometer, model power puck

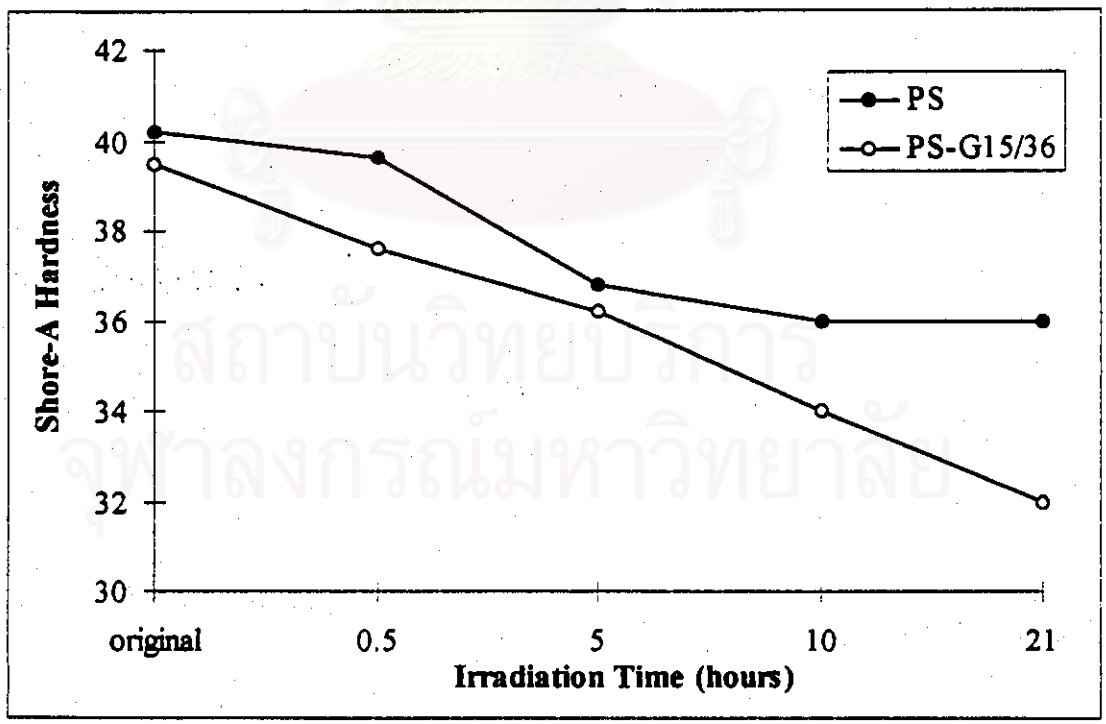

Figure 4.63 Shore A hardness measurements as a function of UV-irradiation time for PS and PS-G15/36 sheets

Table 4.14 and Figure 4.63 show that the shore A hardness of PS and PS-G15/36 sheets decreases with increasing UV irradiation time, particularly the hardness of PS sheet decreases rather slowly than that of PS-G15/36 sheet, i.e. the initial hardnesses of PS and PS-G15/36 sheets were 40.2 and 39.5, respectively. After 21-hour UV irradiation time, the hardness of the two samples became 36.0 and 32.0, respectively. The decreasing of shore A hardness can be described by the formation of degradation reaction to result in degraded materials lower molecular weights.

4.3.5.2 Fourier Transform Infrared Absorption Measurements

The FTIR spectra of the PS and PS-G15/36 sheets under UV irradiation are given in Figures 4.64 through 4.69. The carbonyl indexes of the samples are shown in Table 4.15 and Figure 4.70.

Table 4.15 Change in the carbonyl indexes of PS and PS-G15/36 sheets at control, 10 and 21-hour UV irradiation

Samples Irradiation Time (hours)	Carbonyl Index (I_{co})	
	PS	PS-G15/36
Control	0.41	0.27
10	0.41	0.32
21	0.44	0.39

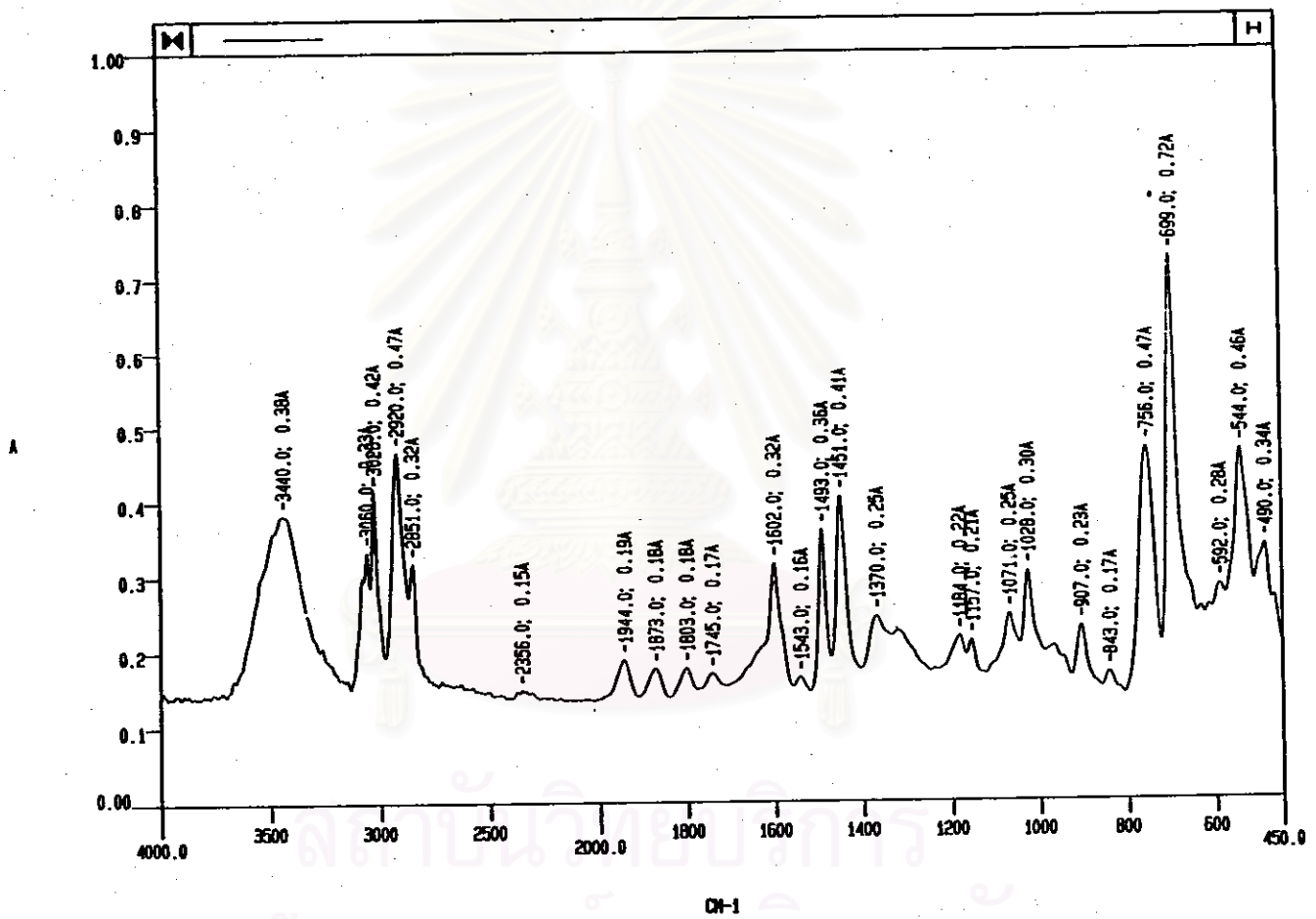

Figure 4.64 Infrared spectrum of Control PS sheet

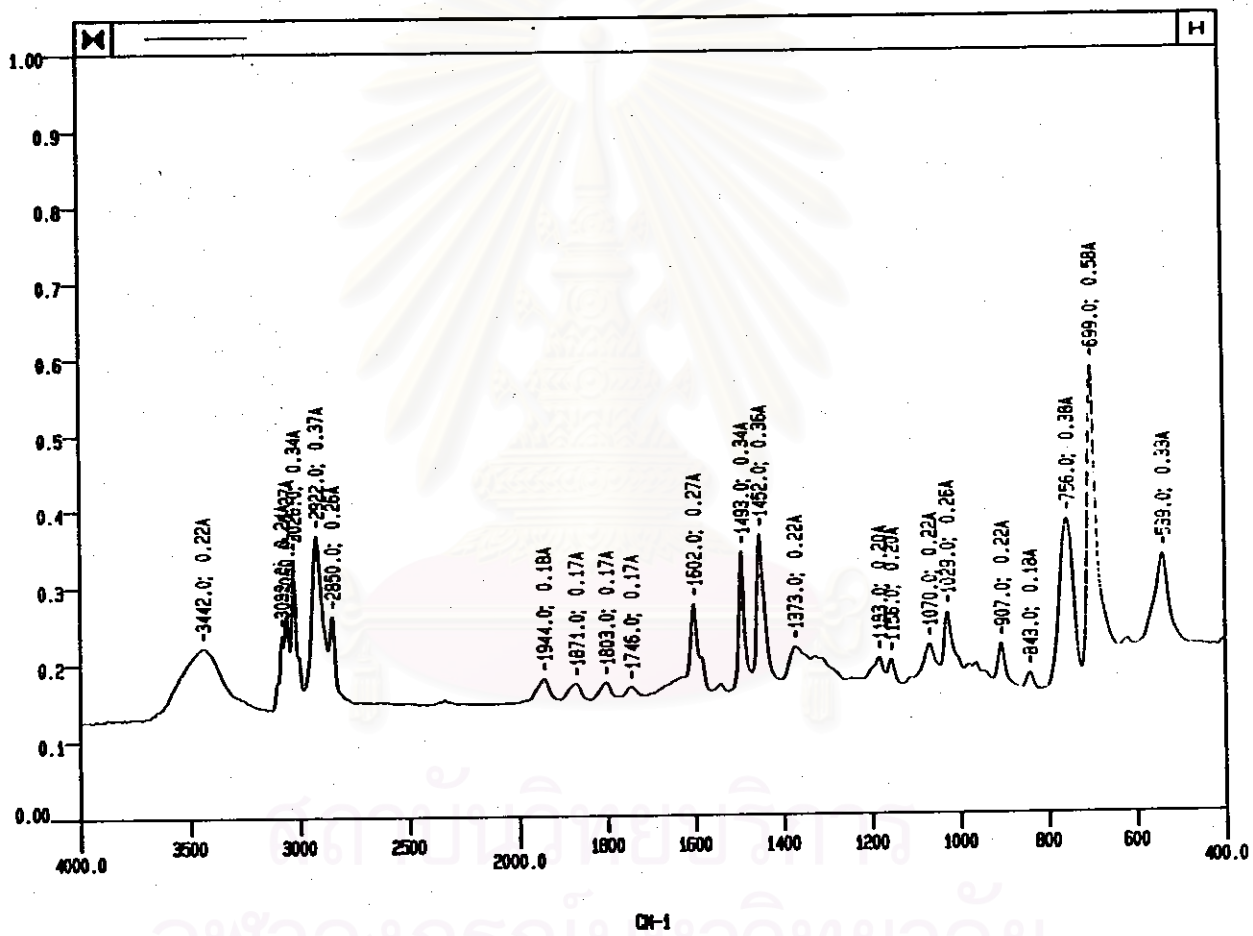

Figure 4.65 Infrared Spectrum of PS sheet at 10-Hour Irradiation Time

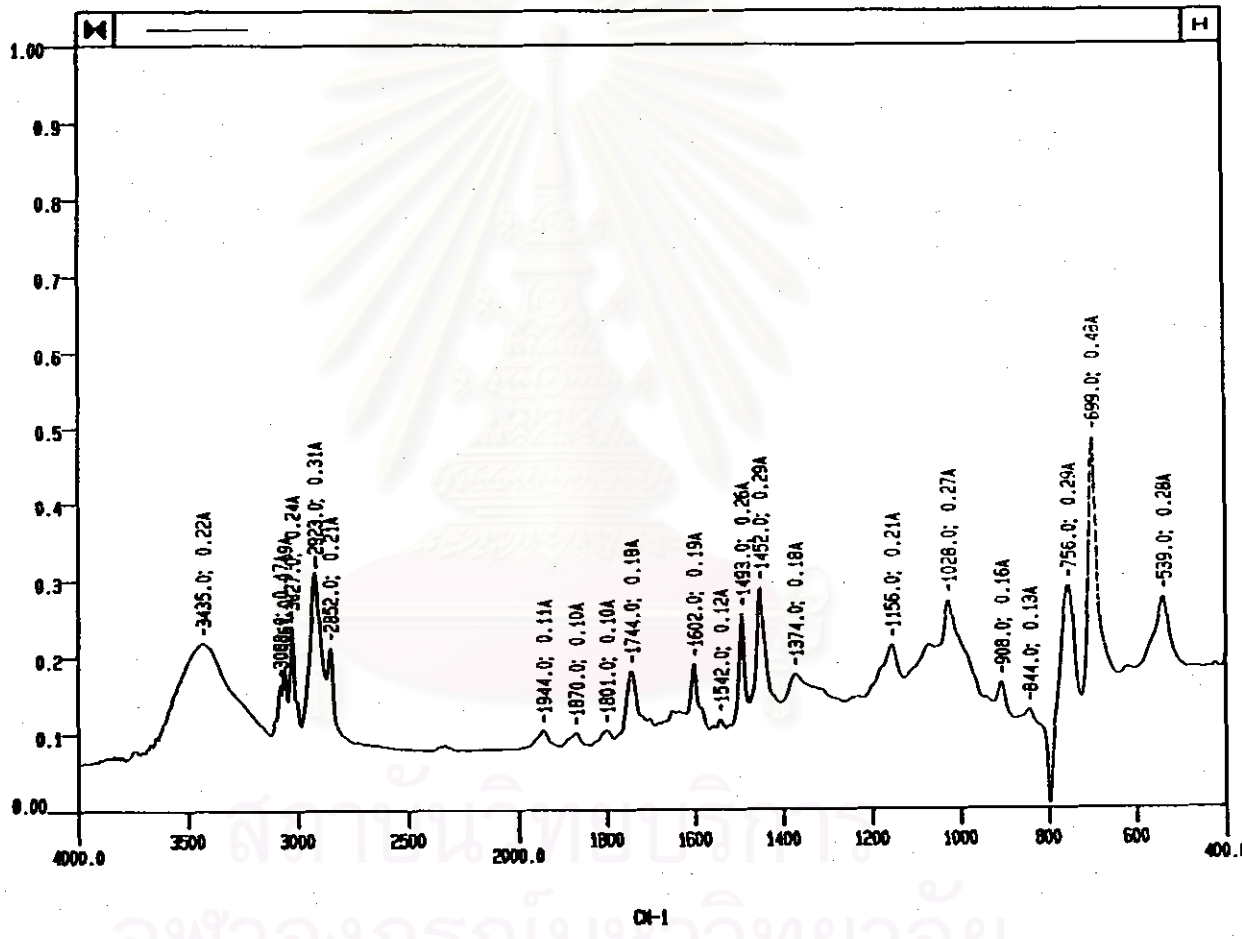

Figure 4.66 Infrared Spectrum of PS sheet at 21-Hour Irradiation Time

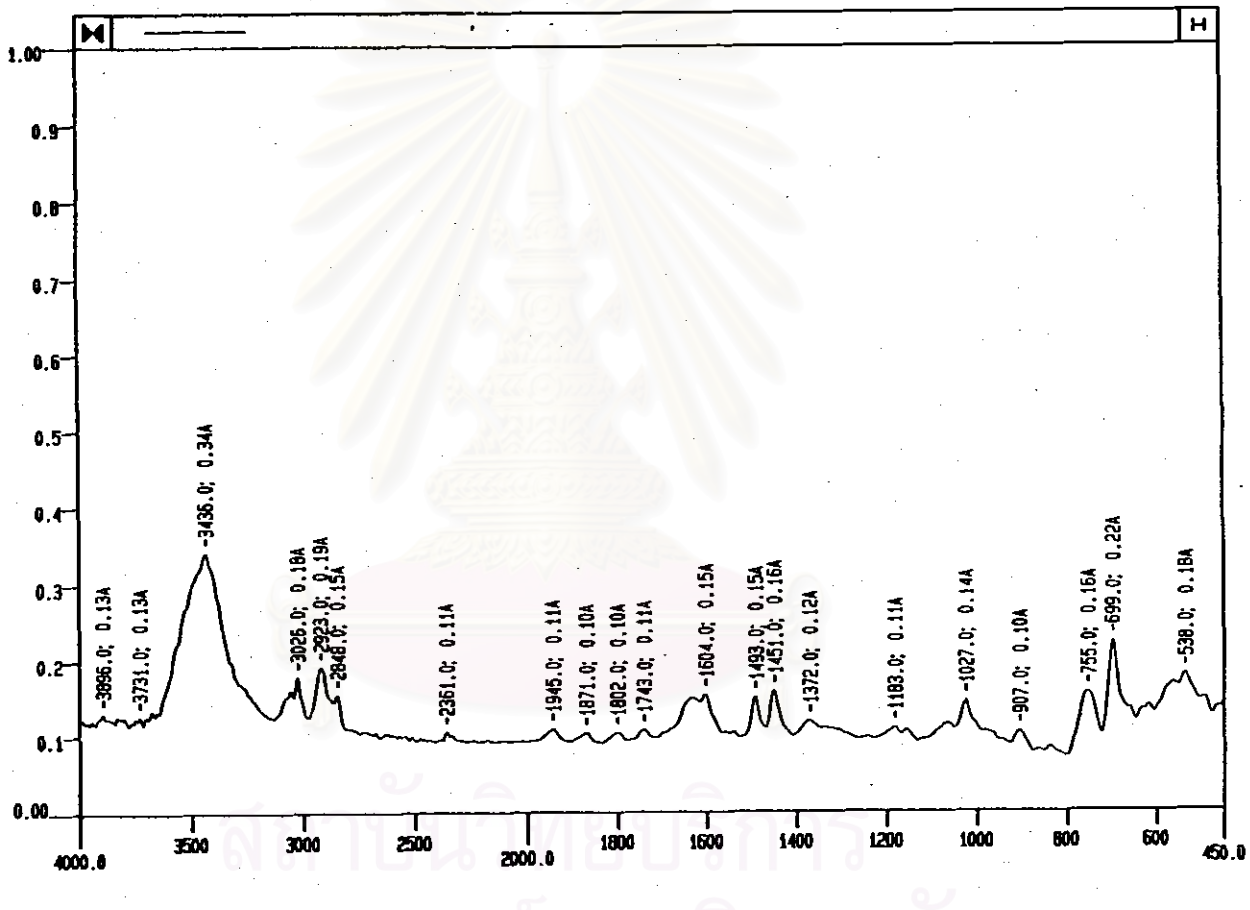

Figure 4.67 Infrared Spectrum of Control PS-G15/36 sheet

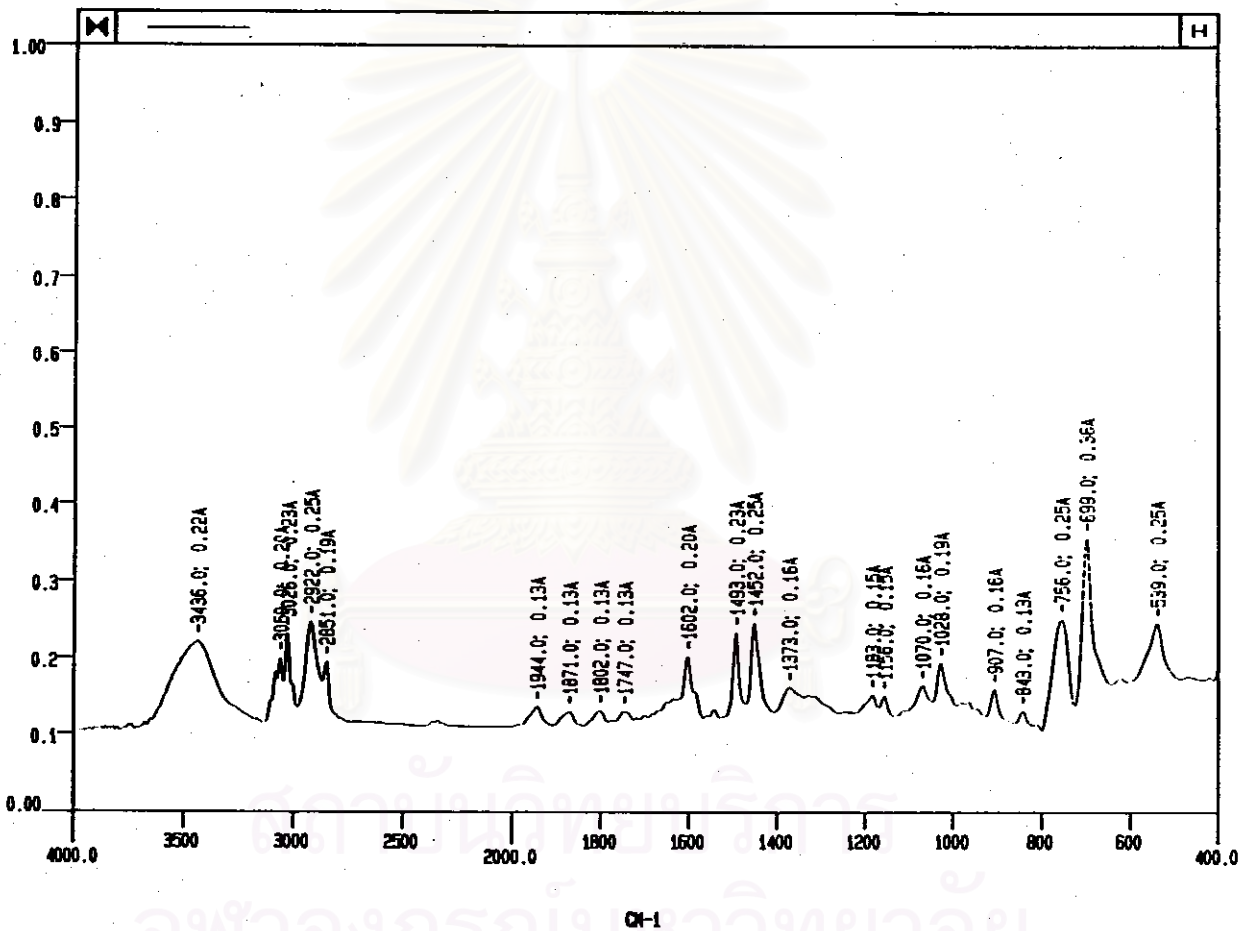

Figure 4.68 Infrared Spectrum of PS-G15/36 sheet at 10-Hour Irradiation Time

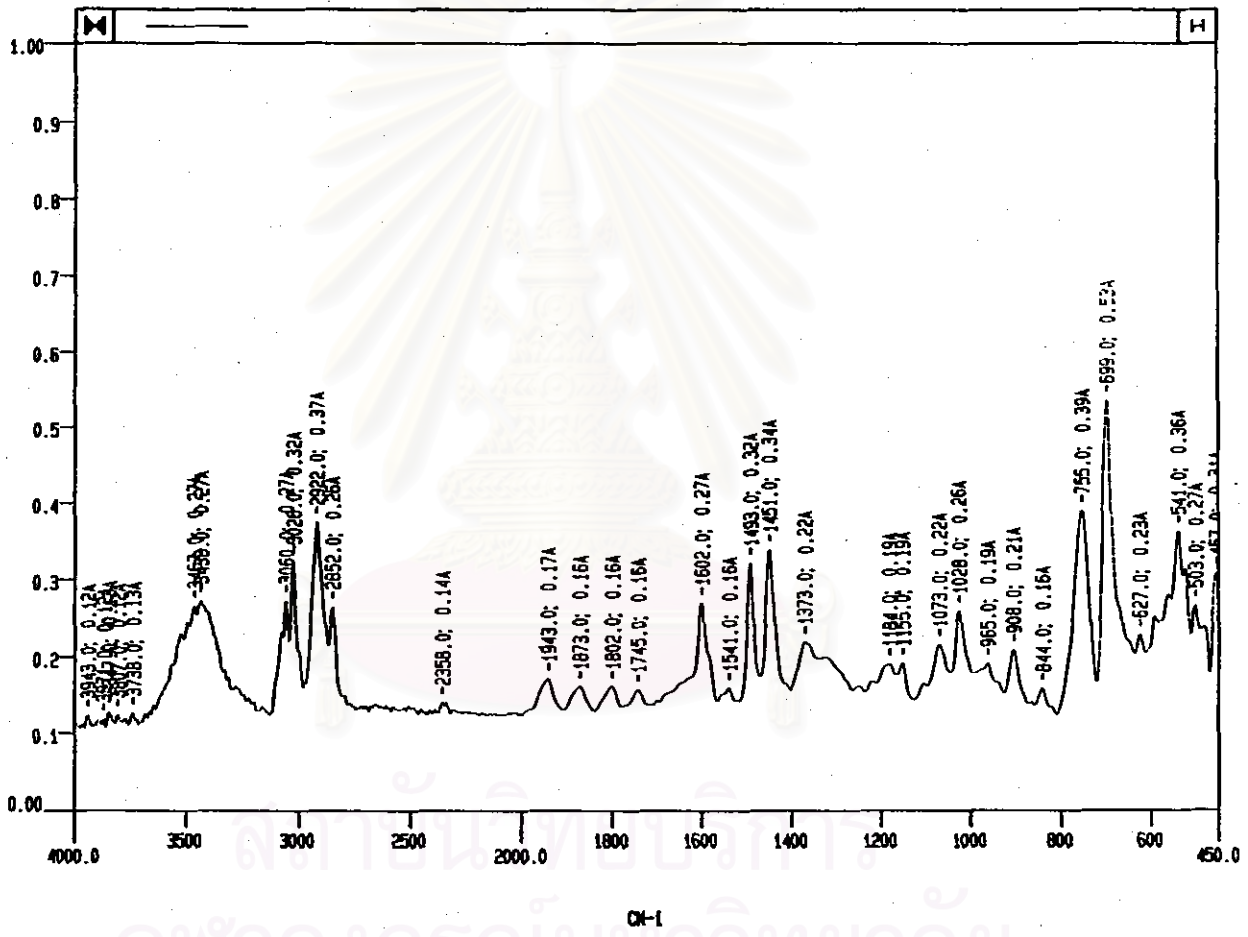

Figure 4.69 Infrared Spectrum of PS-G15/36 sheet at 21-Hour Irradiation Time

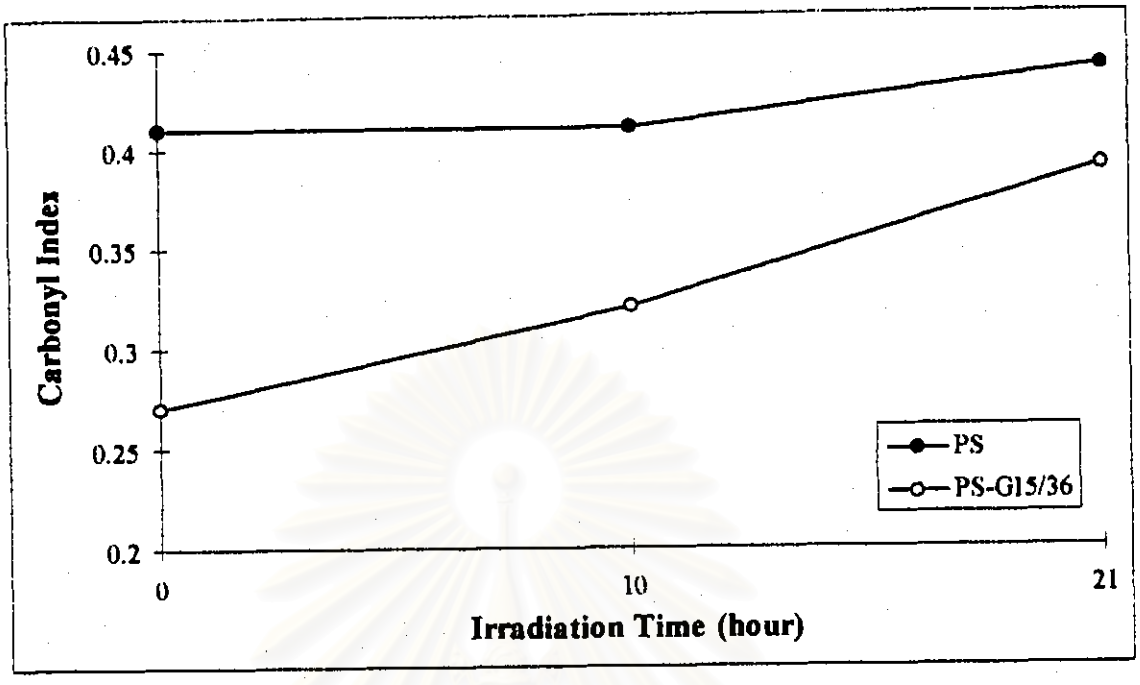

Figure 4.70 The carbonyl indexes of PS and PS-G15/36 sheets at control, 10 and 21-hour UV irradiation time

From Table 4.15 and Figure 4.70, it can be seen that the carbonyl indexes of PS and PS-G15/36 sheets increased with increasing irradiation time, particularly, the carbonyl indexes of PS-G15/36 sheets are higher than PS sheets.

4.3.5.3 Molecular Weight Measurements

The data of average molecular weights and molecular weight distribution of PS and PS-G15/36 sheets during UV irradiation are shown in Table 4.16 and Figure 4.71, respectively.

Table 4.16 Average molecular weights and molecular weight distribution of PS and PS-G15/36 sheets during UV irradiation

a) PS sheet

Data	Samples Irradiation Time		
	Control	10 hours	21 hours
$\overline{M}w$	484,040	407,692	403,652
$\overline{M}n$	10,754	3,654	1,128
$\overline{M}z$	1,171,640	1,017,637	981,543
$\overline{M}v$	424,063	354,521	348,021
$\overline{M}w / \overline{M}n$	45.01	111.57	358.00
$\overline{M}z / \overline{M}w$	2.42	2.50	2.43
$\overline{M}v / \overline{M}n$	39.43	97.02	308.66
I. VISC	14,376.74	12,547.03	12,371.80

b) PS-G15/36 sheet

Data	Samples Irradiation Time		
	Control	10 hours	21 hours
$\overline{M}w$	395,008	346,086	304,196
$\overline{M}n$	6,823	3,445	1,073
$\overline{M}_z$	924,450	923,749	18,092,544
$\overline{M}v$	344,981	298,772	184,072
$\overline{M}w / \overline{M}n$	57.90	100.46	283.43
$\overline{M}z / \overline{M}w$	2.34	2.67	59.48
$\overline{M}v / \overline{M}n$	50.56	86.73	171.50
I. VISC	12,289.58	11,017.21	7,624.36

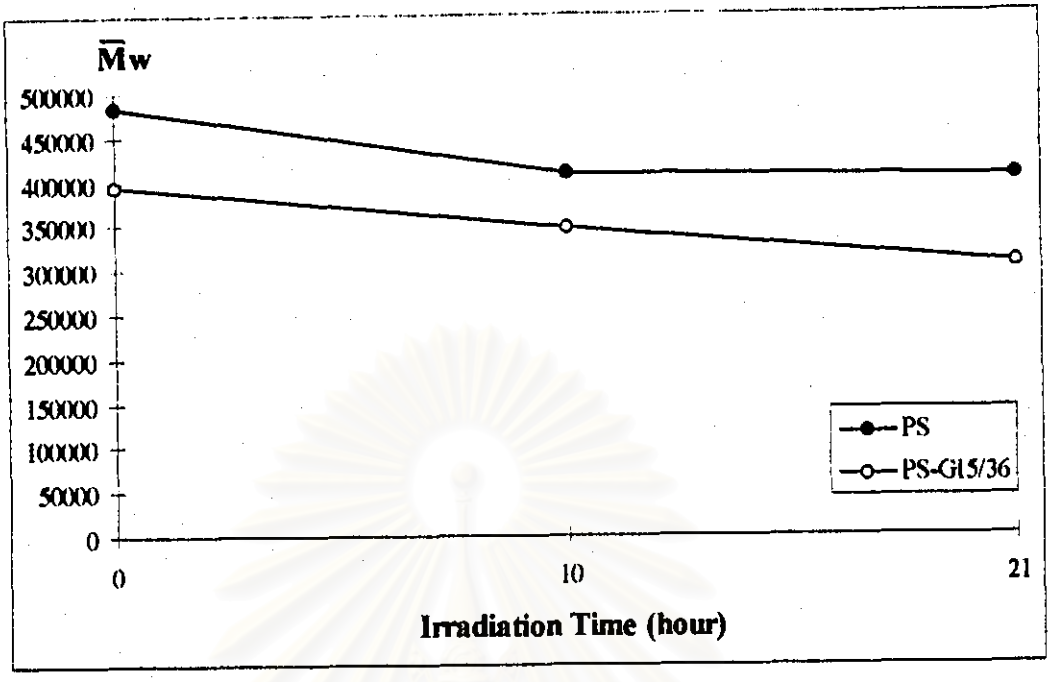

Figure 4.71 Weight-average molecular weights of PS and PS-G15/36 sheets during UV irradiation

The changes of weight-average molecular weight of PS and PS-G15/36 sheets at various irradiation time are shown in Figure 4.71. From this figure, the molecular weights of both the PS and PS-G15/36 sheets decrease slowly. It can be seen that the molecular weight of PS sample decreases slower than that of PS-G15/36 sheet. The decreasing of molecular weight can be described by the oxidative degradation as in FTIR absorption measurements. Comparing the polydispersity of the PS sheet ($\overline{M}w/\overline{M}n$ = 358) with that of the PS-G15/36 sheet ($\overline{M}w/\overline{M}n$ = 283), the former has a wider distribution. The UV irradiation method gives the similar result and trend with the outdoor exposure. It is undoubted that most of the outdoor radiation is ultraviolet radiation and others. The importantly UV radiation imposes more degradation effect than do the others.

4.3.5.4 Thermal Property Measurements

Figures 4.72 through 4.75 show the TGA thermograms of PS and PS-G15/36 sheet at various UV irradiation times. The initial percent weight loss of PS sheet was 99.95%; and that at 21-hour UV irradiation time, the percent weight loss became 99.26%. The TGA thermograms of PS-G15/36 sheet as a control and this under 21-hour UV irradiation time showed two steps of weight loss, the first one involving the decompose of cassava starch and the second one for the decompose of polystyrene plastic. The percent weight loss of control PS-G15/36 sheet at 21-hour UV irradiation time was 97.63%, the percent weight loss became 97.23%. It was found that the percent weight losses of PS and PS-G15/36 sheets change slightly or even unchanged under UV irradiation. The result may conclude that PS and PS-G15/36 sheets degrade slowly under UV irradiation.

From equation 4.13, the initial activation energy of PS sheet was 201.3 $kJ.mol^{-1}$, after 21-hour UV irradiation, the activation energy became 204.6 $kJ.mol^{-1}$. For PS-G15/36 sheet, the initial activation energy was 97.8 $kJ.mol^{-1}$, after 21-hours UV irradiation, the activation energy became 109.6 $kJ.mol^{-1}$. It can be seen that the activation energy of PS and PS-G15/36 sheets change slightly or even do not change at all for UV irradiation.

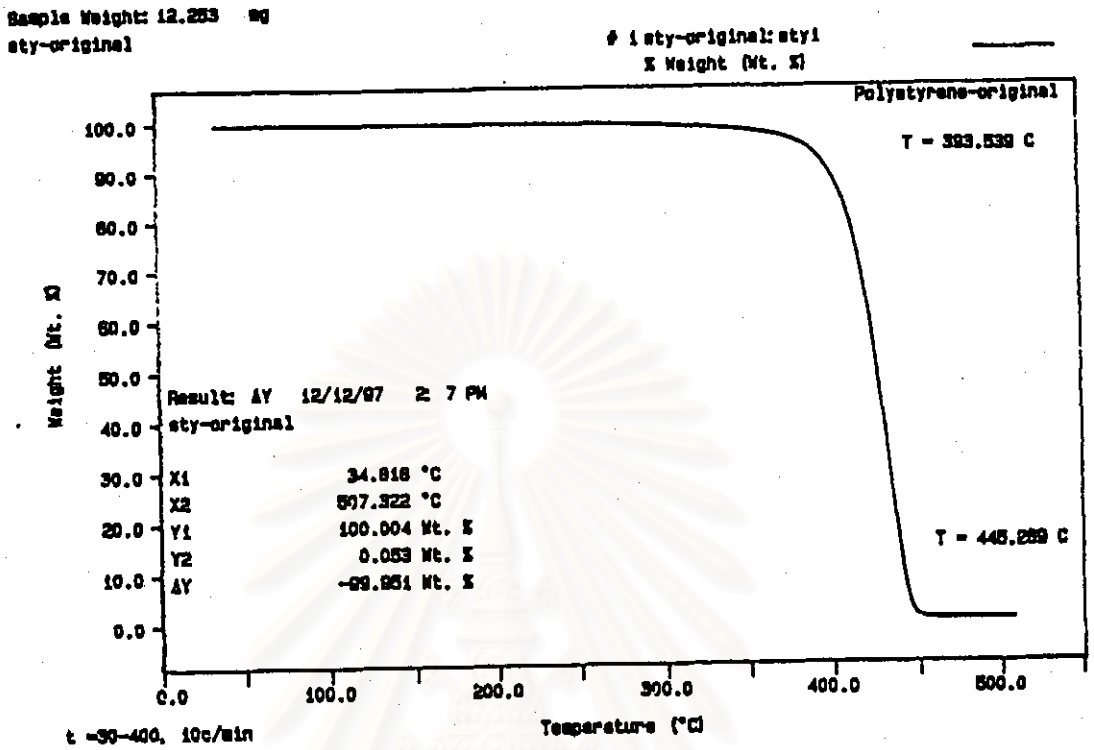

Figure 4.72 TGA thermogram of control PS sheet

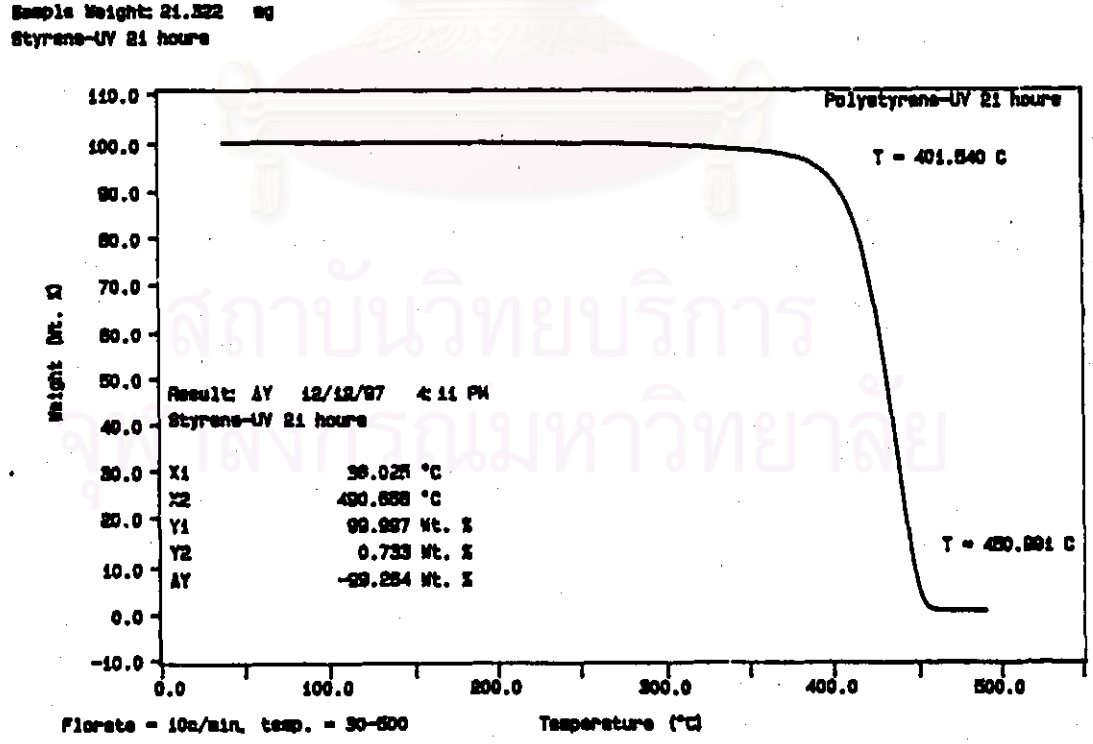

Figure 4.73 TGA thermogram of PS sheet at 21-hour UV irradiation time

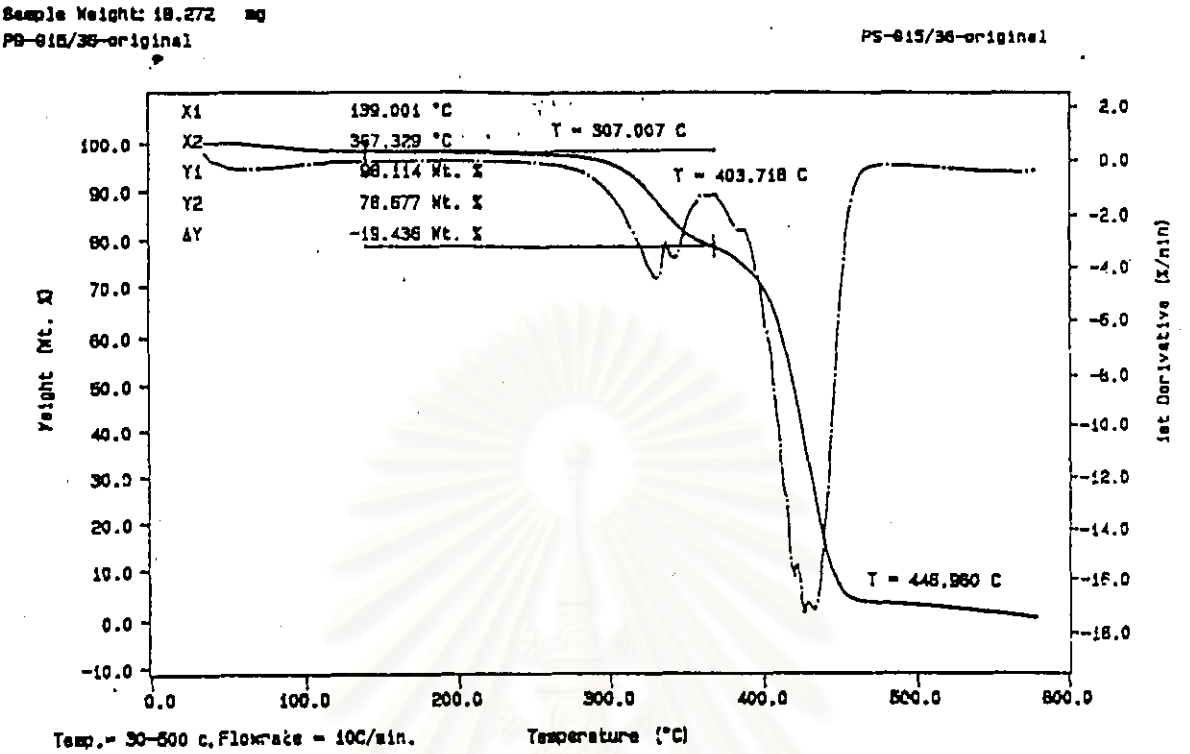

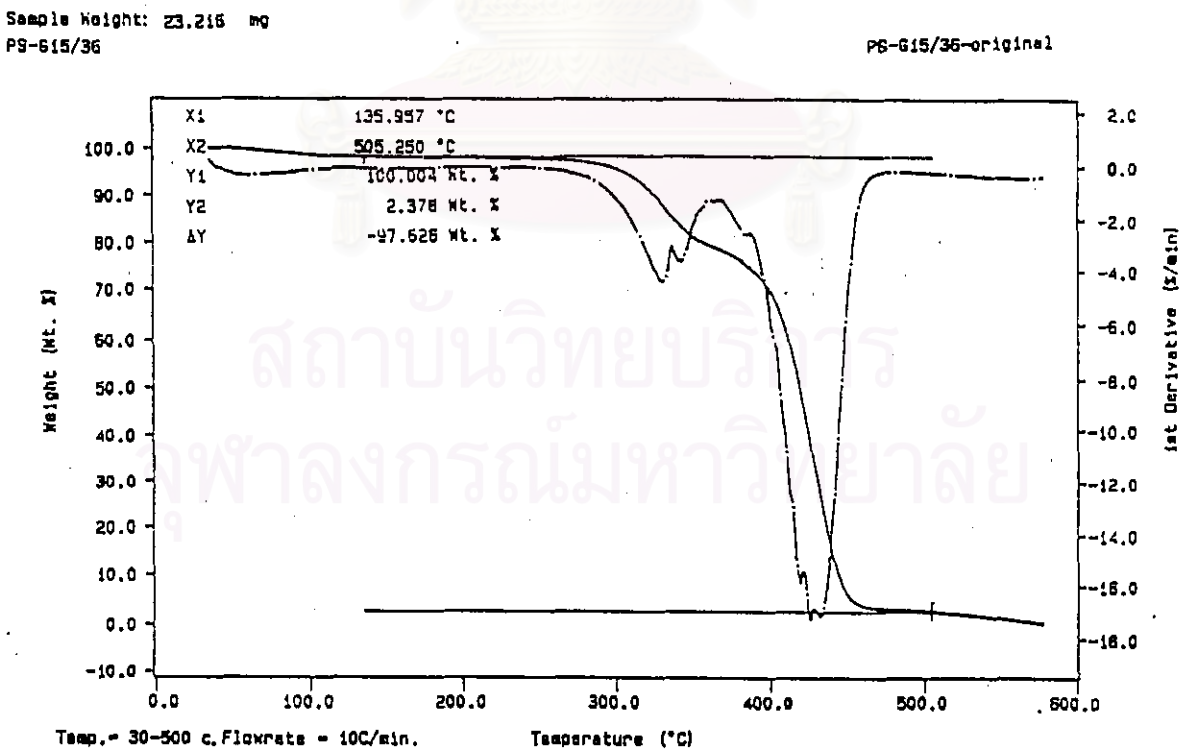

Figure 4.74 TGA thermograms of control PS-G15/36 sheet

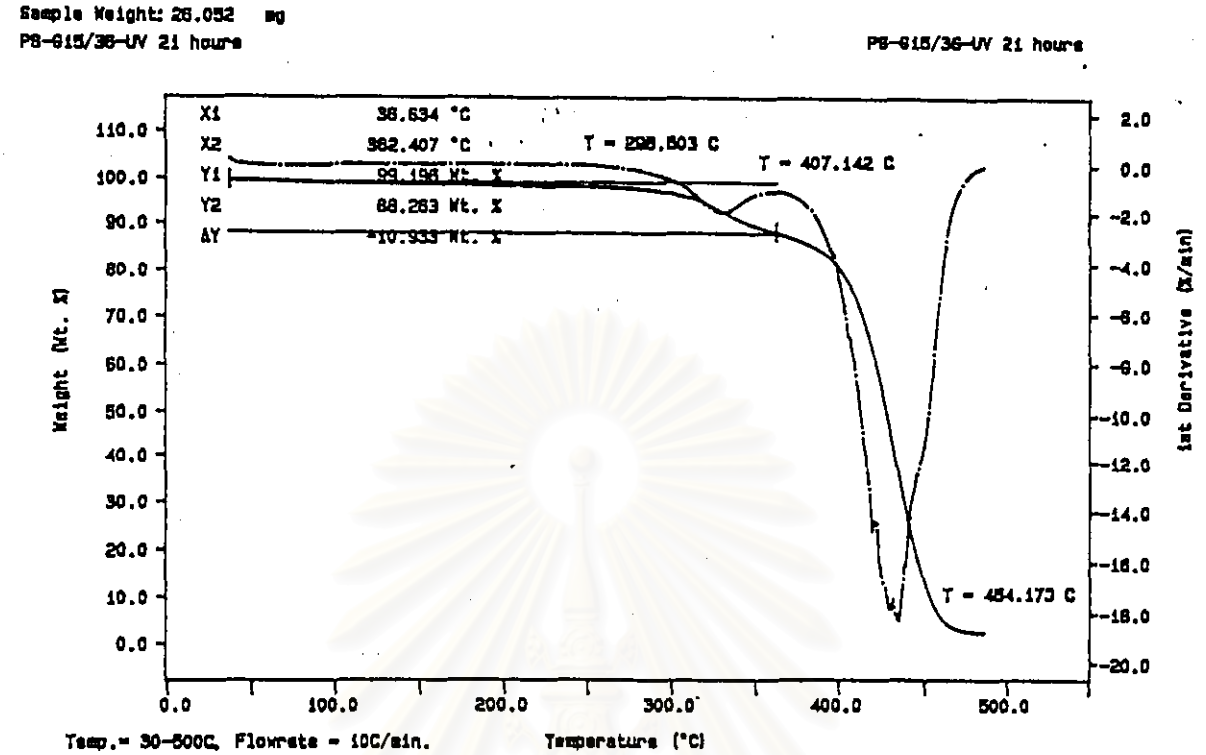

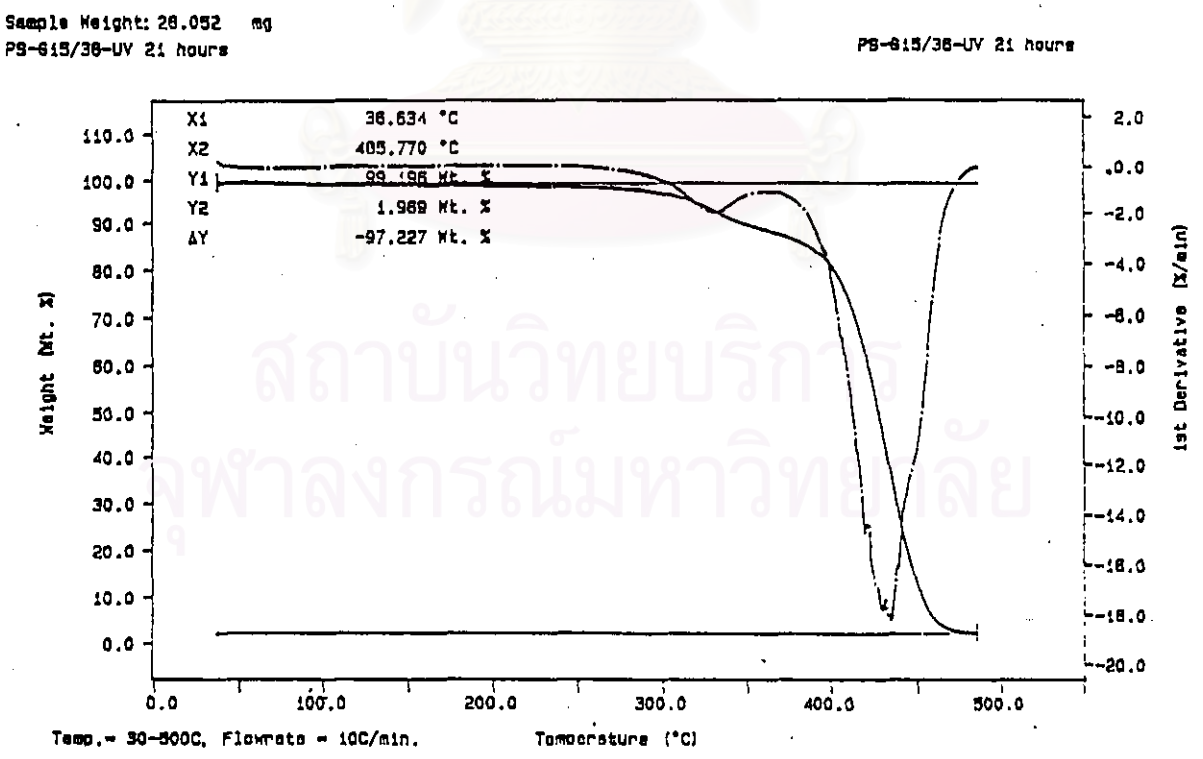

Figure 4.75 TGA thermograms of PS-G15/36 sheet at 21-hour UV irradiation time.

4.3.6 Bacteria Resistance of the PS and Composite PS Sheets

The degradability resistance of PS and composite PS sheets was carried out in accordance with ASTM G22-76. In this experiment, *Bacillus coagulans* 352 was used and the nutrient-salt selected for this study contained no carbon source. The microorganisms used for this research can survive by utilizing only the nutrient sources from the cassava starch in the plastic samples. The effects of liquid and solid media on the microbial degradation of plastic sheets were carried out to observe contact surface areas. In a liquid media, both sides of the plastics contact more intimately with the bacteria in the solution. Microbial degradation occurred by microorganisms consuming the materials (starch and the plastics) leading to increased porosity, void formation and the loss of integrity of the plastic matrix was observed on both plastics. The side of PS plastic contacted with the solid media became yellowish while the other side remained unchanged. Both sides of the PS plastics immersed in the liquid media are yellowish in color. This result indicates the importance of contacted surface area on microbial degradation.

The scanning electron micrographs of the composite PS sheets as shown in Figures 4.76 to 4.79, reveal the destroyed areas of starch that are the starting point of degradation. From SEM micrographs, there was some significant effect in terms of damaged holes between the samples in solid and liquid media. Diffusion or partition of substants on the plastic surfaces to the bulk solution and vise verse is better so that new areas for bacterial attack are increased. The number of pores on the immersed surfaces is thus increased. The primary mechanism must be microbial production of amylase in or near a pore, followed by diffusion of the enzyme into pores and diffusion of soluble digestion products back to the surface where they are metabolized. This mechanism is the only possibility when the pore diameter (≈ presently measured of 3-4 μm) is too small to admit a microbial cell. An alternative mechanism could be diffusion of a water-soluble starch to the plastic surface, at which point degradation would occur [35].

a) solid media

b) liquid media

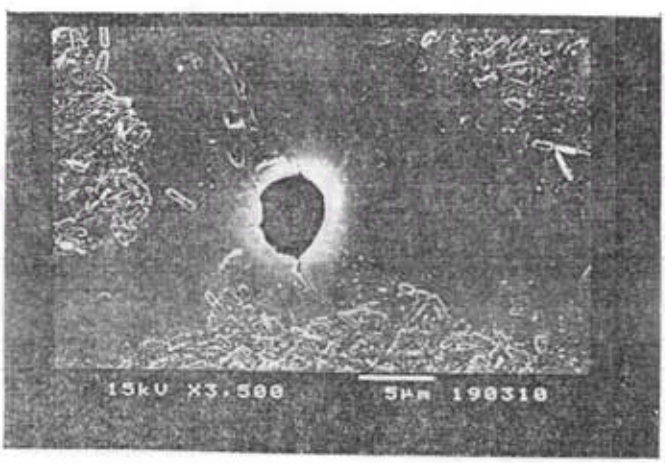

c) liquid media

Figure 4.76 SEM micrographs of PS-S5-G5/9 sheets attacked by bacteria *Bacillus coagulans* 352

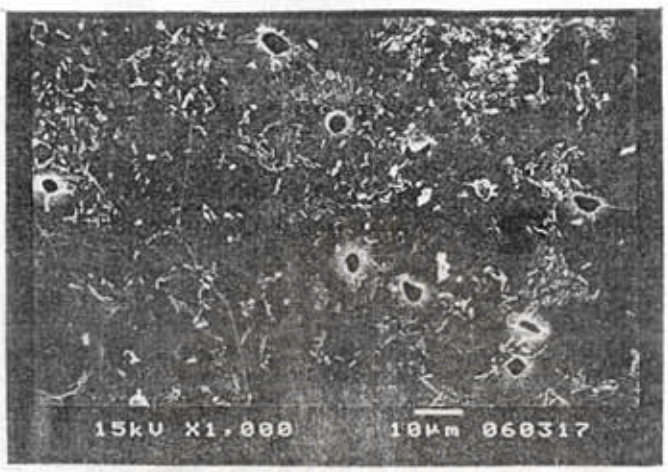

a) solid media

b) liquid media

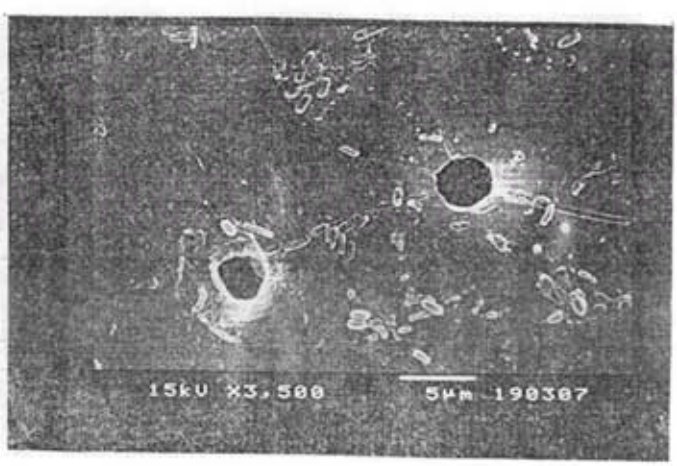

c) liquid media

Figure 4.77 SEM micrographs of PS-S5-G10/18 sheets attacked by bacteria *Bacillus coagulans* 352

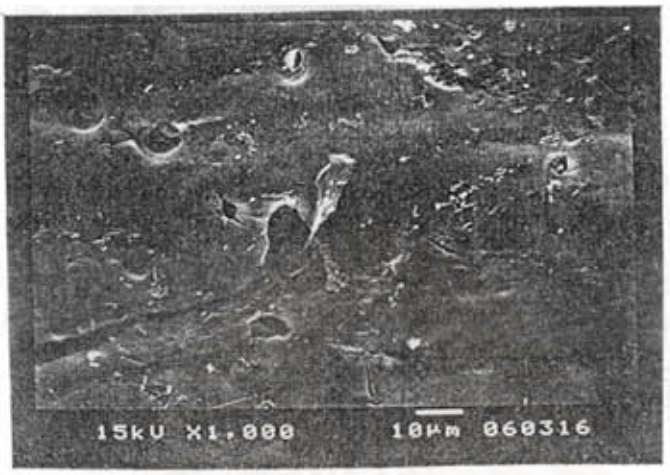

a) solid media

b) liquid media

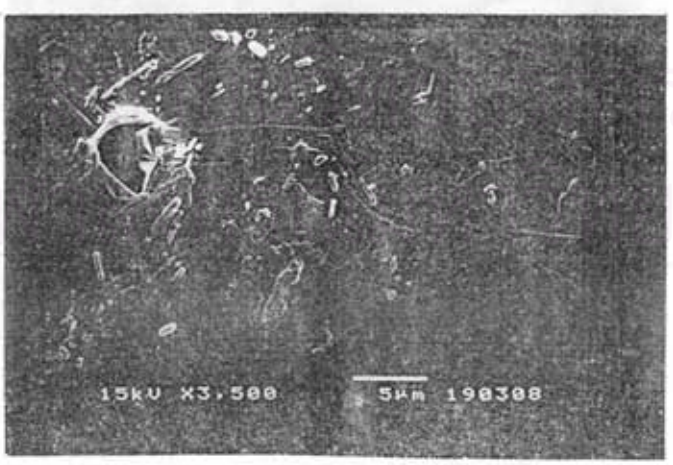

c) liquid media

Figure 4.78 SEM micrographs of PS-S15/27 sheets attacked by bacteria *Bacillus coagulans* 352

a) solid media

b) liquid media

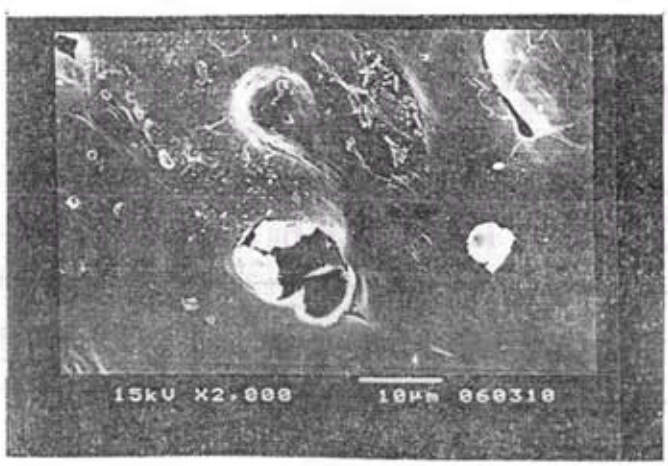

c) liquid media

Figure 4.79 SEM micrographs of PS-G15/36 sheets attacked by bacteria *Bacillus coagulans* 352